A thesis submitted for the degree of Doctor in Philosophy (PhD) in co-tutelle between:

Laboratoire de physique-chimie / Université de Paris XI, France

School of Chemistry / University of Sydney, NSW Australia

By

Anne Bunner-Pilotelle

Lipid-protein and protein-protein interactions in the mechanisms of photosynthetic reaction centre and the Na^+,K^+-ATPase

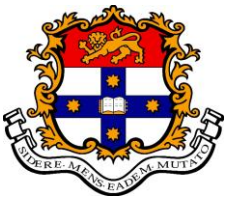

September 2008

M. Champeil P. Examiner

M. Clarke R.J. Examiner

Mme Demachy I. Examiner

M. Mahy J.P President

M. Sebban P. Examiner

Table of Contents

Table of Contents

Acknowledgements

First of all I would like to express my sincere gratitude to my supervisors Ron Clarke and Pierre Sebban. They have given invaluable support throughout these three years with their enthusiasm, endless inspiration, patience (when we spent five hours in a bus to cross LA, and when we went back and forward to Saclay!).

Merci à tous les membres du laboratoire de chimie-physique de Paris XI-Orsay qui ont participé à rendre ce travail agréable.

Tout au long de ma thèse j'ai pu bénéficier d'aide technique formidable, un grand merci à Valérie Derrien, Mireille Benoit et Christine Dubois.

Merci a ma collègue Hélène Cheap pour avoir partagé son expérience du laser et les sympathiques pauses discussion. Et aussi tant de bon souvenirs à courir après un PM de remplacement!! ….N'était-ce pas plutôt l'alimentation électrique?

Un grand merci à mon collègue Thomas, partager le bureau avec lui m'a permis de voir un lien entre le football et la musique cubaine!! A special thank for all the pictures you sent to warn me about all the venomous animals living in Australia …you're a true friend!

Thanks to all the mates from room 330 and 331 for making this year such an enjoyable time, especially to Connie, thank you for your friendship, the tea (detox)-muffin breaks (for chocolate emergency!), piano times (and music sheets!!) and those endless travel plans: you certainly are a legend!!! Muay for her great Thai food suggestions; Bill with whom it was always a pleasure to speak about everything, Nguyen, Izy and Jeannette.

I would like to thank all my friends that reminded me there is a life outside the laboratory.

Finalement je voudrais remercier ma famille: Mes parents, Auguste et Simone ; Céline ; Lucas et bien sûr Alexis. Sans leur soutien cette thèse n'aurait certainement pas pu se réaliser.

Abstract

Lipid-protein and protein-protein interactions are likely to play important roles in the function and regulation of charge-transporting membrane proteins. This thesis focuses on two different membrane proteins, the photosynthetic reaction centre (RC) from purple bacteria and the Na^+,K^+-ATPase. The influence of the lipid surroundings and cholesterol derivatives on the kinetics of electron transfer of the RC were investigated by reconstituting the protein in phosphatidylcholine vesicles containing cholesterol and derivatives known to modulate the membrane dipole potential. The experiments performed on the Na^+,K^+-ATPase were designed to contribute to a better understanding of the role that oligomeric protein-protein interactions have in the enzyme's mechanism.

Our results show that the cholesterol derivatives significantly modify the electron transfer kinetics within the RCs and their multiphasic behavior. These effects seem to be associated with the extent of the dipole potential change experienced by the RC within the phospholipid membrane. Indeed, the largest effects on the rates are observed when 6-ketocholestanol and cholesterol are present, consistent by with their previously demonstrated significant increase of the dipole potential. We interpret this data as indicating an increased free energy barrier for protons to enter the protein. The consequences of the increased dipole potential seem to be experienced across the entire protein, since the rates of the $P^+Q_A^-$ charge recombination in the presence of AQ^- acting as Q_A are also modified by the same effectors.

Also interesting is the effect of the dipole potential on the two conformational states of the RCs (previously reported) as revealed by the biphasic decays of the electron transfer kinetics. In particular, we report for the first time a biphasicity of the $P^+Q_A^-$ charge recombination in the WT RCs. This non exponential behaviour, absent in the phospholipid membrane or isolated RCs, is induced by the presence of the cholesterol derivatives,

suggesting that the equilibration time between the two RC conformations is slowed down significantly by these molecules. According to this work, the dipole potential seems to be an important parameter that has to be taken into account for a fine understanding of the charge transfer function of the RCs.

Reported literature values of the dissociation constant, K_d, of ATP with the E1 conformation of the Na^+,K^+-ATPase based on equilibrium titrations and kinetic methods disagree. Using isothermal titration calorimetry (ITC) and simulations of the expected equilibrium behaviour for different binding models, this thesis presents an explanation for this apparent discrepancy based on protein-protein interactions. Because of the importance of Mg^{2+} in ATP hydrolysis, kinetic studies of Mg^{2+} binding to the protein were also carried out. These studies showed that ATP alone is responsible for Mg^{2+} complexation, with no significant contribution from the enzyme environment.

Abbreviations

AMP-PCP: Adenylylmethylenediphosphonate

ATP: Adenosine tri-phosphate

BCls: Bacteriochlorophyll dimer

BPh: Bacteriopheophytin

CDTA: Trans –1,2-diamino cyclohexane-N,N,N',N'-tetraacetic acid

Cyt c_2: Cytochrome c_2:

Di-8-ANEPPS:4-(2-(6-dioctylamino)-2-naphthalenyl)ethenyl)-1-(3-sulphopropyl)-pyridinium inner salt

EDTA: Ethylene diamine tetraacetic acid

k_{AB} (1): rate constant associated with the first electron transfer

PLPC: proteoliposome composed with phosphatidylcholine

PC: Phosphatidylcholine

P: Primary electron donor

RH421: N-(4-sulphobutyl)-4-(4-(p(dipentylamino) phenyl) butadienyl)-pyridinium inner salt

RCs: Photosynthetic reaction centres

U10: Ubiquinone10

Chapter 1

Introduction

1.1 Lipid bilayers

Both the plasma and organelle membranes of living cells are bilayers of lipid containing proteins. The lipids are diverse in composition and the proportion of each type of lipid in any given membrane varies depending on the organism and the nature of the membrane. The membrane architecture is neither completely rigid nor fluid and the lipid structural diversity enables non-random lipid mixing in each leaflet of the bilayer, resulting in regions or microdomains with specific physical and functional properties. Some lipids are surrounded by neighbouring lipids whereas others are involved in interactions with membrane proteins.

Phospholipids are amphipathic molecules **(Fig. 1.1)** containing hydrophilic polar head groups and hydrophobic hydrocarbon chains (usually 12-20 carbons). Most phospholipids belong to the class of phosphoglycerides, which contain a glycerol group joining the polar head group and the hydrocarbon chain. The most common phospholipids found in the bimolecular lipid matrix are phosphatidylcholine, phosphatidylethanolamine and phosphatidylserine.

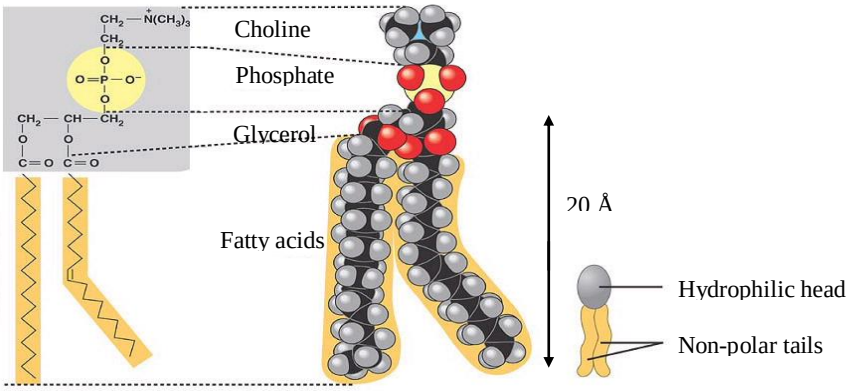

Figure 1.1: Structure of the phosphatidylcholine (PC) containing a hydrophilic head composed of a choline group, a phosphate and a glycerol group. The non-polar tail is composed of two fatty acids chains of ~ 20Å.

Proteins embedded in the membrane bilayer may pass entirely through the bilayer as transmembrane proteins or may be inserted at the cytoplasmic or extracellular face.

1.2 The dipole potential

The electrical potential profile experienced by lipid bilayers **(Fig. 1.2)** in biological cells is composed of two major components. The first is the transmembrane potential ($\Delta\psi$) determined by the concentration difference of the ions in the aqueous phases on both sides of the membrane which is reflected by a charge separation across the membrane. The second component is the boundary potential, including two subcomponents: a surface potential (ψ_s), and the dipole potential (ψ_d) that have both been shown[1] to be pH-dependent. ψ_s arises [2-4] from charged surface groups on the membrane. $\Delta\psi$ and ψ_s have been widely examined by electrophysiological measurements, unlike ψ_d.

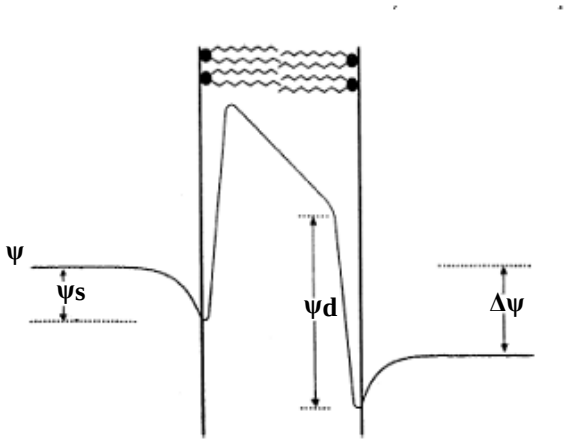

Figure 1.2: The electrical potential, ψ, profile across a phospholipid bilayer. The transmembrane potential ($\Delta\psi$) is due to the difference in ion concentrations between the two bulk aqueous phases. The surface potential (ψ_s) results from charged residues at the bilayer/solution interface. The dipole potential (ψ_d) results from the alignment of dipolar residues moieties of the lipids and associated water molecules within the membrane.

The dipole potential of a lipid membrane is manifested between the hydrocarbon core of the membranes and the first few water molecules adjacent to the lipid headgroups. It is caused by the uniform orientation of the phospholipid moieties, the carbonyl groups of the

ester linkage, and water dipoles which penetrate into the membrane. It can vary between both leaflets as they have different composition. The lipid-bound polarized water molecules are thought[5] to make the major contribution to ψ_d.

Recently, ions have been recognized[6, 7] to have an influence on ψ_d and on various membrane-related physiological processes. It has been shown[8] that Li^+, Na^+, Ca^{2+}, Mg^{2+}, Sr^{2+} and Ba^{2+}, but not K^+, bind to lipid-head groups containing oxygen and that ion binding influences lipid order, area per lipid, orientation of the lipid head dipole, the charge distribution in the system, and therefore the electrostatic potential across the head-group region of the bilayer. Furthermore, lyotropic anions like perchlorate are known[7] to have an effect on the kinetics of the Na^+,K^+-ATPase enzymatic cycle, which might be explained by electrostatic interactions with the protein due to the binding of such ions at the membrane-aqueous solution interface. Clarke and Lüpfert[6] noticed that the capacity of anions or cations to affect the dipole potential depends on their ability to partition between the membrane surface and the aqueous phase, thereby controlling the ion transport activity of the Na^+,K^+-ATPase. Furthermore, increasing the sodium chloride concentration decreases the self-diffusion of phosphatidylcholine lipids within the bilayer[9].

A common component found in biological membrane is cholesterol. Its role in the bilayer will be detailed in a later section. The primary effect of cholesterol or its derivatives on the dipole potential is thought[10] to occur by the alignment of their dipole moments either opposite to or in the same direction as the net dipole moment arising from the phospholipids of the bilayer and their associated water molecules. However, a more precise picture of the mode of action of lyotropic anions and cholesterol derivatives on membrane proteins could lead to a better understanding of dipole potential participation in the mechanism of membrane protein activity.

Depending on the structure of the bilayer, the magnitude of ψ_d can vary from around 100mV to 400mV[11]. It has been reported[12] that the inclusion of molecules such as cholesterol and some of its derivatives may either increase or decrease the magnitude of the dipole potential. Cholesterol itself can increase ψ_d by up to 100mV when added to a phosphatidylcholine bilayer[13], resulting in an enormous electric field strength within the membrane.

Over the past decade, a large number of membrane proteins have been shown to be sensitive to a change in their electrostatic surroundings. ψ_d affects the activity of proteins as well as their insertion and folding into the membrane[14]. Recently for instance it has been shown that ψ_d affects the interaction of the viral gp41 fusion peptide with the cell membrane[15, 16]. Other proteins affected include ion channels[17-19], phospholipases[20], but also pumps like the sodium potassium pump[21, 22]. In this study we have analysed the effect of the lipid environment and the presence of cholesterol derivatives on the functioning of two membrane proteins, the photosynthetic reaction centre of purple bacteria and the Na^+,K^+-ATPase from shark.

1.3 Lipids

1.3.1 Phospholipids

a. Phosphatidylcholine and Dimyristoylphosphatidylcholine

Phosphatidylcholine (PC) is one of the major components in biological membranes. We used here to form liposomes. It can be chemically extracted from either egg yolk or soybeans. Phosphatidylcholine can be found with various molecular weights due to the various lengths of its hydrocarbon chains.

Recently it has been found[23] that the value of the dipole potential decreases with increasing unsaturation, with a drop of between 50 and 100mV depending on the degree of unsaturation. This can be accounted for by effects of *cis* carbon-carbon double bonds on chain packing and hence the spacing between the headgroups. In a membrane of fully saturated phosphatidylcholine, ψ_d was found to have a value of around 220-280mV[10].

In previous investigations, the influence of the phase state of lipid bilayers on the photosynthetic reaction centre was investigated using dimyristoylphosphatidylcholine (DMPC) (14:0/14:0). It was shown that the gel-liquid crystalline phase transition of DMPC modifies the thermodynamic parameters associated with the second (but not the first) electron transfer process[24]. Studying proteoliposomes where RCs from Rhodopseudomonas viridis where incorporated in DMPC and dieladoylphosphatidylcholine (DEPC) Baciou *et al*.[25] have suggested that, *in vivo*, protein-protein interactions play a role in the thermodynamic parameters associated with the energy stabilization process within reaction centres reconstituted in DMPC liposomes. Later, Agostiano *et al*.[26] also showed that the charge-separated state of reaction centres is highly stabilised in protein reconstituted in liposomes due to specific interactions between phosphatidylcholine and reaction centres.

1.3.2 Cholesterol and its chemical analogues

a. Cholesterol and lipid rafts

Cholesterol (structure of cholesterol shown **Fig. 1.3 (B)**) and sphingolipid-enriched microdomains are known as lipid rafts[27]. The biological membrane contains a variety of lipid and protein molecules that are segregated and distributed in microdomains. Lipid rafts represent a concept of membrane microdomains that are enriched in cholesterol and sphingolipids. Lipid rafts were discovered due to their resistance to cold detergent

extraction[28]. Recently, lipid rafts have received considerable attention because they are thought to be involved in the regulation of the activity of numerous proteins[29-32].

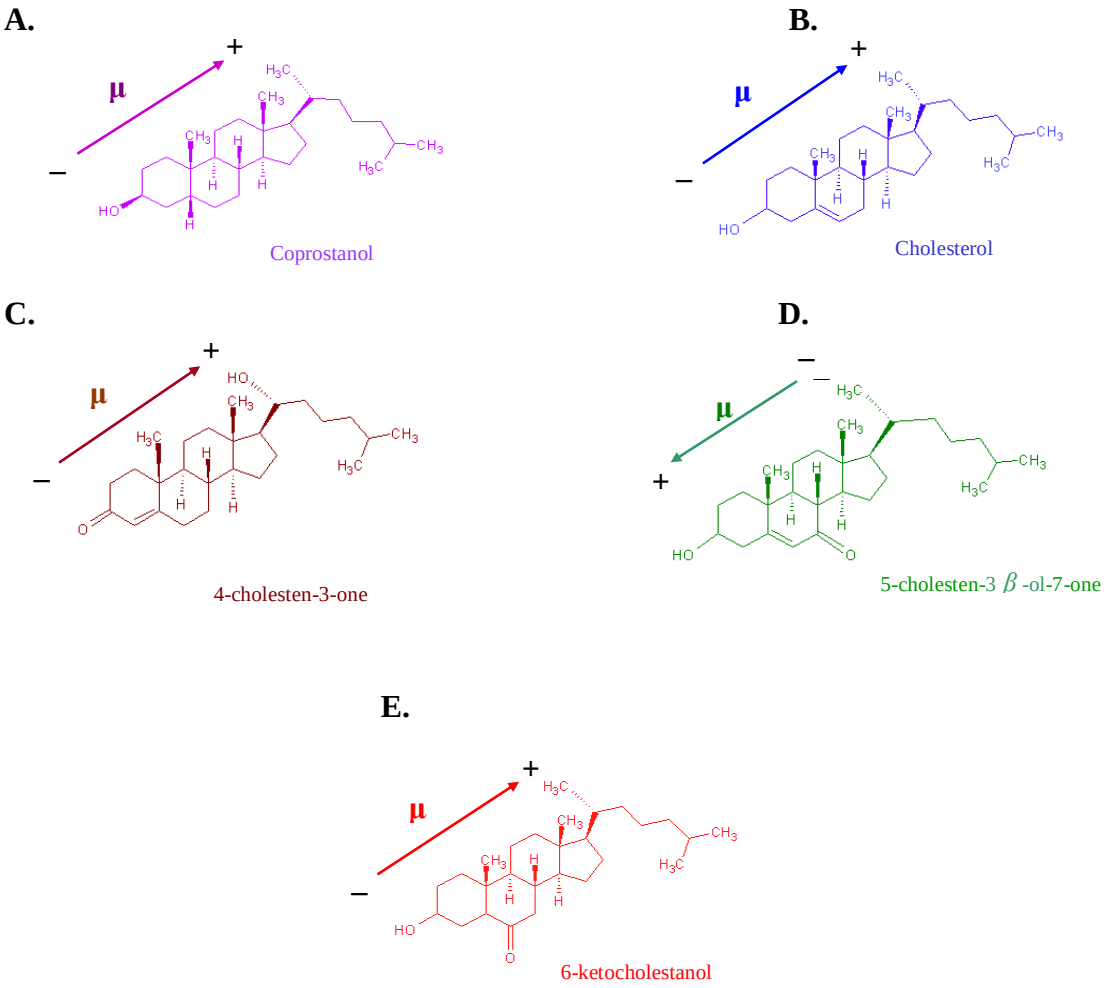

Figure 1.3: Chemical structure of cholesterol and its derivatives: 6-ketocholesterol, 5-cholesten-3β -ol-7-one and 4-cholesten-3-one, coprostanol and their dipole moments (μ) orientation.

Different subtypes of lipid rafts can be distinguished according to their protein and lipid composition. Recent work[33] indicates that the glycosylation of cholesterol reduces the percentage of cholesterol present in microdomains.

In general, cholesterol is known to induce an internal positive dipole potential that enhances the permeability of anions but decreases the permeability of cations. When the cholesterol concentration is increased in phospholipid bilayers, the degree of motional order of the phospholipid hydrocarbon chains in the membrane is decreased [34].

Recently, it has been demonstrated[35] that a preferential interaction exists between cholesterol and tryptophan residues of membrane proteins located near the membrane-water interface. Evidence has been presented[36] that the complex of phosphatidylcholine and cholesterol is held together by hydrogen bonding between the hydroxyl group of cholesterol and the carbonyl groups of the phosphatidylcholine situated in the polar part of the lipid bilayer. The importance of the hydroxyl group is supported by the fact that cholestane which has a molecular structure similar to cholesterol except for the absence of the OH group[37] has no preferential orientation in the bilayer membrane.

Furthermore, replacing the cholesterol hydroxyl group by a ketone group facilitates sterol flip-flop which gives the lipid bilayers increased fluidity[38]. The change in the field strength caused by incorporation of cholesterol into phosphatidylcholine bilayers is theoretically capable of modulating membrane protein function by affecting the orientation of dipolar or charged protein segments.

b. Phloretin, 6-ketocholestanol and 5-cholesten-3-β-ol-7-one

6-ketocholestanol **(Fig. 1.3 (E))** and phloretin **(Fig. 1.4)** have been used[39] as penetration enhancers in the transdermal delivery of certain drugs. Different mechanisms have been proposed to explain the effect of these molecules in this process. Phloretin and 6-ketocholestanol are believed[40] to increase the fluidity of the lipid bilayer by interacting with the lipid layer and changing its structural parameters. They strongly decrease the lipid phase transition temperature of DMPC and DPPC liposomes, which induces a decrease in the strength of intermolecular forces within the membrane. Furthermore, it has been shown[40] that increasing amounts of phloretin and 6-ketocholestanol to phospholipid bilayer caused an increase of the enthalpy change of the transition. Additionally, phloretin can alter[39, 41] the

structure of the interface by changing the water dipoles' orientation and the orientation of the ester carbonyls of the lipids.

A study from Antonenko *et al.*[42] suggested that the change in the dipole potential caused by phloretin **(Fig. 1.4)** affects carrier-mediated ion fluxes through the bilayer lipid membrane. This could be explained[43] by the change in dipole potential produced by phloretin altering the electrical component of the energy barrier from ion transport.

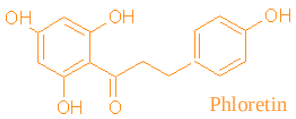

Figure 1.4: Chemical structure of phloretin

The effect of 5-cholesten-3-*β*-ol-7-one **(Fig. 1.3 (D))** on the dipole potential is related to a twisted planar cyclic structure possessing a hydrophobic tail and a different dipole moment direction compared[13] to the other cholesterol derivatives, which have the positive end of their dipole moment directed towards the hydrophobic interior of the membrane **(Fig. 1.3)**. In contrast, the positive end of the dipole moment of 5-cholesten-3-*β*-ol-7-one is directed towards the interface with the aqueous solution.

1.4 Liposomes

The studies described in this thesis have concentrated on model systems of one phospholipid, phosphatidylcholine, which was used to form liposomes. A second step was to include cholesterol, its derivatives (6-ketocholestanol, 5-cholesten-3-*β*-ol-7-one, coprostanol, 4-cholesten-3-one) or phloretin within the membrane and to compare the effect of each molecule on the RC and Na^+,K^+-ATPase respective activities.

1.5 Orientational polarizability

Ion transfer by the Na^+,K^+-ATPase involves the movement of charges across the membrane and simultaneous protein conformational changes. Lipids and associated water molecules surrounding the enzyme possess permanent dipole moments and are free to rotate and align with the electric field direction. Charged and dipolar moieties in the surrounding lipids could reorient around the changing charge distribution caused by its conformational transitions. The ability to reorientate with the applied electric field is called orientational polarizability (Δf). Therefore, it is important to take into account not only the static charge distribution of the membrane's hydrophilic part, reflected in the dipole potential but also the possibility of dynamic changes in charge distribution, reflected in the orientational polarizability. Phloretin **(Fig. 1.4)**, cholesterol, 6-ketocholestanol, coprostanol, 4-cholesten-3-one and 5-cholesten-3-β-ol-7-one **(Fig. 1.3)** are known to change the dipole potential value when incorporated in liposomes[13]. In this thesis the effect of cholesterol and its derivatives on the function of Na^+,K^+-ATPase has been investigated not only through their impact on the dipole potential but also through their effect on the orientational polarizability of the membrane surroundings.

1.6 The Photosynthetic Reaction Centre from *R. sphaeroides*

1.6.1 Introduction

All microorganisms can survive either using chemotrophy or phototrophy. In the former process they extract their energy from the oxidation of organic (chemoorganotrophs) or inorganic (chemolithotrophs) compounds. In the latter process, they use solar energy, in other words, photosynthesis. All of them have one "goal", producing ATP.

Photosynthesis is a biological oxidoreduction process by which electromagnetic energy (light energy) converted into chemical free energy. It is essential not only because it allows plants to grow but also because this stored chemical energy sustains all other forms of life on earth.

According to fossils and CO_2 markers in the rocks, photosynthesis has very likely emerged on earth more than 3 Ga ago and possibly earlier than 3.5 Ga.

The first organisms to have developed this survival mode were probably the green sulphur bacteria using H_2S as the essential electron donor compounds. The purple non-sulphur bacteria arose shortly after. The (accidental) cooperation of both of them gave rise to cyanobacteria, the first oxygen evolving organisms. This main event in the earth history gave rise to oxygenic atmosphere ~2 Ga later and to the emergence of mammals and human: 3 Ga later (amongst others!).

1.6.2 Anaerobic photosynthetic organisms

As mentioned above, higher plants are not the only organisms performing photosynthesis. Algae and many bacteria (including cyanobacteria, purple and green bacteria) are able to use photosynthesis as a process for obtaining energy. Algae, cyanobacteria and higher plants (collectively known as oxygenic organisms) extract electrons from water (evolving oxygen as a by-product) and use them to convert carbon dioxide to hexose:

$$\mathbf{6CO_2 + 12\ H_2O \rightarrow C_6H_{12}O_6 + 6O_2 + 6H_2O}$$

Since they use solar energy and their main source of carbon is CO_2, these organisms are called *photoautotrophic*.

Other organisms do not evolve oxygen and are anaerobic (all of which are prokaryotes), microaerophiles or facultative anaerobes. All of them extract electrons from donor molecules

with a lower redox potential than that of water, such as elementary sulphur, sulphide, thiosulphate, organic compounds, alcohols, or hydrogen. Since they use solar energy and their sources of carbon are diverse, these organisms are called *photoheterotrophic*.

Oxygenic organisms use two different types of reaction centres which operate in series and which are designated photosystem 1 (PS I) and photosystem 2 (PS II). Differing from these, anoxygenic organisms function with a single reaction centre. Two different types of reaction centres have been described in photosynthetic bacteria. Green sulphur bacteria contain membrane bound iron-sulphur centres of low redox potentials as secondary electron acceptors. These are called 'Fe-S type' reaction centres. This type of reaction centres is found in photosystem I of oxygenic organisms.

Reaction centres (RCs) of purple and green nonsulfur bacteria contain bacteriopheophytin as an intermediate electron acceptor and two quinones of moderately low redox potentials as secondary electron acceptors. They show structural similarities with the more complex photosystem II of oxygenic organisms and are named 'pheophytin-quinone type' reaction centers.

The anoxygenic photosynthetic organisms have been traditionally divided into four families (purple sulphur, purple nonsulphur, green sulphur and green nonsulphur bacteria) based on their respective sources of electrons and redox properties of electron carriers in the reaction centres[44, 45]. Another (and more precise) classification scheme has been introduced by Woese[46] based on sequence similarities of the 16 S ribosomal RNA. The purple bacteria and their relatives fall into a phylum called Proteobacteria. This phylum has four major subdivisions, α, β, γ and δ. The α subdivision includes purple nonsulphur bacteria such as *Rhodopseudomonas (Rps.) viridis*, *Rps. acidophila*, *Rhodobacter (Rb.) capsulatus*, *Rhodospirillum rubrum* and *Rhodobacter sphaeroides* whose structural and functional properties of the photosynthetic apparatus have been studied in detail. This will be used

here..*Rubrivivax (Rv.) gelatinosus* and *Rhodocyclus tenuis* are classified into the β-subdivision. The γ-subdivision contains purple sulphur bacteria (e. g. *Chromatium okenii*, *Thiocystis violacea*) and the δ-subdivision does not involve photosynthetic species (it is assumed that these organisms have lost the photosynthetic capacity during evolution).

Photosynthesis initially requires the cooperation of a large number of membrane proteins, soluble proteins and pigment molecules. All chlorophyll–based photosynthetic organisms share the existence of an antenna system tunnelling light energy to a reaction centre where light energy is transformed into chemical energy. The overall principle of the mechanism of energy storage appears to be the same in all kinds of photosynthetic organisms: a chlorophyll dimer (or perhaps monomer in photosystem I complexes) or bacteriochlorophyll dimer in a specific protein environment is excited to its singlet state by excitation energy transfer from the antenna pigments. In this state, chlorophyll molecules are very strong reductants which are able to transfer an electron to the nearby electron acceptor molecule. The electron transfer reaction leads to the formation of a radical-ion pair state, consisting of an oxidized chlorophyll or bacteriochlorophyll dimer on one side of the membrane and a reduced acceptor on the other side of the membrane. Energy conservation is achieved by coupling the electron flow to proton translocation across the photosynthetic membrane. The energy stored in the electrochemical gradient thus formed can be used to synthesize ATP and other molecules serving as the energy source of living organisms.

1.6.3 Structure

As mentioned above, photosynthetic RCs **(Fig. 1.5)** are membrane-spanning proteins binding pigments and cofactors that catalyse the first steps of light energy conversion into chemical free energy.

The 3D structure of the RC from *Rb. sphaeroides* has been previously determined[47]. More recently Koepke *et al.*[48] have determined its structure at different pH values, in dark and light conditions. At pH 8, in the dark, they obtained the best resolution so far, of 1.87 Å.

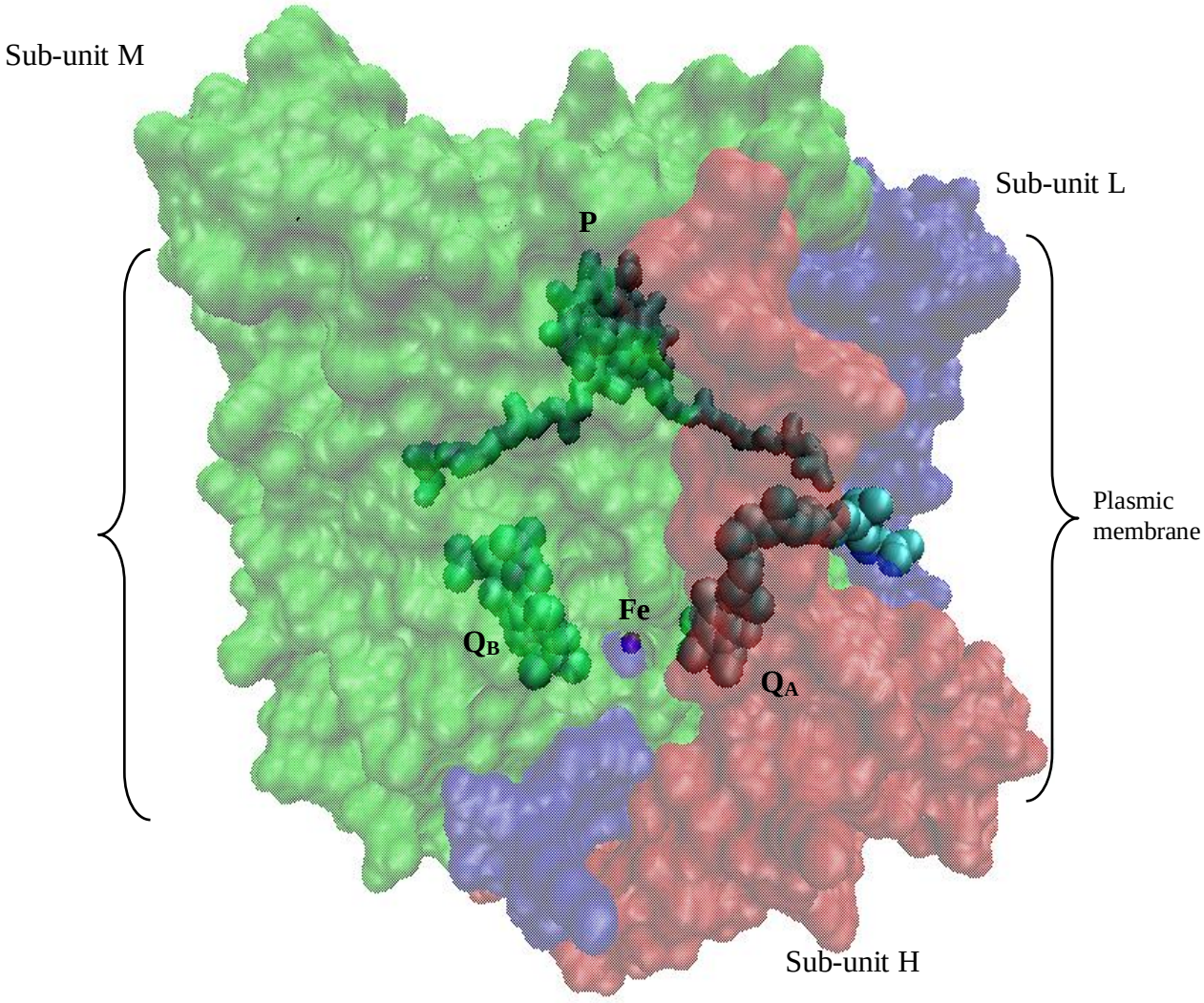

Figure 1.5: Structure of the *Rb. sphaeroides* reaction centre[49] composed of three sub-units L, M and H. Land M carry a dimer of BChls, P, two quinones, Q_A and Q_B and a non-heme iron Fe. The light-energy conversion is achieved through a series of coupled electron-proton transfer reactions from the primary electron donor (P). The electrons are transferred to a primary quinone molecule Q_A through B_A to form the Q_A^-. The electrons are then transferred to Q_B. This leads after the successive absorption of two photons to the formation of the doubly reduced and doubly protonated, Q_BH_2.

The isolated bacterial RC is composed of three polypeptides: L, M and H. L and M subunits bind all pigments and cofactors: a dimer of BChls, which is also the primary electron donor, P situated on the periplasmic side of the membrane; two monomers of

bacteriochlorophyll, B_A and B_B; two monomeric bacteriopheophytins, H_A and H_B; one non-heme ferrous ion, Fe^{2+}, which is symmetrically bound between two quinone molecules situated on the cytoplasmic side of the protein, Q_A and Q_B. Q_A is the primary stable electron acceptor and Q_B is the secondary (and ultimate) stable electron acceptor. The subunits L and M share the same secondary structure (5 transmembrane α helixes), arising from the ~ 30 % identity between their primary sequences.

The polypeptide backbones of L and M subunits show a high degree of local twofold symmetry, with the symmetry axis (joining P to Fe^{2+}) perpendicular to the membrane plane. On either side of the membrane-spanning region the L-M complex forms a flat surface parallel to the membrane plane. The H subunit consists of three distinct segments: the first one is the N-terminal segment which contains the only transmembrane helix of H subunit; the second one is a surface segment, which is mostly in contact with the cytoplasmic side of the L-M complex; and the third one is a globular segment consisting mainly of β-sheets.

The ferrous ion is bound near the cytoplasmic membrane surface, between Q_A and Q_B. Fe^{2+} is bound to four histidine residues (two provided by the L subunit, L190His and L230His and two by the M subunit, M219His and M266His) and one glutamic acid, provided by the M subunit, M234Glu.

The role of the ferrous ion is not clear but studies have shown[50] that if the iron is removed or exchanged with several other divalent metal cations the function of the RC is not altered. In addition, it has recently been demonstrated[51] that Fe^{2+} does not change its oxidation state during electron transfer. Upon light excitation of P to its singlet excited state of lowest energy, P*, an electron is transferred to H_A and then to the primary electron acceptor Q_A in about 3.5 and 200 ps. All electron transfer reactions from P* to Q_A^- are considered to be "fast", *i.e.*, with no activation energy, in other words as fast at the maximum rate achievable according to the Marcus theory.

1.6.4 Marcus electron transfer theory

In bacterial reaction centres, the electron transfer reactions take place over distances from 3 to 25 Å. The lifetime of these processes ranges from picoseconds to seconds. They are driven by free energy barriers of 1-30 kcal mol^{-1}. Most of the electron transfer processes taking place within reaction centre proceed with negative activation energies between room and cryogenic temperature[52].

Marcus electron transfer theory[53, 54] provides a quantitative description of these processes. According to this theory, the rate constant of an electron transfer reaction (k_{ET}) varies according to the formula:

$$k_{ET} = \frac{4\pi^2 H_{AB}^2}{h\sqrt{4\pi\lambda RT}} e^{\left[-(\Delta G^\circ+\lambda)^2/4\lambda R\,T\right]} \quad (1)$$

where h is Planck's constant, R is the gas constant and ΔG° is the standard free energy change of the electron transfer reaction. The electronic coupling factor (H_{AB}) depends on the magnitude of the overlap of the molecular orbitals of the electron donor and acceptor. Marcus defined λ as the reorganization energy factor. Introducing this term was one of the main contributions of Marcus theory. λ relates to the energy needed to rearrange the electron donor and acceptor as well as the surrounding "solvent" in order to produce an activated complex allowing electron transfer to proceed. For electron transfer reactions in polar solvents, the dominant contribution to reorganization energy arises from a reorientation of solvent molecules in response to the change in charge distribution of the reactants. Embedding reactants in a low dielectric medium (e. g. a membrane) can reduce the reorganization the energy, but the effect on electron transfer rate depends on the response of ΔG° to the non-polar environment[55].

The original idea of Marcus, which is clearly seen in the equation is that the rate constant of electron transfer is maximum when $\Delta G° = -\lambda$ and not at the highest possible values of $\Delta G°$. At low driving forces, rates increase with $-\Delta G°$, but as the driving force moves into the region where $-\Delta G° > \lambda$, electron transfer rate is predicted to decrease (inverted region).

It has been proposed[56] that in proteins, electron transfer proceeds at it's a maximum rate, i. e. with λ values close to $-\Delta G°$. In this case, rate constant for electron transfer reactions essentially depends on the edge to edge distance between the donor and the acceptor molecules. The main factor governing the electron rate is the electronic factor which was estimated to be 1.4 $Å^{-1}$.

The electron transfer theory of Marcus has been tested in reaction centres of *Rb. sphaeroides* where $\Delta G°$ was varied by substitutions of Q_A with quinones of different redox potential[57, 58]. Reasonably good fits of the rate constants according to the Marcus equation have been obtained with λ values ranging between 200 meV (primary reactions) and 1 eV (interquinone reactions).

In contrast to the majority of electron transfer and charge recombination reactions in the reaction cenrer, the electron transfer from Q_A^- to Q_B for *Rb. sphaeroides* is temperature dependent with activation energy of 560 meV[59].

The reorganization energy related to this electron transfer (λ) of about 0.8 eV[56] seems much larger than the free energy difference between $Q_A^-Q_B$ and $Q_AQ_B^-$. This might be explained by the presence of many polar residues in the Q_B binding site leading to the higher "solvent" reorganization factor compared to that for primary reactions.

We shall come back to this point later, and especially to the rate-limiting process that may slow the Q_A^- to Q_B electron transfer.

Scheme 1.6 presents the kinetic events described above. Typically a stabilized charge-separated state, $P^+Q_A^-$ is created across the membrane in about 200 ps.

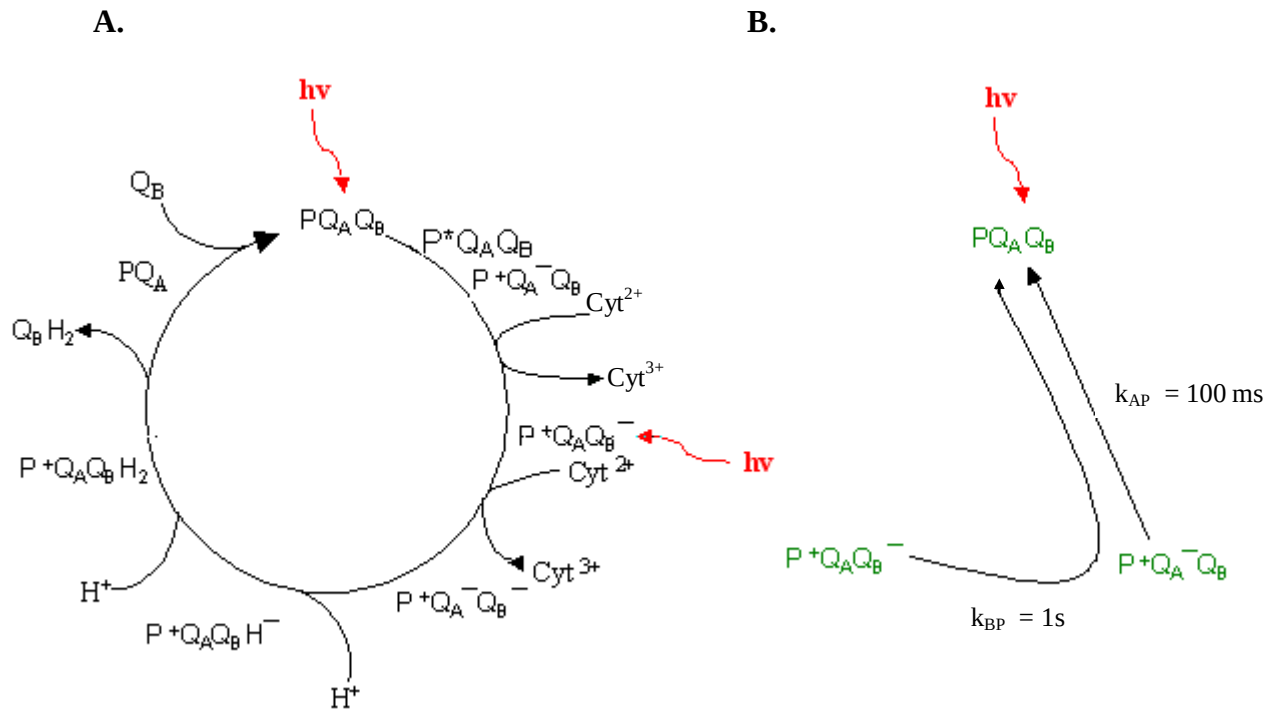

Scheme 1.6: (A) Scheme showing the charge separation process in bacterial RCs. Light absorption by P, the primary electron donor, results into the creation of P*, its first excited singlet state. An electron is transferred from P* to a first ubiquinone-10 electron acceptor (Q_A), generating the primary charge separated state $P^+Q_A^-$. The electron present on Q_A is then transferred to the secondary electron acceptor quinone Q_B generating the $P^+Q_B^-$ state. This leads after the absorption of two photons to the formation of the doubly reduced and doubly protonated secondary quinone molecule, Q_BH_2. (B) The electron can recombine from Q_B^- through Q_A to P^+ in 1s or from Q_A^- to P^+ in 100 ms.

The electron present on Q_A is then transferred to Q_B in 20-200 µs depending on the bacterial species. P^+ is reduced by a c2-type cytochrome in few µs. A second photochemical event activates the formation of Q_A^-, which finally leads to the double reduction and double protonation of the Q_B species to form the dihydroquinone molecule Q_BH_2.

Due to the competition for the binding site of Q_B, Q_BH_2 is displaced from its site and replaced by an oxidized quinone from the pool floating in the membrane. Q_BH_2 is reoxidised

at the level of the cytochrome b/c1 complex. Since the RC spans the membrane, the initial charge separation generates a transmembrane electric field.

In order to investigate the influence of the RC environment and in particular of the dipole potential on the Q_A^- to Q_B electron transfer process, we have studied the influence of phloretin, cholesterol, 6-ketocholestanol and 5-cholesten-3-β-ol-7-one on the kinetics of the first electron transfer.

Phloretin, cholesterol and its derivatives all have a capacity for changing the dipole potential value when included in a vesicle composed of phosphatidylcholine and thus are potentially able to electrically modify RC function.

1.7 The Na^+,K^+-ATPase

1.7.1 Introduction

The Na^+,K^+-ATPase **(Fig 1.7)** is central to all animal life. It transports three sodium ions from the cytoplasm to the outside of the cell and two potassium ions from the extracellular environment into the cytoplasm by using the free energy of ATP hydrolysis.

The enzyme thus allows cells to maintain a low intracellular Na^+ concentration and a high intracellular K^+ concentration, which (because the cell membrane is generally more permeable to K^+ ions than Na^+ ions) establishes a net negative electrical potential inside the cell. These transmembrane Na^+ and K^+ electrochemical potentials which the enzyme produces provide the driving force for such basic functions as nerve, muscle and kidney function[60].

The Na^+,K^+-ATPase also contributes to the osmotic regulation of the cell volume and is a major determinant of body temperature. For all of these functions the enzyme derives its energy from the hydrolysis of ATP.

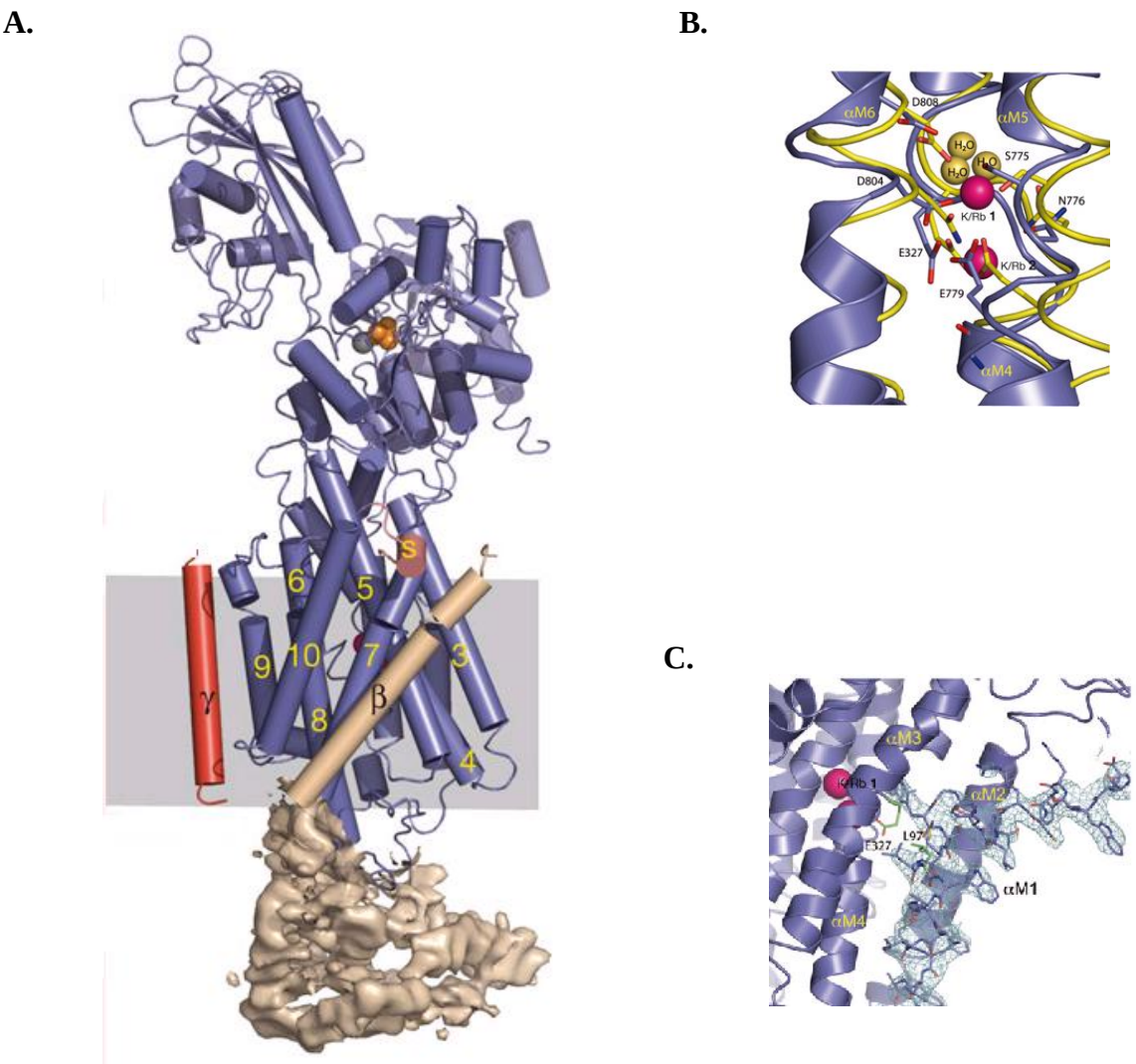

Figure 1.7: (**A)** The α-, β- and γ-subunits of the Na^+,K^+-ATPase are coloured blue, wheat and red, respectively. Helices are represented by cylinders and β-strands by arrows. The yellow numbers on the α-subunit indicate the position of the transmembrane segments starting with the most N-terminal. The C-terminal helix from α-subunit is indicated by a S (light red). $Mg^{2+}$and Rb^+ ions are orange and pink, respectively. **(B)** Magenta spheres represent the position of K^+/Rb^+ ions in Na^+,K^+-ATPase. Oxygen-containing side chains within and close to the coordination sphere are shown. **(C)** Interaction between Glu 327 and Leu 97. The figures are reproduced from Morth *et al.*[61].

The first identification of the Na^+,K^+-ATPase was made by Jens Christian Skou, who won the Nobel Prize in chemistry in 1997 for this discovery[62]. The pump is known[63, 64] to be involved in diseases such as diabetes, epilepsy, hypertension and congestive heart failure. More recently, it has been found[65] that a mutation in the Na^+,K^+-ATPase alpha subunit causes

familial hemiplegic migraine type 2. The understanding of this protein could thus have therapeutic implications.

The Na^+,K^+-ATPase is situated in the plasma membrane of the cell. Depending on cell type, there are between 800,000 and 30 million pumps[66] on the surface of a cell. Because the Na^+,K^+-ATPase transports ions against their electrochemical potential gradient this is an *active* transport process. This is in contrast to passive transport, where ions flow along an electrochemical potential gradient.

The Na^+,K^+-ATPase is a member of the P-type ATPase family, which refers to the formation of a phosphorylated intermediate, a phosphate covalently bound to an aspartate of the enzyme.

The phosphate is transferred to the enzyme from ATP. This requires the presence of magnesium ions which act as a cofactor[67]. Despite research based on metalloenzyme crystal structures, the detailed role the magnesium ion plays in ATP hydrolysis is still unclear. Catalysis is rationalized by complexing of the magnesium ion around the phosphoryl oxygens of ATP to stabilize a highly negatively charged transition state[68]. However, in aqueous solution, the hydrolysis of ATP follows a dissociative mechanism, where the bond to the leaving group (ADP) is largely broken before the bond to the incoming water forms to any extent [69].

The goal of the research on the Na^+,K^+-ATPase described in this thesis is to contribute to the elucidation of the role that protein-protein interactions play in the enzyme's mechanism and investigate the role of magnesium ions in the Na^+,K^+-ATPase's kinetics. This is a prerequisite for later investigations of the role of lipid-protein interactions, because it may well be so that the lipid environment of the protein modulates enzyme function via an indirect effect on the strength of protein-protein interactions.

1.7.2 The structure of Na^+-K^+-ATPase

The structure of Na^+,K^+-ATPase in one of its conformations **(Fig. 1.7 A)** was solved by Morth *et al.*[61] by X-ray crystallography in 2007. The enzyme is composed of three subunits: alpha, beta and gamma.

The alpha subunit[70] (~113 kD) binds ATP and both sodium and potassium ions, contains the phosphorylation site and is similar to single-subunit P-type ATPases like the Ca^{2+}-ATPase of sarcoplasmic reticulum. Several isoforms of both the alpha and the beta subunits have been identified which have different tissue distributions, and different kinetic and thermodynamic characteristics. The cytoplasmic domain of the alpha subunit is subdivided into three smaller domains: an N-domain containing the site where the ATP molecule binds, a P-domain containing the phosphorylation site and an A-domain involved in the conformational changes. A recent study [71] has found that a Tyr 771 might play a central role in Na^+ binding to the alpha subunit. Two Rb^+ (a K^+ congener) sites in the alpha subunit were identified[72] in the crystal structure **(Fig. 1.7 B)**. Glu 327 is associated exclusively with K^+/Rb^+ and may control the extracellular gate of the occlusion cavity, possibly guided by contact with Leu 97 **(Fig. 1.7 C)**. It has also been suggested that Phe 475 and Glu 446 on the alpha subunit cytoplasmic domain play important roles in the binding of ATP to the enzyme[73].

The beta subunit (~55 kDa) is composed of about 370 amino acids and the gamma subunit is the smallest of the three subunits (~7.1kDa).

Recently it has been suggested [74] that the dipole potential has an effect on the molecular activity of the enzyme by affecting the water structure on the extracellular surface. Furthermore, Morth *et al.*[61] suggested that the carboxy terminus of the alpha subunit is contained within a pocket between transmembrane helices and may be a regulatory element controlling sodium affinity, possibly influenced by the membrane potential.

1.7.3 Inhibition of the Na^+-K^+-ATPase by cardiac glycosides

The Na^+,K^+-ATPase is inhibited by cardiac glycosides such as ouabain. The chemical structure of ouabain is shown in **Fig. 1.8**. This steroid has been used as a heart medicine for centuries. It can be extracted from a plant called the foxglove (*Digitalis purpurea*). Cardiac glycosides have been widely used to increase the strength of contraction of the heart. Inhibition of sodium pump activity in cardiac myocytes results in an increase in intracellular sodium concentration. This leads to an increase in intracellular calcium because the sodium concentration gradient, which is the driving force for calcium extrusion from the cell is diminished. The increase in the calcium concentration, which is the signalling agent for muscle contraction, is thought to enhance muscle contractibility.

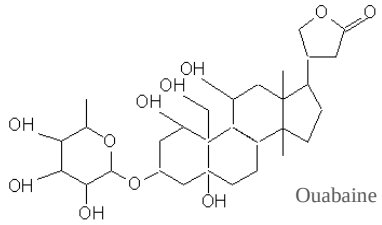

Figure 1.8: Chemical structure of ouabain, which is a natural inhibitor of the Na^+,K^+-ATPase.

The highest affinity of ouabain for the enzyme, with a K_D ~5 nM, occurs when the enzyme is in its E2P state. Three residues (Phe783, Thr797, and Asp804) of the enzyme located[75] on the alpha sub-unit appear indispensable to confer high affinity ouabain binding.

Different tissues containing the Na^+,K^+-ATPase can have different affinities for ouabain that can vary from 3 to 5 fold[76, 77]. For example, the brain hemisphere tissue has a dissociation constant of 0.040 µM for ouabain, whereas for brain stem the value is 0.082µM.

1.7.4 Albers-Post Cycle

The Albers-Post cycle **(Fig. 1.9)** is the most widely accepted model for describing the series of reactions constituting the Na^+,K^+-ATPase catalytic cycle. This mechanism describes the enzyme as a monomer undergoing a catalytic cycle of ion binding and release steps by using the free energy from the hydrolysis of an ATP molecule.

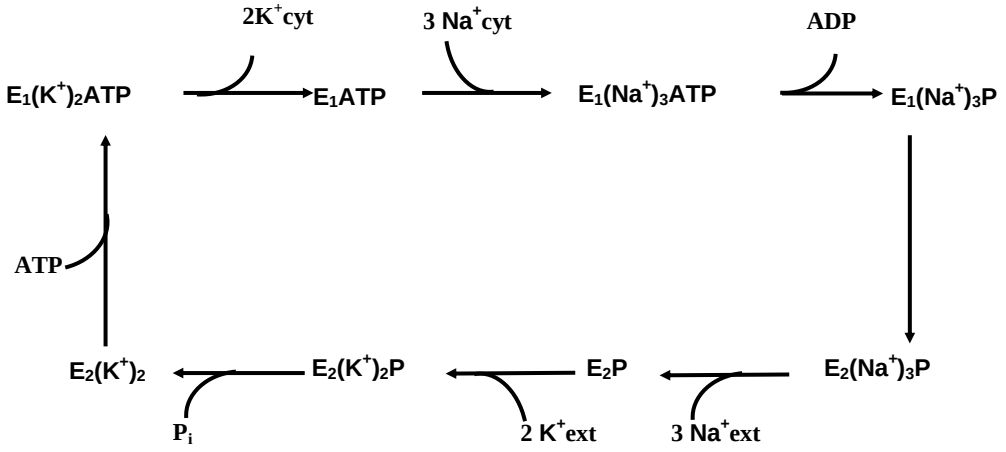

Figure 1.9: E_1/E_2 Albers-Post model of the Na^+-K^+-ATPase reaction cycle.

When radioactivity was measured after membrane fragments containing the enzyme were exposed to γ^{32}P-ATP, the existence of phosphorylated intermediates in the enzyme cycle were discovered in the presence of Na^+ and Mg^{2+}. Additionally, K^+ stimulated the release of the phosphate[78].

Albers *et al.*[79, 80] suggested the existence of two conformations of the phosphoenzyme, the initially formed compound, E_1P, and E_2P, formed subsequent to the phosphorylation reaction. The E_1 conformation has a high affinity towards Na^+ ions and ATP, and its cation-binding sites are in contact with the cytoplasm. E_2P, on the other hand, binds K^+ ions (or its congeners Rb^+ and Li^+) with a high affinity with the binding site facing the extracellular medium.

The reaction cycle of the enzyme proceeds as follow. Three intracellular Na^+ ions bind to the E_1 state of the enzyme, which has previously bound ATP. The aspartic acid residue (Asp 369) of the enzyme is phosphorylated. A change in the conformation from the state $E_1(Na^+)_3P$ to the state $E_2(Na^+)_3P$ reduces the Na^+ affinity and the previously occluded Na^+ ions are released to the extracellular medium, thus leading to the E_2P state. K^+ ions bind to this state from the extracellular medium. The binding of the K^+ ions stimulates the release of the phospho-group and leads to the formation of the state $E_2(K^+)_2$. The phosphorylated enzyme is relatively stable[79] and there is only a low rate of spontaneous dephosphorylation. ATP has an allosteric effect in this part of the enzyme cycle. When ATP binds to the $E_2(K^+)_2$ conformation of the enzyme, it stimulates the transition of E_2 to E_1 and accelerates the release of K^+ ions. The enzyme is then in the E_1 state , ready to bind Na^+ ions from the cytoplasm again and start a new cycle. The conformational change from $E_2(K^+)_2$ to $E_1(K^+)_2ATP$ is the rate limiting step[81] for the reaction cycle with a rate constant of approximately 30 s^{-1}, while the conformation change from $E_1(Na^+)_3P$ to $E_2(Na^+)_3P$[78] occurs with a rate constant of approximately of 300 s^{-1}.

However, there is a significant amount of experimental data which cannot be explained by the monomeric Albers-Post model. Recently, Clarke and Kane[82] investigated via the stopped-flow technique the kinetics of phosphorylation and subsequent conformational change of the Na^+,K^+-ATPase. The ATP concentration dependence of the time course and the amplitude of the kinetic traces they obtained could be explained by a dimeric model, in which the enzyme cycles at a low rate with ATP hydrolysis by one α-subunit or at a high rate with ATP hydrolysis by both α-subunits. Thus, they proposed a two-gear bicyclic model **(Fig. 1.10)** to replace the classical monomeric Albers-Post model for Na^+,K^+-ATPase. They suggested that the reason for the two different rate constants was an ATP-induced change in protein-protein interactions within the $(\alpha\beta)_2$ diprotomer.

The bicyclic dimer model of Na^+,K^+-ATPase function proposed provides an explanation for a longstanding paradox regarding ATP binding, i.e. equilibrium measurements of ATP binding have consistently revealed an ATP dissociation constant approximately 40 fold lower than that obtained from pre-steady-state kinetic studies based on enzyme phosphorylation. Within the framework of the dimer model both dissociation constants could be explained by a negative cooperative interaction between the two protein monomers, with ATP binding to one monomer inducing a decrease in the ATP affinity of the adjacent monomer.

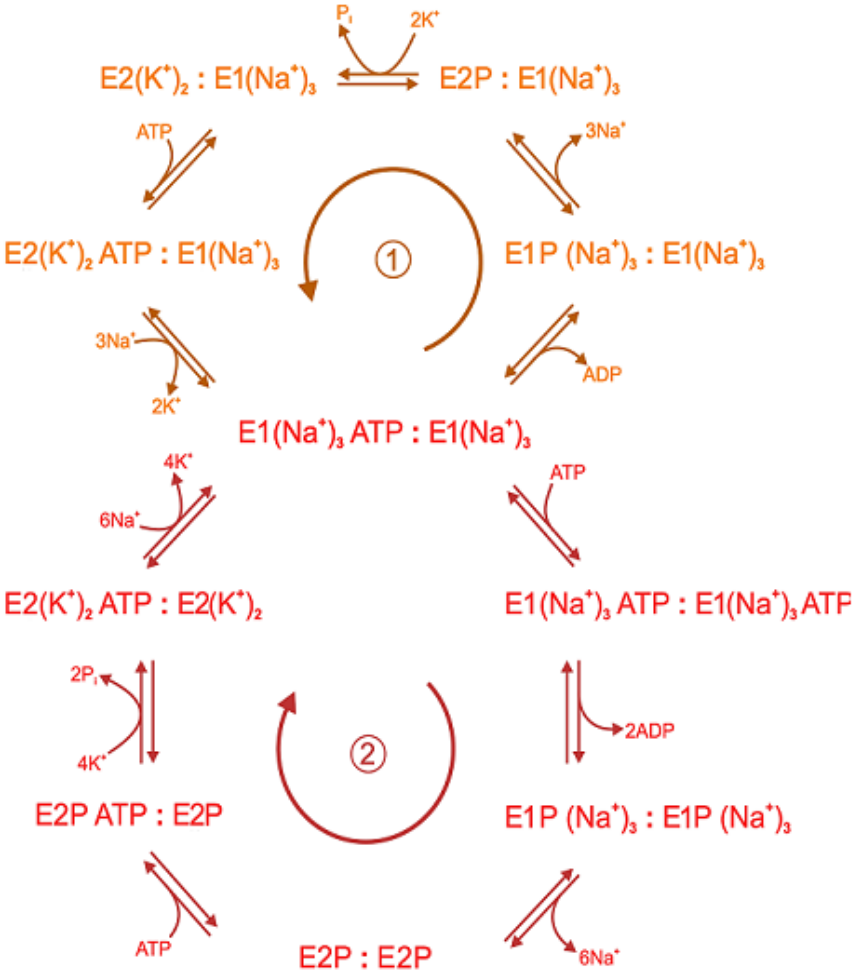

Figure 1.10: Two-gear dimeric model of sodium potassium pump function. The upper cycle (1) represents the low gear pathway followed at low concentrations of ATP when only one of the ATP sites on one of the monomers is occupied. The lower cycle (2) represents the high gear pathway followed at high concentrations of ATP, when both ATP binding sites of the dimer are occupied.

The thermodynamics of ATP binding to the Na^+,K^+-ATPase is, thus, a crucial aspect of the dimer model which must be investigated further in order to critically test the model's predictions. One of the purposes of this thesis is to improve the comprehension of the enzyme mechanism by shedding further light on the monomer/dimer question.

Chapter 2

Materials and Methods

2.1 Preparation of Photosynthetic Reaction Centres from *Rhodobacter Sphaeroides*

2.1.1 Methods of RC purification and reconstitution in liposomes

1. Growth of His-tagged Reaction Centres (RCs)

Rb. sphaeroides cells were grown semiaerobically on RM medium (see appendix for the RM medium composition) containing 30 μg ml^{-1} kanamycin to ensure the presence of the plasmid. Ten litres of culture were routinely used for one preparation of reaction centres. The culture was grown in the dark, at 34°C on a shaker and after one day the cells were harvested by centrifugation (30,000xg, for 30 min). The cell pellets were washed with sodium phosphate buffer (0.1 M, pH 7.5), spun down again and stored at - 70°C.

2. Preparation of isolated His-tagged Reaction Centres

The cell pellets (~30 g) were resuspended in 200 ml of 10 mM Tris-HCl, pH 8.0, 100 mM NaCl buffer with ~10 mg of DNAse I (Roche, France) and 200 μl $MgCl_2$ (1 M). Cells were then sonicated for 1 h 15 min ice to break the external cell membrane. The unbroken cells were removed by centrifugation (11,000xg, for 20 min at 20 °C) and the chromatophores were collected by centrifugation (200,000xg) at 5°C for 3 hours. The chromatophore membranes were solubilised by adding 1% (w/v) of the detergent LDAO (N, N-dimethyldodecylamine) drop by drop and stirred for 15 min at 30°C in the dark. Membranes were separated initially by centrifugation for 10 min at 4°C and 10,000xg

(Beckmann J 2-21, rotor JA20). After the first centrifugation the supernatant was taken and ultracentrifuged for 1 h 15 min at 5°C, at 120,000xg (Beckmann L8M, rotor Ti 50). The crude RC suspension was added to a HIS-select^{TM} Nickel affinity gel (Sigma, Germany) preequilibrated with 10 mM Tris-HCl, pH 8, 0.1% LDAO and 5mM Imidazole buffer. A 10 mM Tris-HCl, pH 8, 0.1% LDAO containing 40 mM imidazole buffer was used to elute RC bound to the column. The purity of the RC suspension was determined by UV-visible spectrophotometry by recording the absorbance ratio 800 nm/280 nm, which corresponds to the absorbance of the pigments (essentially BChls) at 800 nm and the absorbance of the protein at 280 nm. A ratio of 1.2 indicates an excellent purity of the protein. Ratios of ~ 1.3-1.5, with a good yield, *i.e.*, ~ 0.5 µmole of protein/30 g of cells, were routinely obtained.

3. Preparation of depleted ubiquinone Q_A Reaction Centres

To remove the primary ubiquinone Q_A, the method of Okamura *et al.*[83] modified by Sebban[84] was used. Reaction centres were mixed with an equal volume of DEAE-Sepharose CL-6b (equilibrated with 10 mM Tris-HCl and 0.05% LDAO, pH 8.0) and poured onto a glass column (bed volume 15 ml, diameter 3 cm). The column was then washed with 150 ml of depletion buffer (10 mM Tris-HCl, 3.5% LDAO, 10 mM o-phenanthroline and 1mM dithiotreitol, pH 8.0) at 28 ºC and in the dark. After this, 200 ml of 10 mM Tris-HCl and 0.05% LDAO, pH 8 was passed through the column at 4 °C. Depleted reaction centres were eluted by 10 mM Tris-HCl, 0.05% LDAO and 200 mM NaCl, pH 8. About 85 % of the reaction centres were depleted of ubiquinone as judged from the disappearance of the amplitude of P^+ signal after a flash.

Restoration of the Q_A activity was achieved by adding ~ 80 µM of anthraquinone or 1-amino-5-chloro-anthraquinone (dissolved in dimethylsulfoxide or in ethanol, respectively) to the suspension of reaction centres. The almost complete reconstitution by anthraquinones

was estimated from the reappearance of absorbance changes associated with the formation of $P^+Q^-_A$ after a flash.

4. Reconstitution of purified reaction centres into phosphatidylcholine liposomes containing cholesterol and derivatives

50 mg of PC from egg yolk (Sigma, Germany) was mixed with 20 mol% of cholesterol, 6-ketocholestanol, phloretin or 5-cholesten-3-β-ol-7-one (Sigma, Germany) in chloroform. The lipid/cholesterol (or its derivatives) solution was dried using a rotary evaporator (BÜCHI R-114) leaving a lipid film on the wall of the flask. The ethanolic lipid solution was maintained on ice and under N_2 to minimize lipid oxidation. The lipid film was then re-hydrated in a 10 mM Tris-HCl, pH 8, 100 mM NaCl and 0.1 mM EDTA buffer to obtain a 50 mg/ml final lipid concentration. The lipid suspension was shaken for few minutes to form multilamellar vesicles. The mixture was sonicated for 25 mins using a titanium micro tip (Dr. Hielscher GmbH, model UP 200 S). The transition from a white cloudy solution to a more transparent one was indicative of a decrease in the ratio multilamellar/bilayer vesicles in the solution. The solution was centrifuged at 40,000xg (Beckmann L8M, rotor Ti 50) at 4°C for 2 h to pellet the remaining multilamellar vesicles and titanium from the probe. Finally, a 60 µM RC suspension was mixed with the liposomes drop by drop, using a vortex for a good mixing. A lipid/protein ratio of 3 was used when cholesterol or phloretin were present and a ratio of 4 for the other cholesterol derivatives. A 20 mol% ratio of phloretin, cholesterol and its derivatives /lipid was used for all the experiments carried out on RC. An attempt was made to use 30 mol% of phloretin, cholesterol and its derivatives but this was unsuccessful, as the proteins could not be inserted into the vesicles. The result was a biphasic suspension of RC and the liposomes even after mixing.

2.1.2. Flash photolysis

1. Steady state absorption

The absorption spectra of RCs were recorded on a Beckman (DU-800) spectrometer. The concentration of the RCs was determined from the absorbance at 800 nm using a molar absorption coefficient, ε_{800} = 288 l.mmol^{-1}.cm^{-1} as determined for *Rb. sphaeroides* RC[85].

The absorption spectrum of the RC from *Rhodobacter sphaeroides* is presented in **Fig. 2.1**. In the near-infrared region, three absorption bands at 860, 800 and 760 nm correspond essentially to the BChls l dimer, the bacteriochlorophyll monomers, and bacteriopheophytin, respectively. Bands at 600 nm and 540 nm belong to the monomeric bacteriochlorophylls and bacteriopheophytins, respectively. The light-induced oxidation of the BCls dimer (P) leads to the bleaching of the band at 860 nm.

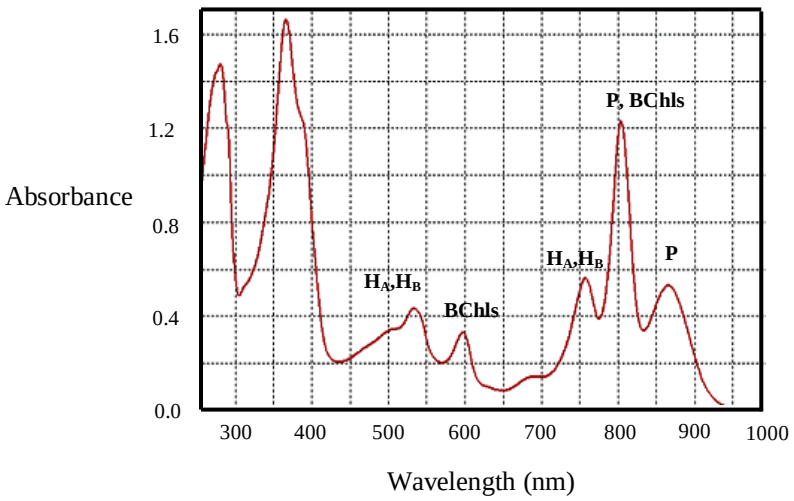

Figure 2.1: The steady state absorbance spectrum of purified reaction centre of *Rhodobacter sphaeroides*. The photooxidation of P is indicated by a bleaching at 860 nm. Conditions: 10 mM Tris-HCl, 0.05 % LDAO, pH 8.0.

The absorbance changes obey the Beer-Lambert equation (equation 1):

$$\mathrm{Log}_{10}\,(I_t/I_0) = \varepsilon Cl \qquad (1)$$

where I_0 is the intensity of the incident light, I_t is the transmitted light intensity, ε is the extinction coefficient, l is the pathlength of the cuvette, and C is the RC concentration.

2. Kinetic absorption spectroscopy

The kinetics of absorption changes were determined using a single beam spectrophotometer of local design[86] shown **Fig. 2.2**. The amplified output signal was digitalized via an acquisition card. Light flashes were provided by a pulsed YAG laser (Spectra Physics, USA) (200 mJ per pulse at 532 nm, 5 ns flash duration). The source of monitoring beam was a tungsten lamp (250 W). Wavelength selection was performed by a Jobin-Yvon H25 monochromator. Signals were detected by a photomultiplier tube (S20 photocatode, Hamamatsu, Japan). A Labview homemade program using a card was used to trigger measurements, accumulate signals and analyse the kinetic traces. The time resolution (few µs) was limited by the recovery time of the electronics (photomultiplier and amplifier).

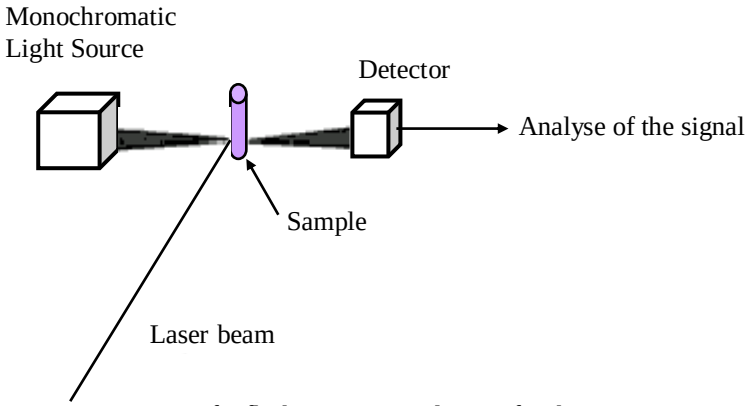

Scheme 2.2: Schematic representation of a flash experimental setup for the measurement of charge separation in an electron transfer process.

Fitting of the decay kinetics by multiexponential decomposition was performed using a Marquardt non-linear least-square algorithm. The kinetics were decomposed into a sum of first order exponential decays (equation 2):

$$\Delta A(t) = A_1 \exp(-t/\tau_1) + A_2 \exp(-t/\tau_2) + A_3 \exp(-t/\tau_3) \qquad (2)$$

where τ_i represents the lifetime of the absorption decay of component *i* and A_i its initial amplitude.

3. Charge recombination rate

1. *In vitro*, and in the absence of an exogenous donor, after a flash, the $P^+Q_B^-$ state decays to the ground state PQ_B by charge recombination. In the case of WT, this reaction proceeds predominantly via the intermediate state $P^+Q_A^-Q_B$ **(Scheme 1.6)** and is thermally activated[87, 88].

2. The rate constant of k_{BP} representing the rate of reaction between P and Q_B may be described as (equation 3):

$$k_{BP} = k_{AP}.e^{-\Delta G‡/kT} + k \text{ direct} \qquad (3)$$

where, k_{AP} is the rate constant of charge recombination from the $P^+Q_A^-$ state. ΔG°_{AB} represents the free energy barrier between the $P^+Q_B^-$ and $P^+Q_A^-$ states and k_{direct} is the rate constant of direct charge recombination from the $P^+Q_B^-$ state to the ground state. Therefore, k_{BP} depends on the free energy barrier between $P^+Q_A^-$ and $P^+Q_B^-$ and is sensitive to any variation of the free energy level of Q_B^- due to for example electrostatic interactions with nearby amino acid residues. In contrast to charge recombination from the $P^+Q_B^-$ state, the $P^+Q_A^-$ charge recombination proceeds directly to the ground state via an electron tunnelling mechanism. The activation energy of this process is negative, the rate constant increasing slightly with decreasing temperature.

The charge recombination rates were determined from the absorbance changes of the bacteriochlorophyll dimer at 430 nm (26 $mM^{-1}.cm^{-1}$ at 430nm). For the reaction centre of *Rb. sphaeroides* at neutral pH, the $P^+Q_A^-$ and $P^+Q_B^-$ charge recombination rates are about 10 s^{-1}

and about 1 s^{-1}, respectively. UQ-6 was routinely added to the assay solution because Q_B was lost during the isolation of the reaction centres. When needed the occupation of the Q_B site was increased by addition of UQ-6.

4. Measurements of the $Q_A^- \rightarrow Q_B$ first electron transfer rate

The measurement of the rate of the first electron transfer (ET) $Q_A^-Q_B \rightarrow Q_AQ_B^-$ (k_{AB} (1)) can be performed at different wavelengths. In the visible part of the spectra, the absorbance changes are dominated by the P^+-P spectrum. The absorption changes for the reduction of Q_A and Q_B are quite similar and are very close to that obtained for ubisemiquinone in alcoholic solution. Hence, there is no primary optical marker to easily distinguish between the different semiquinone states of Q_A^- and Q_B^-. In contrast, larger absorption changes can be detected at around 750 nm, where the formation of Q_A^- and Q_B^- induces electrochromic shifts in the bacteriochlorophyll and the bacteriopheophytin absorbance bands. In addition, 750 nm is an isosbestic wavelength for the $P \rightarrow P^+$ absorbance changes. In this region, the most prominent changes produced by the formation of Q_A^- are the red shift of the absorption band of the bacteriopheophytin and the blue shift of bacteriochlorophyll dimer. The magnitudes of the bacteriochlorophyll and bacteriopheophytin shifts caused by Q_B^- are smaller than those caused by Q_A^-. The ET process can therefore be followed at 750nm.

The Eyring expression[89] was used for the analysis of the temperature dependence of the first ET kinetic rates (k_{AB}) and is given by equation 4, which relates the reaction rate to the temperature:

$$k_{AB} = (k_B T / h) \exp [(\Delta S^{\ddagger} / R) - (\Delta H^{\ddagger} / RT)] \qquad (4)$$

where $\Delta H^{\ddagger}$ is the activation enthalpy of the reaction, $\Delta S^{\ddagger}$ is the activation entropy of the reaction, k_B is Boltzmann's constant, T is the absolute temperature, R is the gas constant and h is Planck's constant.

A plot of ln (k_B/T) versus 1000/T gives a straight line with a slope of $-\Delta H/RT$, from which the activation enthalpy can be derived, and with an intercept of $\ln(k_B/h) + \Delta S/R$, from which the activation entropy can be derived. Therefore, $\Delta G^{\ddagger}$, the free activation energy of the reaction can be derived from the thermodynamic equation (equation 5):

$$\Delta G^{\ddagger} = \Delta H^{\ddagger} - T\Delta S^{\ddagger} \qquad (5)$$

2.1.3. Transmission electron microscopy of proteoliposomes

Transmission electron microscopy (TEM) observations were performed with a JEOL JEM 100CXII transmission electron microscope at an accelerating voltage of 100 kV. Drops of the solutions of RC at 20ºC in a 10 mM Tris-HCl, pH 8, 0.1% LDAO, 40 mM imidazole buffer, were deposited on carbon-coated copper grids (and dried under N_2 flow).

2.2 Preparation and analysis methods of Na^+,K^+-ATPase

2.2.1 Purification of Na^+,K^+-ATPase and reconstitution of Na^+,K^+-ATPase in liposomes

1. Preparation of membrane fragments containing Na^+,K^+-ATPase from rabbit kidneys

Rabbit kidneys were stored at -70°C in 250 mM sucrose, 30 mM L-histidine, 30 mM imidazole and 5 mM EDTA pH 7.5 (buffer S) and defrosted the day before the preparation. The cortex and inner medulla were removed to keep the outer medulla containing the

enzyme. The dissected tissue was placed in a 30 ml mortar tissue grinder (Crown Scientific, Australia) with an adequate supply of buffer (~60 mg of tissue to 20 ml of buffer S) and placed on ice. After homogenisation for 1 min, the lysate was centrifuged for 20 mins at 20,000xg, at 4°C (Beckmann/Sorvall J 2-21, SS34 rotor). The supernatant was kept aside and the pellet was re-homogenised with the same volume of buffer S as for the first dissected tissue and re-centrifuged for 15 mins at 20,000xg (Beckman/Sorvall J 2-21, SS34 rotor), at 4°C. Finally the first and the second supernatants were mixed and centrifuged at 90,000xg for 30 mins at 4°C (Beckmann L8M, rotor Ti 50). The pellets of the microsomes obtained were re-suspended in 1 ml of buffer S and homogenised in a 2 ml mortar tissue grinder (Crown Scientific, Australia) for 1 min. They were transferred to cryotubes and frozen in liquid nitrogen.

On the following day, a 5.4 mg/ml stock solution of SDS was prepared and diluted in 50 mM imidazole, 2 mM EDTA and 0.0364 g/20 ml Na_2ATP pH 7.5 (buffer B). The SDS was added to the microsome preparation to obtain a final concentration of 0.54 mg/ml. The microsome suspension was defrosted and incubated at 26°C for 30 min with SDS. Six tubes were placed on ice and filled with 11ml of a 24% (w/v) sucrose solution. After 10 min, 7 ml of a 15% sucrose solution were added on top of the first 11 ml of 24% sucrose and finally, after a further 15 min, 4 ml of a 10% sucrose solution were added. The final microsome suspension was loaded on the top of the sucrose gradient and centrifuged overnight at 40,000xg at 4°C (Beckmann/Sorvall J 2-21, SS34 rotor). A small fraction of the pellet was kept for an activity test based on the assay procedure of Schwartz *et al* [90] and to measure the protein concentration using the DC Protein Assay (Bio-Rad, USA). The rest of the pellet was resuspended in a 4% sucrose solution dissolved in buffer S and frozen in liquid nitrogen.

2. Reconstitution of purified Na^+,K^+-ATPase into phosphatidylcholine liposomes containing cholesterol and derivatives

Enzyme preparation

The reconstitution of Na^+,K^+-ATPase was based on a method described by Cornelius[91]. Liposomes with different lipid compositions and incorporating Na^+,K^+-ATPase were prepared by co-solubilisation of lipids, protein and detergent in a weight-ratio of 10: 1: 12.5. Initially, 2 mg/ml of pure non-ionic detergent $C_{12}E_8$ was solubilised in 1.5 ml of membrane-bound Na^+,K^+-ATPase (0.5 mg/ml) at room temperature. After 1 h centrifugation at 40,000xg at 10°C (Beckman/Sorvall J 2-21, SS34 rotor), the solubilised enzyme was collected from the supernatant.

Proteoliposome preparation

25 mg of solid phosphatidylcholine from egg yolk (Roche, Australia) mixed with 20 to 50 mol% of cholesterol or its derivatives (coprostanol, 6-ketocholestanol, 5-cholesten-3β-ol-7-one and 4-cholesten-3-one (Sigma, Australia)) were solubilised in 2 ml of pure chloroform and were dried using a rotary evaporator. Then 1000 µl (10 mg/mls) of $C_{12}E_8$ (Sigma, Australia) in 130 mM NaCl, 30 mM imidazole pH 7.4 buffer was added to the lipids and the resulting suspension was sonicated for 20 mins.

The Na^+,K^+-ATPase-detergent solution was mixed with the lipid-detergent solution and kept on ice for 10 min. Liposomes containing reconstituted Na^+,K^+-ATPase spontaneously formed when $C_{12}E_8$ was removed by the addition of 200 mg/ml of biobeads (BioRad, USA) and the mixture was incubated for 12 h at 4°C. The biobeads were removed by centrifugation at 4,000xg for 10 min at 4°C (Beckman/Coulter L-100XP, SS34 rotor).

2.2.2 Calorimetry

1. Isothermal Titration Calorimetry(ITC)

General aspects of ITC

Any reaction which generates or absorbs heat can be directly studied by calorimetry. ITC **(Fig. 2.3)** is a useful technique to study both protein-ligand and protein-protein interactions. It is the only technique that determines directly the thermodynamic parameters of molecular interaction of a given reaction, ΔG, ΔH, and ΔS, in a single experiment. The ITC instrument is a heat-flux calorimeter operating according to the dynamic power compensation principle that measures the amount of power required to maintain zero temperature difference between the sample and the reference cell.

Two identical coin-shaped cells, sample and reference, are enclosed in an adiabatic shield **(Fig. 2.3)**. The temperature difference between the reference cell and the shield is continuously monitored to maintain a constant temperature. A feedback control system monitors the difference in temperature between the two cells through a semi-conductor between them. The temperature difference is kept constant and as close to zero as possible at any point in time. The feedback signal is the measured signal. One reagent is placed in the sample cell and the other is placed in the injection syringe. The reference cell serves only as a temperature reference. ITC uses stepwise injections of one reagent into the calorimetric cell containing the second reagent to measure the heat of the reaction for both exothermic and endothermic processes.

Here the multiple injection method was used to measure the change in instrument thermal power supplied to the reaction cell after mixing the two reagents. Each addition of the reagent contained in the syringe into the sample cell gives rise to a spike in the instrument power due to the formation of a complex accompanied by the release or absorption of heat. The heat released or absorbed upon their interaction is monitored over time.

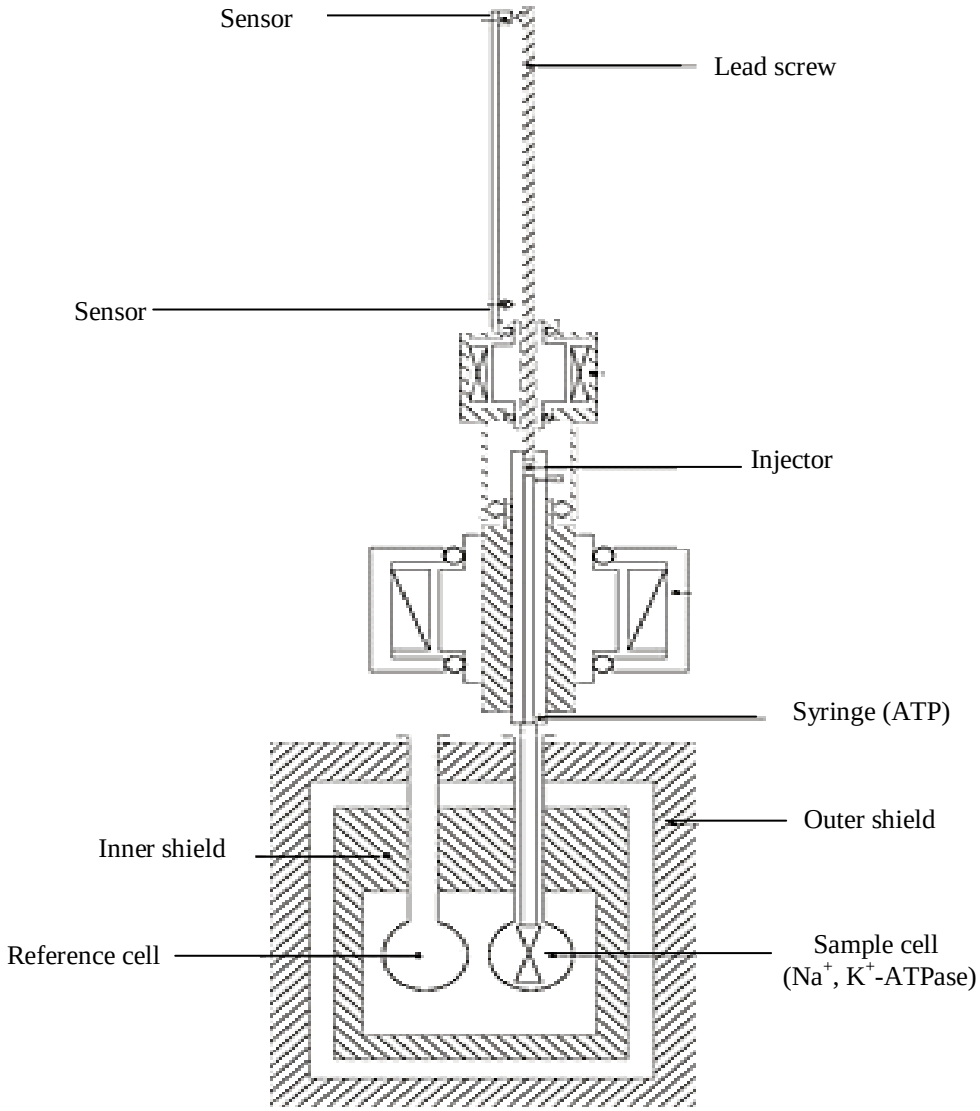

Figure 2.3: Schematic diagram of an ITC instrument. Two lollipop-shaped cells are contained within an adiabatic jacket. A small continuous power is applied by the heater on the reference cell. Thermocouple detectors sense temperature differences between the reference and sample cells. On interaction of ligand and macromolecule, heat is either taken up or evolved. Depending on the nature of the association, the feedback circuit will either increase or decrease power to the sample cell to maintain equal temperature with the reference cell. The heat per unit time supplied to the sample cell is the observable signal in an ITC experiment and a direct measure of the heat evolved on binding of a ligand to a macromolecule.

Then, the feedback system either lowers or raises the thermal power applied to compensate for the temperature unbalance. After each injection the system reaches equilibrium and the temperature balance is restored.

For an exothermic reaction, the temperature in the sample cell will increase, and the feedback power will be deactivated to maintain equal temperatures between the two cells.

For endothermic reactions, the reverse will occur, meaning the feedback circuit will increase power to the sample cell to maintain the temperature. The heat absorbed or evolved during a calorimetric titration is proportional to the fraction of bound ligand.

For the initial injections, all or most of the added ligand binds to the macromolecule, resulting in large endothermic or exothermic signals depending on the nature of the association. As the ligand concentration increases, the macromolecule becomes saturated and subsequently less heat is evolved or absorbed on further addition of titrant.

A parameter, *c,* was defined to relate the binding affinity and experimental conditions required to allow data analysis to be performed (equation 6):

$$c = [P] / K_d \qquad (6)$$

where P is the protein concentration and K_d the dissociation constant.

The value of *c* must be < 1000 to determine the K_d by ITC, which in practice, sets an upper limit of 10^{-9}-10^{-10} M on the measurable dissociation constant. When the protein concentration is too high or the K_d is too small, i.e. for values of c beyond 1000, ITC curves lose their characteristic sigmoid shape and instead resemble a step function. Under these conditions only a lower limit to the value of the dissociation constant can be estimated.

Binding enthalpy and heat capacity

The quantity of heat (q_n) absorbed or released in the injection n is equal to:

$$q_n = \nu \, \Delta H \, \Delta[L_{n,bound}] \qquad (7)$$

where v is the volume of the reaction cell, $\Delta L_{n,\,bound}$ is the change in concentration of bound ligand after the nth injection and ΔH is the enthalpy change of the reaction. So q_n is proportional to the amount of ligand that binds the protein.

Initial considerations and samples preparation

The concentrations of macromolecule and ligand are critical, especially when one partner of a complex is difficult to obtain in large quantities. Thus, for the measurement of the association constant, suitable initial concentrations of both the ligand and the macromolecule were determined by carrying out simulations using the ITC200 software. Both the titrant and macromolecule were dialyzed for 42 hours in buffer to minimize artifacts arising from mismatched buffer components. The final dialysis buffer was saved and used for any necessary concentration adjustments of the macromolecule or titrant solutions.

Loading the sample and reference cells and the injection syringe

Typically, 300 µl of the solution is prepared to fill a cell with a volume of 205 µl. The utmost care is required to fill the sample cell without introducing air bubbles. Great care must also be taken to avoid bending of the needle while the injection syringe is loaded into place. Bending of the injection syringe needle can result in some of the titrant solution being expelled into the macromolecule solution, causing the first injection to be unusable. Any minor bending in the syringe can also result in high noise levels.

Experimental conditions

ITC experiments were carried out on Microcal VP-ITC and ITC 200 isothermal titration calorimeters at 24 °C. 2 mls of purified Na^+,K^+-ATPase were prepared by 12 hours dialysis at 4°C in 1 litre of a buffer containing 30 mM imidazole, 130 mM NaCl and 5 mM ouabain pH 7.4. A volume of 1 ml of the same dialysed buffer was used to make a 2 mM ATP solution to avoid possible heat changes due to the interaction between the buffer components during mixing. The ATP solution was readjusted to pH 7.4 with NaOH. The samples were titrated by 25-30 sequential injections of 1 µl of a solution of 1 mM ATP into a ~13 µM Na^+, K^+-ATPase sample (after dialysis). Control experiments were performed, in which Na^+, K^+-ATPase was omitted. ITC titrations of CDTA, EDTA and ATP with injections of $MgCl_2$ solution were also performed with a stirring speed of 1300 rpm and a reference power of 0.5 µcal.s^{-1}.

Data analysis

Baseline selection is an important factor in ITC data analysis and for the results presented in this thesis the baseline was adjusted manually. Each peak was integrated automatically by routines provided in the software package. Normalized and baseline corrected data were fitted by the single binding site model using the analysis software ORIGIN (Microcal 200 Software, USA) provided with the ITC200. The association constant was used to determine the free energy of binding. The entropy of binding at 25°C was determined from the free energy and enthalpy of binding.

2.2.3 Stopped-flow

The stopped flow instrument uses compressed air or nitrogen to rapidly fire two solutions contained in separated drive syringes together into a mixing device. The solution

flows into the observation cell replacing the previous contents with freshly mixed reactants. A stopping syringe serves to abruptly stop the flow of the solution and trigger data collection. The fresh reactant in the optical cell is illuminated by a light source and the change in fluorescence can be measured as a function of time **(Fig. 2.4)**.

Stopped-flow experiments were carried out using a SF-61 stopped flow spectrofluorimeter from Hi-Tech Scientific (England). The two solutions equilibrated in the drive syringes at 24°C were prepared in the same buffer, so that no buffer concentration change occurred during mixing. 1 litre of buffer containing 130 mM of NaCl and 30 mM imidazole, adjusted to pH 7.4 was prepared.

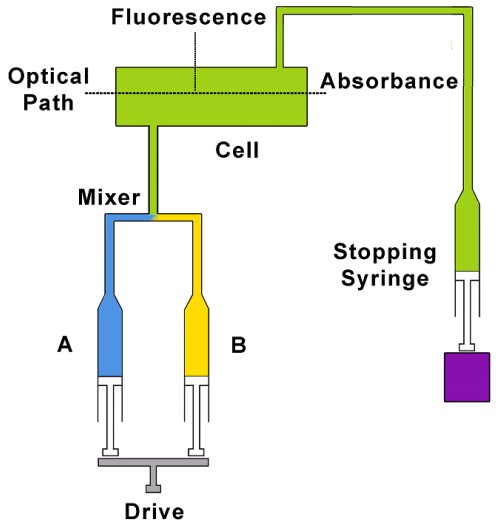

Figure 2.4: Schematic diagram of a stopped-flow instrument

The solution was split into two equal volumes of 500 ml each and in one of them 5 mM of $MgCl_2$ was added. From these two solutions a range of concentrations from 0.0004 mM to 5 mM of $MgCl_2$ were prepared. A measurement was made for each concentration of $MgCl_2$. One of the syringes contained 5 ml of 20 nM Na^+,K^+-ATPase prepared in buffer

containing the respective $MgCl_2$ concentration and labelled with 160 nM RH421 before mixing. The second syringe contained an equal volume of buffer at the same $MgCl_2$ concentration together with 2 mM of ATP.

The solution in the observation cell was excited with a 100 W short-arc mercury lamp (Osram, Germany), and the fluorescence was detected at right angles to the incident light beam with an R928 multialkali side-on photomultiplier. The exciting light was passed through a grating monochromator with a blaze wavelength of 500 nm. The mercury line at 577nm was used for excitation, and the fluorescence of RH421 was collected at wavelengths ≥665nm using an RG665 filter (Schott, Germany) placed in front of the photomultiplier. The kinetic data were collected and analysed using software developed by Hi-Tech Scientific. To increase the signal to noise ratio, 10-40 experimental traces were averaged. Non-linear fits with one or two exponential equations of the experimental traces were performed using a program from Hi-Tech (England).

2.2.4 Enzyme activity assay

Enzyme activity measurements were performed at 340 nm on a Shimadzu UV-2450 UV-visible spectrophotometer using a coupled enzyme assay[90]. The activity of Na^+,K^+-ATPase is linked to the oxidation of nicotinamide adenine dinucleotide (NADH) by the inclusion of the enzymes pyruvate kinase and lactate dehydrogenase in the reaction mixture. The reaction sequence is as follows:

$$\text{ATP} \xrightarrow{Na^+,K^+\text{-ATPase}} \text{ADP} + \text{Pi}$$

$$\text{PEP} + \text{ADP} \xrightarrow{\text{pyruvate kinase}} \text{pyruvate} + \text{ATP}$$

$$\text{Pyruvate} + \text{NADH} \xrightarrow{\text{lactate dehydrogenase}} \text{lactate} + \text{NAD}^+$$

The Na^+, K^+-ATPase activity can be easily determined by continuously monitoring the oxidation of NADH, via the drop in its absorbance at 340 nm. At the beginning of the measurement the reference and the sample cuvette contained 250 µl of 5 mM $MgCl_2$, 25 mM Tris-HCl and 2.5 mM phosphoenolpyruvate pH 7.4 (buffer A). The cuvettes were completed with 2.5 mM Tris-ATP, 130 mM NaCl (for the measurement of the Na^+, K^+-ATPase activity in presence of perchlorate, Chapter 7, NaCl was replaced by sodium perchlorate from 10 mM to 100 mM), 10 mM KCl and 0.02 ml of a combined pyruvate kinase-lactate dehydrogenase suspension (Sigma, Australia). After starting a time scan of the spectrophotometer the reduced NADH was added to the sample cuvette to give a minimum absorbance of 2. The absorbance was then recorded for about 1min to obtain a zero activity line. The reaction was then started by the addition of 20 µl of ~30 µM Na^+,K^+-ATPase, which leads to a decay in the absorbance. 100 µl of 5 mM ouabain solution was added after 5 min to stop the reaction. The enzyme activity was calculated from the slope of the decreasing absorbance after the enzyme sample was added. The calculation of the specific activity (SA) of the Na^+,K^+-ATPase (in µmolPi/mg/h) took into account the protein concentration given by the DC Protein Assay (Biorad) and was determined by the equation 8:

$$SA = \frac{-dA}{dt} \times \frac{V \times 10^6}{\varepsilon_{NADH} \times l \times m_{protein}} \qquad (8)$$

where dA/dt is the absorbance decrease in function of the time (hr^{-1}), V is the volume of the suspension in the cuvette, ε_{NADH} the extinction coefficient of NADH, l is the cell pathlength (1 cm) and $m_{protein}$ is the quantity of protein added to the preparation (mg).

2.2.5 Fluorescence measurements

Fluorescence measurements were performed on a Shimadzu RF-5301 PC spectrofluorophotometer. Quartz semimicro cuvettes (Starna Pty Ltd, Australia) were used for all measurements and the temperature was maintained at 24°C using a constant temperature circulating water bath. All emission spectra were recorded over a range of excitation wavelengths in order to confirm the wavelength of maximum fluorescence emission. Solutions of proteoliposomes or membrane fragments containing Na^+, K^+-ATPase and the dye di-8-ANEPPS **(Fig. 2.5)** were mixed by vortexing for a few seconds and the preparations were left overnight to allow the dye to be incorporated into the membrane.

The orientational polarizability was calculated from equation (9)[12] using the Stokes shift:

$$\Delta f = \frac{\text{Stokes shift } (cm^{-1}) - 207\ (\pm 542)}{19503\ (\pm 2000)} \qquad (9)$$

where the Stokes shift is the difference, in wavelength between the positions of the band maxima of the absorption and fluorescence emission spectra of the same electronic transition. Upon excitation di-8-ANEPPS undergoes a large electronic redistribution with the positive charge generally located on the pyridinium nitrogen in the ground state moving towards the amino nitrogen in the excited state[92].

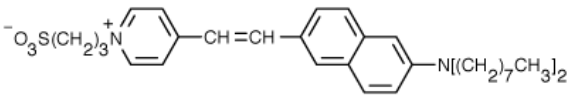

Figure 2. 5: Structure of di-8-ANEPPS

After excitation lipid dipoles surrounding the dye undergo a reorientation in response to the excited electronic configuration of the dye. This lowers the energy of the dye's excited state

and increases the Stokes shift, the magnitudes of which depend on the orientational polarizability of the lipid surrounding[93].

The maximum absorbance wavelength and the corresponding maximum fluorescence emission wavelength of di-8-ANEPPS were measured on proteoliposomes containing Na^+, K^+-ATPase and cholesterol derivatives. The effect of sodium perchlorate (from 10-100 mM) on the orientational polarizability was studied by replacing NaCl with sodium perchlorate in the buffer. A control experiment was carried out without sodium perchlorate and in presence of 130 mM of NaCl. A stock solution of dye was prepared in ethanol to obtain a final concentration of 1 mM. The effect of the small volume of ethanol added to the preparations on the fluorescence spectra was found to be negligible[6].

For fluorescence anisotropy measurements **(Scheme 2.6)** polarizers (Shimadzu, Japan) were used in front of the excitation and emission monochromators. The extent of polarization of the emission is described in terms of the anisotropy (R). The origin of the fluorescence anisotropy is the preferential absorption of polarized light by fluorophores which have their absorption transition moments oriented along the electric vector of the incident light. Hence, the excited state population is not randomly oriented. Initially there is a larger number of excited molecules having their transition moments oriented along the electric vector of the polarized exciting light. Hence, the fluorescence emission is also polarized. However, if a fluorophore can undergo rotational motion while in its excited state, this decreases the degree of polarisation of the fluorescence (i.e. the fluorescence anisotropy decreases). In the case of a binding event, the fluorescent dye will have less motion when bound to the enzyme. As a result, the decrease in mobility of the fluorescent dye will lead to an increase in fluorescence anisotropy. The intensity of emission is then measured through a polarizer. The fluorescence intensity is called I_{hv} for horizontally polarized excitation and vertically polarized emission, I_{vh} for vertically polarized excitation and horizontally polarized

emission, I_{vv} for vertically polarized excitation and vertically polarized emission and I_{hh} for horizontally polarized excitation and horizontally polarized emission.

The anisotropy is given by equation (10):

$$R = \frac{I_{vv} - GI_{vh}}{I_{vv} - 2GI_{vh}} \qquad (10)$$

The G-factor is the ratio of the sensitivities of the detection system for vertically and horizontally polarized light and is given by equation (11):

$$G = \frac{I_{hv}}{I_{hh}} \qquad (11)$$

In these experiments, a fluorescent dye di-8-ANEPPS 5 µM was mixed with a constant 1.3 µM concentration of a Na^+, K^+-ATPase membrane fragments solution. Control experiments were performed in which Na^+, K^+-ATPase was omitted.

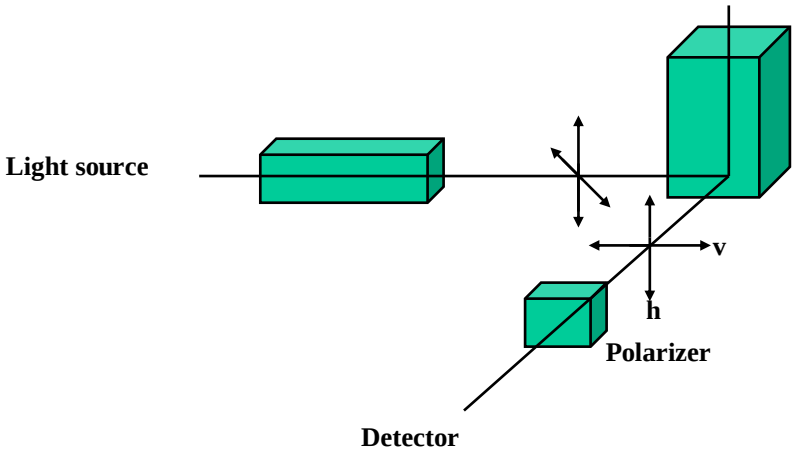

Scheme 2. 6: Schematic diagram for the measurement of fluorescence anisotropy. The light is emitted from the light source along the x-axis and goes through the sample. The fluorescence emitted by the sample is measured at a 90˚ angle along the y-axis and is polarized by a polarized.

Chapter 3

Effects of cholesterol and its oxidised derivatives on the first electron transfer and recombination of photosynthetic reaction centres.

3.1 Introduction

RCs are embedded in the intracytoplasmic membrane (named chromatophores) of photosynthetic bacteria. The RC converts light excitation energy into chemical free energy. Following the absorption of a photon or after the capture of an excitation coming from antenna proteins present in the membrane, the primary electron donor, P, a dimer of bacteriochlorophylls becomes a strong reducer in its singlet excited state P* ($E'_{0\ P^*/P^+}$ ~ -0.9 V)[94]. An electron transfer (ET) chain is then initiated, resulting in ~ 200 ps in the semi-reduction of Q_A (Q_A^-), situated on the cytoplasmic side of the RC (~ 28 Å from P). Therefore, a transmembrane charge separation state ($P^+Q_A^-$) is created. Further ET between Q_A^- and Q_B (with a rate constant k_{AB} (1)), the second quinone acceptor (~ 18 Å from Q_A), is achieved in ~ 150 µs, parallel to the membrane.

In vivo, P^+ is rereduced by endogenous cyt c_2 in a few µs. P can thus absorb a second excitation finally leading to the double reduction and double protonation of Q_B to form the dihydroquinone Q_BH_2. Q_A and Q_B are both ubiquinone$_{10}$ but because of their different respective protein environments they differ in their functional and energetic properties. Q_A is never protonated, in contrast to Q_B, and the $P^+Q_B^-$ state is stabilized by about 60 meV relative to $P^+Q_A^-$ at neutral pH.

In vitro, in the absence of cyt c_2, the $P^+Q_A^-$ and $P^+Q_B^-$ states decay by charge recombination in ~100 ms and ~ 1 s, respectively. $P^+Q_A^-$ decays (with a rate constant k_{AP}) by a tunnelling effect to the ground state whereas the $P^+Q_B^-$ state decays (with a rate constant

k_{BP}) through repopulating $P^+Q_A^-$. Since k_{AP} and k_{BP} are each much smaller than (k_{AB} (1) + k_{BA} (1)) (k_{BA} (1) being the inverse ET rate from Q_B^- to Q_A) $Q_A^-Q_B$ and $Q_AQ_B^-$ are in thermal equilibrium.

In isolated RC re-suspended in detergent or in a phospholipid bilayer, the first ET is not directly coupled to the direct proton transfer to Q_B^-. Instead, pK_a shifts of residues in the cytoplasmic region induced by the formation of either Q_A^- or Q_B^- result in the substoichiometric uptake of protons.

It is accepted that proton are taken up through an anticooperative delocalised proton uptake process over widely spread hydrogen bond networks in the cytoplasmic region that would involve water molecules and residues extending from L210Asp, M17Asp and L209Pro in the Q_B region to M249A in the Q_A region via M266H, M234E as Fe ligands[48, 95, 96]. It has been suggested that the first ET is rate limited by a gating process[97] which might involve conformational rearrangement of the proton distribution[96], of internal water molecules as well as extended hydrogen bond networks.

In isolated RC, the kinetics of the first ET have been shown to be biphasic with a fast phase of ~50-80 µs and a slow phase of ~ 300-900 µs[98, 99]. The origin of these phases has not yet been clearly assigned even if the first phase seems to be more related to ET and the slow one to proton rearrangement.

In *Rhodobacter (R.) sphaeroides* RC, the $P^+Q_A^-$ charge recombination process decays as a single exponential (~ 100 ms) whereas when the native Q_A is replaced by a low potential quinone such as an anthraquinone of lower *in vivo* redox potential, the charge recombination decay is accelerated (~ few ms time range) and the $P^+Q_A^-$ charge recombination process becomes biphasic. The hypothesis of a slow equilibrium between two RC conformational states has been proposed to account for these observations **(Scheme 3.1)**.

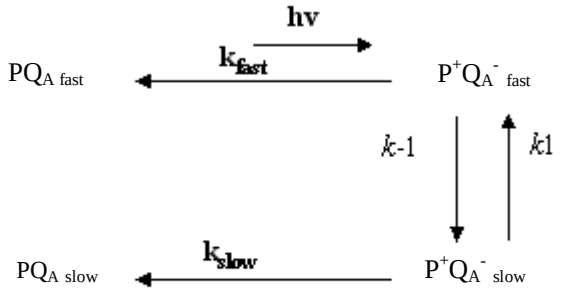

Scheme 3.1: Schematic diagram representing the competition between the recombination to the ground state and the establishment of equilibrium between $P^+Q_A^-$ fast and the $P^+Q_A^-$ slow (modified from Sebban[84]).

In *Rhodopseudomonas (Rps) viridis* RCs where the native Q_A is a menaquinone, the $P^+Q_A^-$ recombination is also biphasic[100]. In the last two examples, $P^+Q_A^-$ no longer decays directly through the ground state but instead *via* a thermally activated state which is a relaxed state of the $P^+H_A^-$ charge separated state (H_A being the bacteriopheophytin intermediate electron acceptor).

In their native *in vivo* state, RCs are embedded in a phospholipid membrane and will therefore experience the dipole potential ψ_d. ψ_d is, thus, generated inside the bilayer. When applied to a membrane (thickness of about 40Å), this electrical potential results in electrical field strengths in the range 10^8 to 10^9 V/m. It has recently been proposed that ψ_d affects very different aspects of membrane protein functioning. Amongst them are the conductance of the gramicidin channel[101], membrane insertion and folding of amphiphilic peptides[102, 103], membrane fusion[15], the kinetics of redox reactions[104], skin permeability[105] and the activity of the Na^+,K^+-ATPase[21].

It was demonstrated in the seventies that the strength of ψ_d can be modulated by the presence in the phospholipid membrane of cholesterol and chemical analogues[106, 107]. This effect has been observed or demonstrated in several biological systems/membranes[106]. Different hypotheses have been proposed to account for this effect. It was initially suggested

that it may arise from a change in the orientation and packing density of molecules at the membrane surface [106]. Alternatively, a cholesterol-induced reorganization of interfacial water was also proposed[107]. Cholesterol could also have an inhibitory effect on vesicle fusion. Indeed, when an increasing concentration of cholesterol is added to PC vesicles, this inhibitory effect on vesicle association is diminished, which might be due to cholesterol's ability to spread apart the PC head groups and reduce the steric repulsion between adjacent bilayers[108]. For PC vesicles, the incorporation of cholesterol would induce a change in the magnitude of the adhesion energy and produce a change in the organisation of dipolar molecules at the membrane surface.

More recently a mixed experimental and theoretical approach suggested that the magnitude of cholesterol derivatives' effect on the dipole potential could be accounted for by the magnitude of the component of the sterol's dipole moment perpendicular to the membrane surfaceand also by sterol-induced changes of lipid packing, modifying the packing density of dipoles in the membrane as well as water penetration[12].

In order to probe the effect of ψ_d on the redox functioning of the RC, we have reconstituted RC proteins in phosphatidylcholine liposomes and varied ψ_d by introducing known ψ_d modifiers in the membrane. We have used cholesterol, 6-ketocholestanol, 5-cholesten-3-β-ol-7-one and phloretin since their respective quantitative effects on ψ_d have been recently evaluated[12, 13, 109]. 6-ketocholestanol and cholesterol are known to increase the dipole potential whereas 5-cholesten-3-β-ol-7-one and phloretin decrease it[13].

We show that modulating ψ_d notably affects the rates of the first ET process as well as the relative amplitudes of both phases. The equilibrium between the two reaction centre populations as revealed by the charge recombination in the presence of AQ as Q_A is also changed. This is the first report of biphasicity of the PQ_A charge recombination at room temperature in native R. *sphaeroides* RC.

In this thesis, possible interpretations of these observations are proposed.

3.2 Results

3.2.1 Electron microscopy

A typical proteoliposome (diameter ~ 100 nm) containing phosphatidylcholine (PLPC), 20 mol % of cholesterol and RC ([lipids]/[RCs] = 3) is presented in **Fig. 3.2**. The black spots represent the RCs (~50-100 Å diameter) (indicated by an arrow in **Fig. 3.2**) which are randomly distributed over the vesicle membrane. It has been previously shown that when lipid stiffness is significantly increased in phospholipid membranes containing *Rhodopseudomonas viridis* RCs (as in DMPC and DEPC vesicles at a temperature below the phase transition, 23ºC), segregation of proteins are observed and protein-protein interactions become dominant[25].

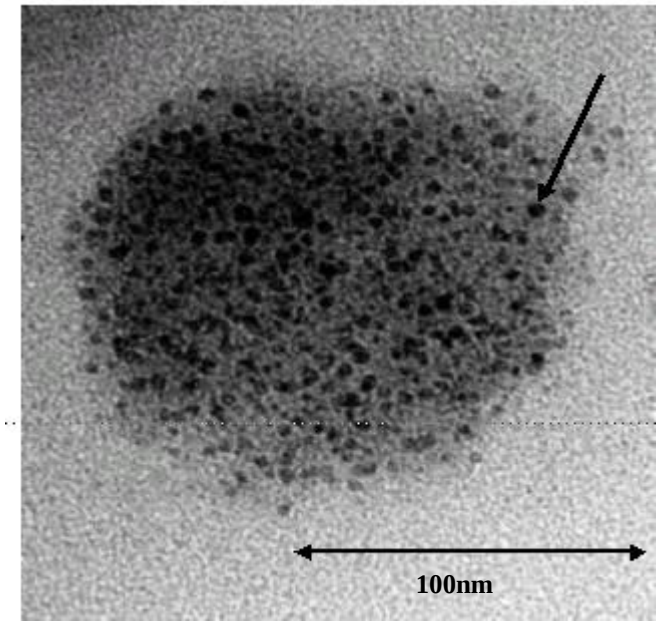

Figure 3.2: Electronic microscopy picture (negative staining) of a proteoliposome containing cholesterol and RCs at 20ºC in a 10 mM Tris-HCl, pH 8.0, 100 mM NaCl and 0.1mM EDTA buffer. One drop of sample was deposited on carbon-coated copper grids before being dried under N_2 flow.

Above the phase transition temperature, this effect was absent, the RCs being randomly distributed all over the DMPC vesicle surface.

Fig. 3.2 shows that cholesterol- (and derivatives, data not shown) containing proteoliposomes protein-protein interactions are unlikely to be a main contributor in influencing the RC energetic/kinetic functioning. Therefore, in the following it is considered that in the RC containing liposomes, the variation of the ET kinetics and the associated energetics are mainly due to the effects of the dipole potential induced by cholesterol derivatives and phloretin. Additionally, direct effects of these chemicals inside phospholipids membranes have previously been demonstrated as being predominantly due to their effects on the dipole potential[13, 21].

3.2.2 Effect of dipole potential modifiers on the first electron transfer

The decay kinetics of the first ET were measured at 750 nm and 20°C in RCs in detergent, in PLPC and in PLPC in the presence of cholesterol, phloretin, 6-ketocholestanol and 5-cholesten-3-β-ol-7-one. The decays are mostly bi-exponential, as previously reported[99]. The decay kinetics measured in isolated RCs, in PLPC and in the presence of 6-ketocholestanol are presented in **Fig. 3.3.** The time window has been truncated to 2 ms. This kinetics have in fact been recorded over 2, 5 and 10 ms time scales. The fits over 5 and 10 ms time windows have been used to determine the rates of the slower components and over 2 ms to determine the rate of the faster phases. The decay lifetimes and the associated amplitudes determined at pH 8.0 are presented in **Table 3.1**.

As can be seen, the decay kinetics are very similar in isolated RCs and in PLPC with, however, a slightly slower kinetics in PLPC. But the main effect is the very noticeable slowing down of the decay kinetics in the presence of 6-ketocholestanol. This effect, although slightly less pronounced, was also observed in the presence of cholesterol.

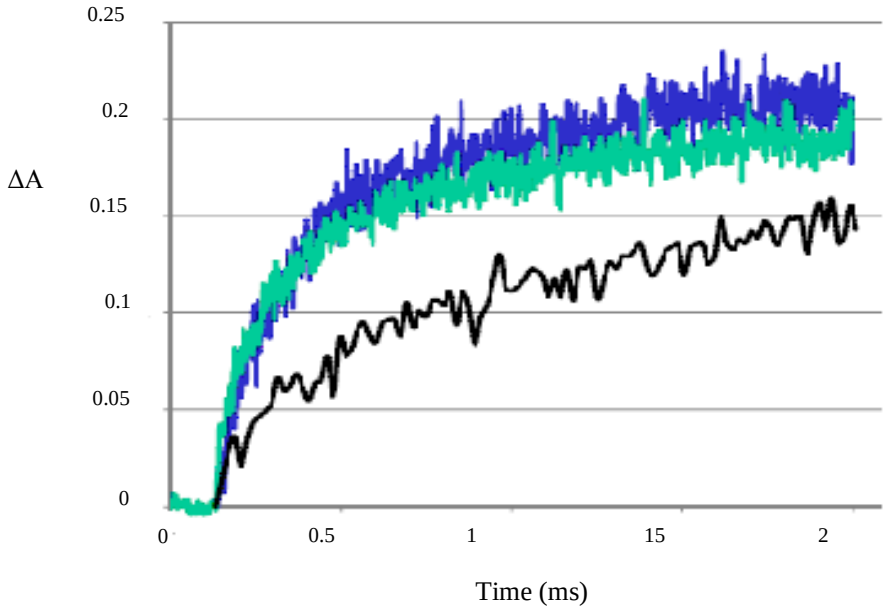

Figure 3.3: Decay kinetics of the first ET measured at 750 nm, 23°C and pH 8.0 in isolated RCs (blue), in PLPC (green) and in PLPC with the presence of 6- ketocholestanol (black). The detergent-RC and the RCs reconstituted in PLPC show almost a similar signal.

The decay lifetimes and the amplitudes of the first ET decay kinetics at 20ºC, pH 8.0 are presented in **Table 3.1**.

20ºC, pH 8.0 (20 mol% of cholesterol and its derivatives in liposomes)	Phases lifetime first ET	Proportion of slow and fast phase (~10% error)	Effect PLPC on dipole potential
Detergent-RC	Fast 85 ± 10 µs Slow 450 ± 50 µs	85 % 15 %	
PLPC	Fast 87 ± 10µs Slow 660 ± 50µs	63 % 37 %	415mV
PLPC+ cholesterol	Fast 350 ± 20µs Slow 2.4 ± 0.2ms	31 % 69 %	+
PLPC+ phloretin	213 ± 20µs	100 %	-
PLPC+ 6-ketocholestanol	Fast 490 ± 50µs Slow 4.4 ± 0.5ms	50 % 50 %	++
PLPC+ 5-cholesten-3β-ol-7-one	434 ± 50µs	100 %	-

Table 3.1: Decay lifetimes of the first ET and associated amplitudes of the first ETin RCs isolated in detergent and in PLPC with the different cholesterol derivatives, measured at 750 nm. Conditions: 20°C in 10 mM Tris-HCl, pH 8.0, 100 mM NaCl, 0.1 mM EDTA.

As shown in **Table 3.1**, a correlation seems to exist between the extent of a cholesterol derivative's effect on the dipole potential and the slowing down of the first ET reaction. Indeed, the major effect on the kinetics is obtained for 6-ketocholestanol for which the fast and the slow components are slowed by ~ 6 and ~7 times, respectively, as compared to PLPC samples **(Table 3.1)**. Moreover, the amplitudes of the two phases invert; the slow component starting to become dominant (~ 50 %). 6-ketocholestanol is the most effective compound in increasing the dipole potential[13]. The molecule which causes the second greatest increase in the dipole potential, is cholesterol **(Table 3.1)**. Interestingly we also observed a clear slowing down of the first ET kinetics: the fast and the slow components are slowed down ~ 4 times and the slow component becomes dominant, (~ 70 %) respectively. Interestingly, when the effect of the molecules on the dipole potential are "negative" (phloretin and 5-cholesten-3-β-ol-7-one), the decay kinetics are found to be single exponential with lifetimes almost unchanged compared to the average lifetimes in RCs or PLPC (respectively ~ 213 and 434 µs). We shall come back to these results below.

3.2.3 Temperature dependence of the rates and amplitudes of the first electron transfer.

The temperature dependencies of the decay lifetimes of the first ET in RCs isolated in detergent and in PLPC with the different cholesterol derivatives, measured at 750 nm and at pH 8.0 are presented in **Fig. 3.4.**

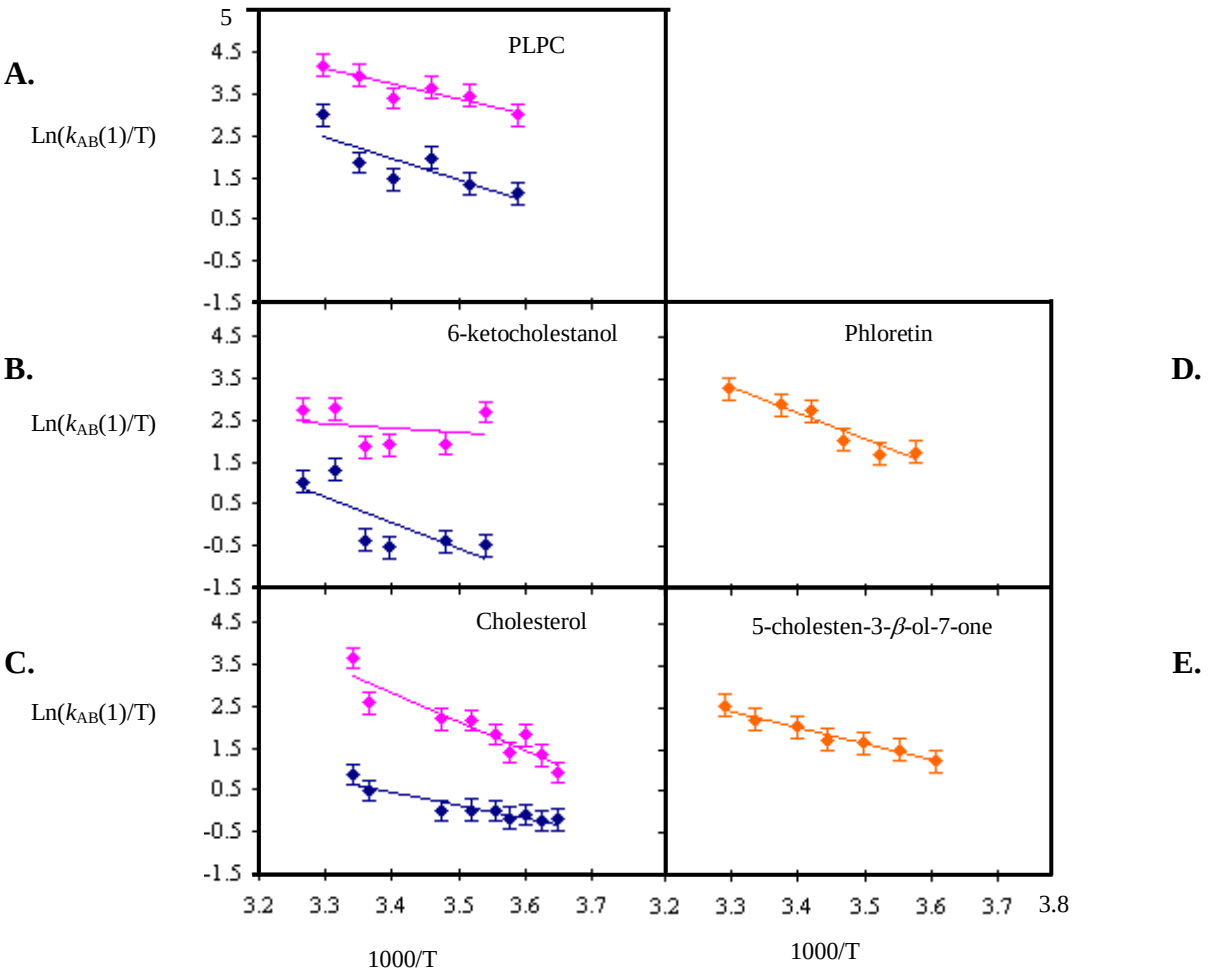

Figure 3.4: Eyring plots of the first ET decays over a temperature range measured at 750 nm, pH 8.0. RCs were reconstituted in PLPC (A) with 6-ketocholestanol (B), cholesterol (C), phloretin (D) and 5-cholesten-3-*β*-ol-7-one (E). The slow phase (blue), fast phase (pink) and the unique phase (orange) are represented for PLPC, cholesterol and each derivatives in blue, pink and orange respectively.

To further characterize the effects of the cholesterol derivatives on the first ET reaction the temperature dependencies of the associated amplitudes were also analysed. These plots are displayed in **Fig. 3.5**. Although noisy, the amplitudes observed in PLPC are rather flat over the observed temperature range, with a ratio slightly favouring the fast component (~ - 63 ± 10 % at neutral pH). The trend is different in the case of 6-ketocholestanol and cholesterol. Indeed, a steep increase in the amplitude of the slow component is observed with increasing temperature. The slow phase becomes the dominant phase ~7°C for cholesterol and above 20°C for 6-ketocholestanol.

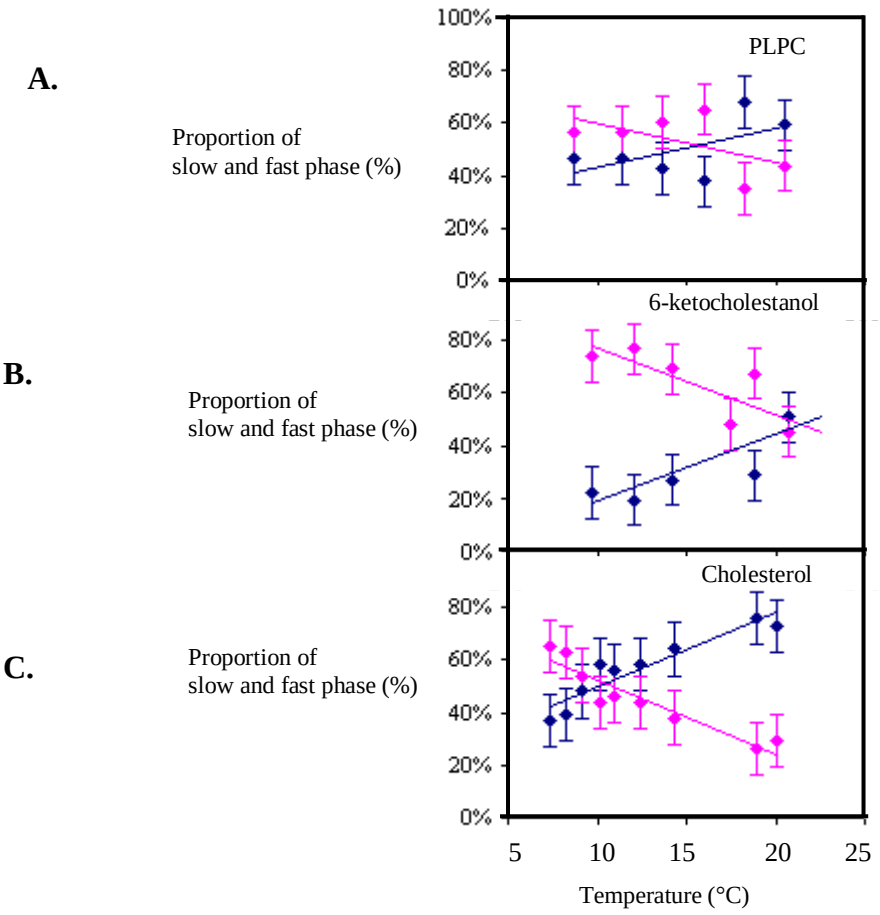

Figure 3.5: Temperature dependence of the amplitudes of the fast (pink) and slow (blue) phases associated with the first ET reaction at pH 8.0, temperature range of 5-25°C. RC were reconstituted in PLPC (A) with 6-ketocholestanol (B) and cholesterol (C).

The thermodynamic parameters derived from the plots of **Fig. 3.4** are presented in **Table 3.2**. As previously mentioned[100, 110], there is a relatively high variability in the enthalpic and entropic terms between different "similar" samples, but "compensating" effects between these terms yield produce free energy values allowing comparison between the different experiments/samples. In other words, the absolute $\Delta G^{\ddagger}$ values are more reliable than the enthalpic or entropic values alone.

As can be seen in **Table 3.2**, the slowest ET reactions logically correspond to higher activation free energy barriers. This is evident from a comparison in a given sample between the fast and the slow phase but also between the different samples. Indeed, the $\Delta G^{\ddagger}$ values

measured for 6-ketocholestanol are significantly higher than those of the PLPC sample by ~ 4 kJ/mol. This also the case for the cholesterol sample. In the case of 5-cholesten-3β-ol-7-one, the measured $\Delta G^{\ddagger}$ value is the same as that measured for the slow phase of PLPC, suggesting that the equilibrium has been entirely displaced towards the slow phase. In the case of phloretin, the measured $\Delta G^{\ddagger}$ value (51.7 kJ/mol) is intermediate between the activation free energies associated with the fast and slow phases of the PLPC sample.

20ºC, pH 8.0 (20 mol% of cholesterol and its derivatives in liposomes)		ΔH (J)	ΔS (J/K)	$\Delta G^{\ddagger}$ (J/mol)
PLPC	Fast	27419	-72	49155
	Slow	39005	-47	53261
PLPC+ cholesterol	Fast	56909	-17	51706
	Slow	26194	-106	57860
PLPC+ phloretin	Unique	44279	-25	51776
PLPC+ 6-ketocholestanol	Fast	8713	-148	52996
	Slow	52253	-19	58120
PLPC+ 5-cholesten-3β-ol-7-one	Unique	24990	-95	53561

Table 3.2: Thermodynamic parameters (derived from the Eyring plots **Fig. 3.4**) of the first ET in RCs reconstituted in PLPC with the different cholesterol derivatives, measured at 750 nm, 20°C at pH 8.0.
.

3.2.4 $P^+Q_A^-$ charge recombination

The $P^+Q_A^-$ charge recombination lifetimes (τ_{AP}) in the presence of the cholesterol derivatives and phloretin are summarized in **Table 3.3**.

In isolated RCs and in PLPC, the $P^+Q_A^-$ decays are exponential (τ_{AP} ~100 ms) as previously observed[24]. The main effect observed here is the biphasic decay kinetics induced by the presence of the four cholesterol derivatives (data not shown). This is displayed in **Table 3.3.** The existence of two reaction conformations has previously been reported in

native RCs from *Rhodopseudomonas viridis*[100, 110] and in the RCs from *R. sphaeroides* either at low temperature[111] or in the presence of a low potential quinone acting as Q_A[84]. We report here for the first time the possibility of revealing these states in the WT *R. sphaeroides* RCs at room temperature, thanks to the influence of cholesterol derivatives.

20ºC, pH 8.0 (20 mol% of cholesterol and its derivatives in liposomes)	Phases lifetime (τ_{AP})	Proportion of slow and fast phase (~10% error)	Effect PLPC on dipole potential
PLPC	102 ± 10ms	100%	415mV
PLPC+ cholesterol	Fast 43 ± 5 ms Slow 100 ± 10 ms	45 % 55 %	+
PLPC+ phloretin	Fast 73 ± 12 ms Slow 171 ± 15 ms	40 % 60 %	-
PLPC+ 6-ketocholestanol	Fast 86 ± 10 ms Slow 237 ± 30 ms	20 % 80 %	++
PLPC+ 5-cholesten-3β-ol-7-one	Fast 74 ± 10 ms Slow 119 ± 20 ms	40 % 60 %	-

Table 3.3: Lifetime decays and associated amplitudes of the $P^+Q_A^-$ charge recombination in RCs isolated in detergent and in PLPC with the different cholesterol derivatives, measured at 430 nm, 20°C in 10 mM Tris-HCl, pH 8.0, 0.1% LDAO, 40 mM imidazole. The lifetimes don't depend on the temperature and the amplitudes for all derivatives are biphasic except for PLPC.

3.2.5 $P^+Q_B^-$ charge recombination

One may also notice the slight increase of τ_{BP} in PLPC (~ 1.6 s as compared to ~1 s in RCs). The $P^+Q_B^-$ charge recombination lifetime decays (τ_{BP}) in the presence of the cholesterol derivatives and phloretin are summarized in **Table 3.4.** In a similar fashion to the $P^+Q_A^-$ decay kinetics, the main effect observed here is the biphasic decay kinetics of $P^+Q_B^-$ induced by the presence of the four cholesterol derivatives, except for 5-cholesten-3-β-ol-7-one . Here too, τ_{BP} is not significantly changed compared to the isolated RCs or in PLPC membranes, where the kinetics are single exponential. The fast phase kinetics for cholesterol, phloretin

and 6-ketocholestanol are ~ 0.80 s. One may note a slight (~2 times) slowing down of the slow phase for phloretin compared to all other samples, with or without cholesterol derivatives.

Interestingly, 5-cholesten-3-β-ol-7-one, which is the only cholesterol derivative displaying a monoexponential decay, is also the only derivative that has its dipole moment in the membrane directed in the opposite direction to that of the other cholesterol derivatives **(Table 3.4)**.

20ºC, pH 8.0 (20 mol% of cholesterol and its derivatives in liposomes)	Phases lifetime (τ_{BP})	Proportion of slow and fast phase (~10% error)	Effect PLPC on dipole potential
Detergent-RC	1.1 ± 0.1 s	100%	
PLPC	1.6 ± 0.2s	100 %	415mV
PLPC+ cholesterol	Fast 0.8 ± 0.1s Slow 1.2 ± 0.1s	70 % 30 %	+
PLPC+ phloretin	Fast 0.8 ± 0.1s Slow 2.3 ± 0.2 s	62 % 38 %	-
PLPC+ 6-ketocholestanol	Fast 0.8 ± 0.2 s Slow 1.4 ± 0.2 s	50 % 50 %	++
PLPC+ 5-cholesten-3β-ol-7-one	1 ± 0.1 s	100 %	-

Table 3.4: Decay lifetimes of the $P^+Q_B^-$ recombination and associated amplitudes in RCs reconstituted in PLPC with the different cholesterol derivatives, measured at 430 nm, 20°C in 10 mM Tris-HCl, pH 8.0, 0.1% LDAO, 40 mM imidazole buffer .

The temperature dependencies of the slow and fast phase of the $P^+Q_B^-$ decays have been determined for cholesterol, 6-ketocholestanol and phloretin. They are presented in **Fig. 3.6**. In the case of 6-ketocholestanol no change in the relative amplitudes was observed. For phloretin and cholesterol the fast phase become dominant at temperatures above 15°C.

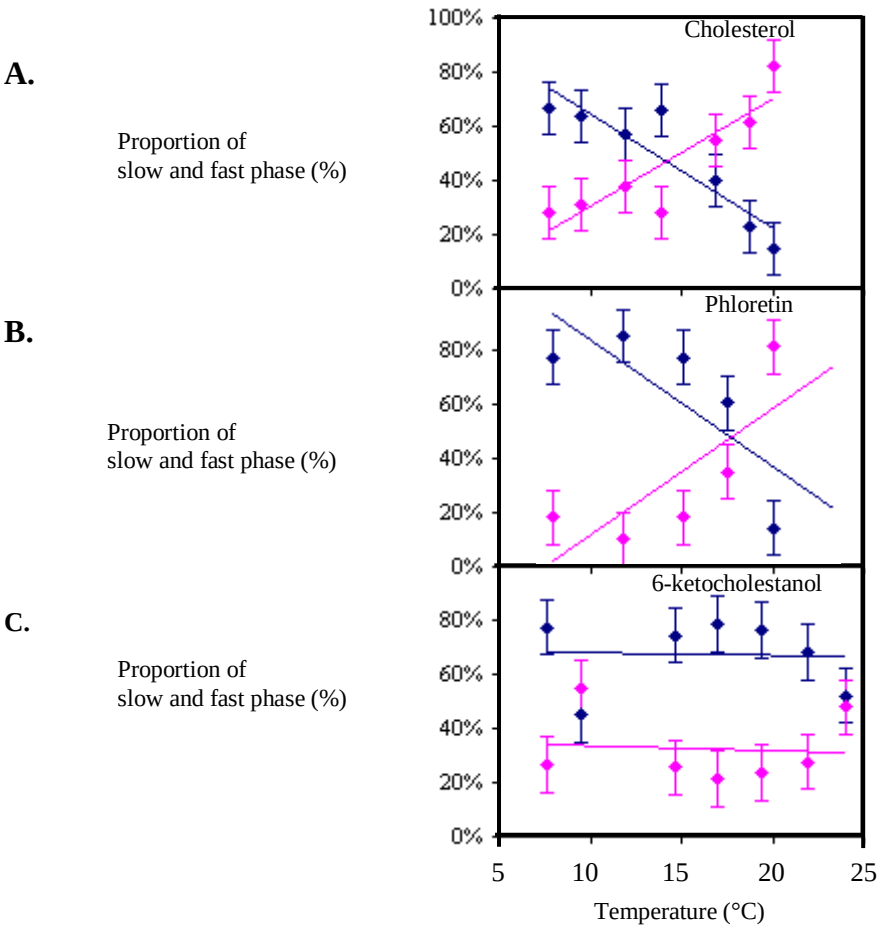

Figure 3.6: Temperature dependencies of the amplitudes of the fast (pink) and slow (blue) phases associated with $P^+Q_B^-$ recombination in RCs reconstituted in PLPC added with cholesterol (A), phloretin (B) and 6-ketocholestanol (C) at pH 8.0 over a temperature range 5-25°C.

3.2.6 $P^+Q_A^-$ charge recombination in the presence of an anthraquinone acting as Q_A

In order to probe the effect of dipole potential modulations on a different redox process and in a different part of the RC molecule spanning a different region of the membrane, the native Q_A was replaced by an anthraquinone and the P^+AQ^- charge recombination kinetics were measured at 430 nm. As mentioned above, this involves the repopulation of the $P^+H_A^-$ state, involving the bacteriopheophytin situated at about mid-membrane. The decay kinetics at 20 ºC are shown in **Table. 3.5**.

20ºC, pH 8.0 (20 mol% of cholesterol and its derivatives in liposomes)	Phases lifetime ($\tau_{AnthraP}$)	Proportion of slow and fast phase (~10% error)	Effect PLPC on dipole potential
PLPC	Fast 2 ± 0.2 ms Slow 27 ± 3 ms	50 % 50 %	415mV
PLPC+ cholesterol	Fast 1 ± 0.1 ms Slow 7 ± 0.7 ms	80 % 20 %	+
PLPC+ phloretin	Fast 2 ± 0.2 ms Slow 11 ± 1 ms	80 % 20 %	-
PLPC+ 6-ketocholestanol	Fast 1 ± 0.1 ms Slow 6 ± 0.6 ms	80 % 20 %	++
PLPC+ 5-cholesten-3β-ol-7-one	Fast 1.5 ± 0.2 ms Slow 12 ± 1 ms	80 % 20 %	-

Table 3.5: Decay lifetimes of the P^+AQ^- recombination and associated amplitudes in RCs reconstituted in PLPC with the different cholesterol derivatives, measured at 430 nm, 20°C in 10 mM Tris-HCl, pH 8.0, 0.1% LDAO, 40 mM imidazole buffer.

As previously reported for *R. sphaeroides,* RCs containing low potential quinones acting as Q_A, the P^+AQ^- charge recombination is biphasic. This is verified here in all samples.

As compared to the PLPC sample, the slow and fast kinetics are significantly accelerated upon addition of cholesterol and 6-ketocholestanol (**Table 3.5**) by a factors of 4-5 for the slow phase and 2 for the fast phase. This effect is less pronounced in the presence of phloretin and 5-cholesten-3β-ol-7-one, where the fast phase kinetics remains nearly unchanged and the slow phase is accelerated by a factor of two.

Considering the amplitudes, the presence of cholesterol derivatives shift the equilibrium between the two phases towards the fast component, *i.e.* A_{fast} becomes > 80% at 20°C and pH 8.0 in all samples, whereas it is about 50 % in the PLPC sample.

3.2.7 Temperature dependences of the amplitudes of P^+AQ^- decays.

We have also investigated the temperature dependencies of the amplitudes of the P^+AQ^- charge recombination process. The results are presented in **Fig. 3.7**. In PLPC samples, the amplitudes of the fast and slow phases are nearly equal, and this repartition does not vary much over the temperature range of 5-25°C.

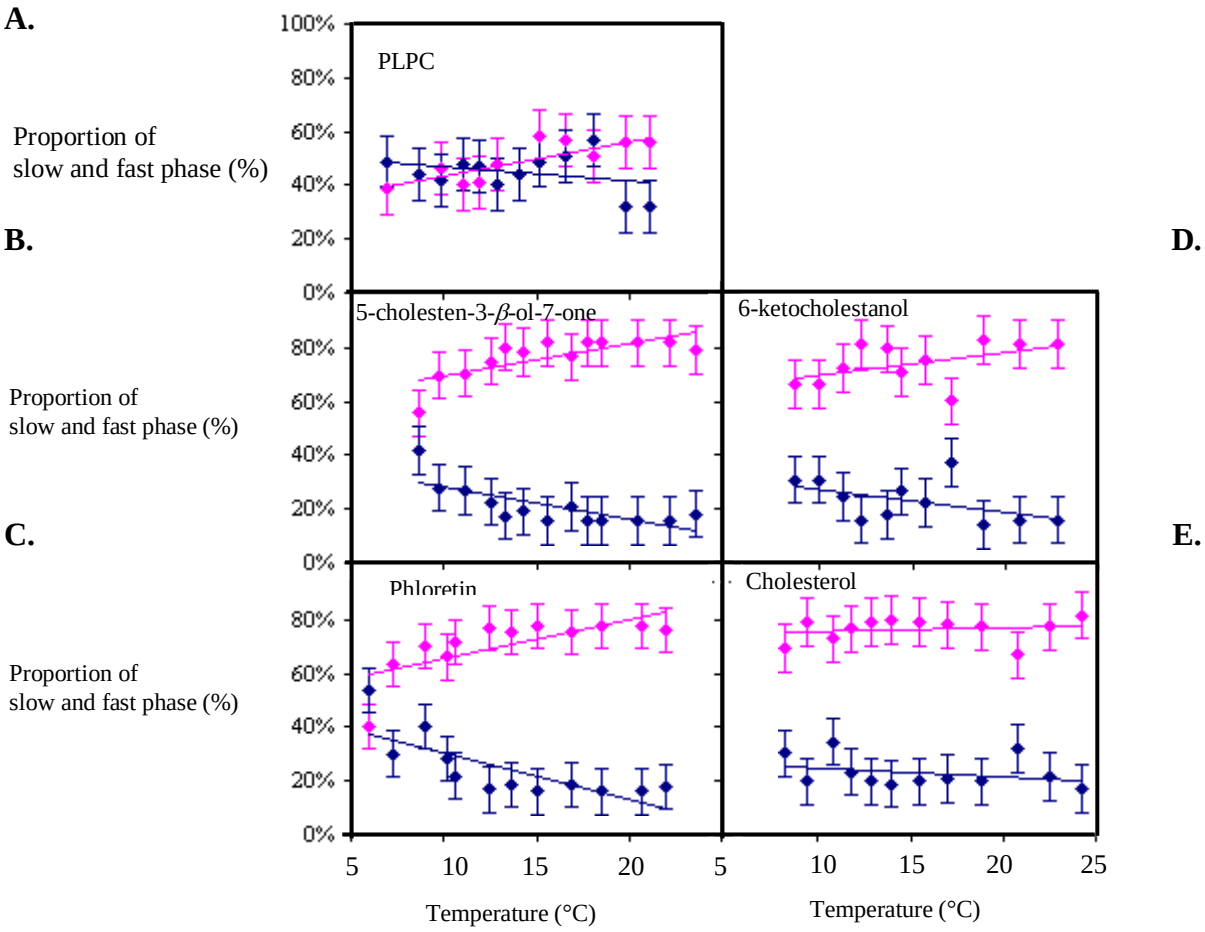

Figure 3.7: Comparison between slow (blue) and fast (pink) phases for cholesterol derivatives when present in PLPC (A) for P^+AQ^- recombination with 5-cholesten-3-β-ol-7-one (B), phloretin (C), 6-ketocholestanol (D), and cholesterol (E) over a temperature range of 5-25°C.

In all samples containing cholesterol derivatives **(Fig 3.7)** the shallow temperature dependence of both amplitudes is also observed, the fast phase remaining largely dominant (> 60-70 %) over the whole temperature range studied.

The thermodynamics parameters

The temperature dependencies of the associated rates have also been measured and the Arrhenius plots of the fast and slow rates of charge recombination from the P^+AQ^- state have been drawn (data not shown). We have analysed our data with Arrhenius plots here in order to compare the obtained values more directly with previously published results concerning the P^+AQ^- charge recombination decays. From the Arrhenius plots the thermodynamic parameters have been calculated and are presented **Table 3.6**.

20ºC, pH 8.0 (20 mol% of cholesterol and its derivatives)		ΔH (eV)	TΔS (eV)	$\Delta G°_M$(eV)
PLPC	Fast	0.291	0.034	0.257
	Slow	0.181	-0.144	0.325
PLPC+ cholesterol	Fast	0.373	0.122	0.251
	Slow	0.326	0.030	0.296
PLPC+ phloretin	Fast	0.385	0.122	0.263
	Slow	0.125	-0.188	0.312
PLPC+ 6-ketocholestanol	Fast	0.417	0.172	0.245
	Slow	0.256	-0.039	0.295
PLPC+ 5-cholesten-3β-ol-7-one	Fast	0.376	0.124	0.252
	Slow	0.229	-0.078	0.307

Table 3.6: Thermodynamic parameters (derived from the Arrhenius plots) of $P^+Q_{Anthraquinone}^-$ recombination of RCs reconstituted in PLPC with the different cholesterol derivatives, measured at 430 nm, 20°C at pH 8.0.

For each phase the same equation was used as in previous work[84, 100, 112].

$$k = k_d \exp - (\Delta G°_M/kT) + k_T$$

where k_d is the rate constant of the $P^+H_A^-$ decay to the ground state. $\Delta G°_M$ represents the free energy difference between $P^+Q_A^-$ and M, a relaxed state of $P^+H_A^-$, the stabilization of which occurs in the ns time range[113, 114]. Following previous work[112], k_d was taken here as 2.10^7 s^{-1}. k_T is the limiting value of the rate constant of P^+Q_A- recombination reached at low temperature. It has previously been measured for anthraquinone as 10 s^{-1}.

The increased rates of P^+AQ^- recombination in the samples containing cholesterol and 6-ketocholestanol is logically reflected in smaller $\Delta G°_M$ values **(Table 3.6)**, especially for the slow components. Indeed, the presence of cholesterol and 6-ketocholestanol increase the free energy level of the slow RC conformation state of Q_A^-, by about 30 meV compared to the PLPC sample **(Table 3.6)**. This effect is less noticeable in the case of the fast component states, for which $\Delta G°_M$ is reduced by ~ 5 and ~ 10 meV, respectively.

3.3 Discussion and conclusion

It has previously been shown that the amplitude of the dipole potential in phospholipid bilayers can be modulated by different cholesterol derivatives due to their different dipole magnitudes as well as their orientations relative to the membrane plane[13]. We took advantage in the present work of these properties to study the possible influence of the dipole potential experienced by the RC protein (when imbedded in PLPC) on its functioning, especially at the level of the electron and proton-coupled ET reactions.

The electronic microscopy images suggest that the presence of cholesterol derivatives, at least at 20 % of the total lipid concentration, does not modify the RC random distribution in the proteoliposomes. No segregation of proteins could be observed as in DMPC or DEPC proteoliposomes (freeze-fractured electron microscopy experiments) when frozen below their transition temperatures (23 and 9°C, respectively)[24, 25, 115]. Therefore, to a first approximation, the effect of cholesterol derivatives on the ET could be interpreted in terms of the

modification of the dipole potential. In other words, the influence of the cholesterol derivatives on the protein-protein interaction is, if any, probably indirect and can likely be neglected here. This statement is supported by the fact that no similar effects to those detected in the present work could be observed in the above described proteoliposomes (DMPC and DEPC) below the phase transition temperatures, where the protein-protein interactions dominate.

Effect of the cholesterol derivatives on the first electron transfer

We observed two different effects of the cholesterol derivatives on the $Q_A^- \rightarrow Q_B^-$ ET parameters. The first observation in the presence of cholesterol and 6-ketocholestanol is the modification of the decay biphasicity associated with this process (the slow phases becoming dominant) and the marked deceleration of the electron transfer. In contrast, in the presence of 5-cholesten-3β-ol-7-one and phloretin, the decays are nearly exponential and the rates are not decreased compared the RC embedded in PLPC membranes or even RCs isolated in detergent. Interestingly, 6-ketocholestanol and cholesterol display the largest increasing effect on the dipole potential whereas 5-cholesten-3β-ol-7-one and phloretin reduce the dipole potential.

The $Q_A^- \rightarrow Q_B$ ET process and the associated two kinetic phases have previously been studied[97-99]. In particular it has been proposed that this process is not a "pure" ET but rather gated (rate-limited)[97] by "conformational changes" that may include protonation events, protein and hydrogen bond network (including waters) rearrangements or even a quinone movement between two positions, although the last hypothesis has recently been ruled out[48, 116].

The two phases have been attributed to different processes, the fast one (~80 µs) to ET *per se*, and the longer one (~ 300-500 µs) to protonation events.

To help in the analysis the above effects of cholesterol derivatives, recent data collected in the Sebban group have been used. These data concern the pH dependence of both first flash electron and proton transfer kinetics measured in wild type RCs from *Rb. sphaeroides*. These data (Julia Tandori, Peter Maroti and Pierre Sebban, unpublished data) show that there is a full correspondence between both the rates and the amplitudes of the two phases associated with electron and proton transfers. This is clearly observed in **Fig. 3.8**.

A.

B.

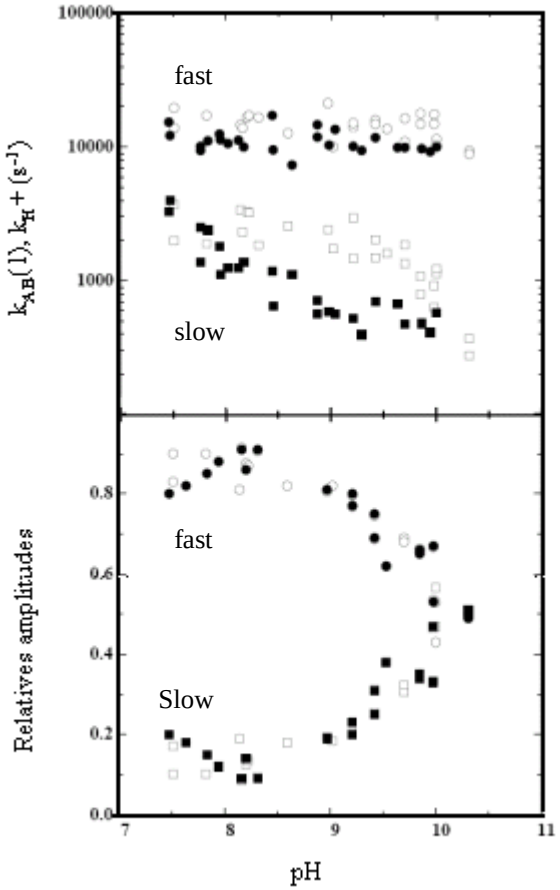

Figure 3.8: (A) pH dependence of the rate constants of the first ET ($k_{AB}(1)$) (open symbols) and of the first flash proton transfer (k_H^+) (closed symbols) in the wild type RCs from *Rb. sphaeroides* at 20°C. (B) Associated amplitudes (same symbols).

This is the first time that a biphasic character has been found for the proton transfer kinetics associated with the first ET process. In other terms, even at the first flash (it is well accepted for the second flash), the $Q_A^- \rightarrow Q_B$ ET is intimately coupled to proton transfer.

Therefore our interpretation of the effects of cholesterol analogues on the $Q_A^- \rightarrow Q_B$ ET has to take this coupling into account. When 6-ketocholestanol or cholesterol are added their strong positive effects on the dipole potential may increase the energy barrier for protons to penetrate to the cytoplasmic side of the RC, perpendicular to the membrane. Indeed, a notable increase of the activation free energy barriers for the ET processes in the presence of the two above molecules is observed. In other words, the effects of 6-ketocholestanol and cholesterol on the rates of ET reflect a slowing down and increased difficulty for protons (whose transfer is coupled to that of the electrons) to penetrate the protein. The significant increase in the amplitude of the slow phase in both samples reflects the greater importance of the proton phase *vs.* the ET itself.

In samples containing 5-cholesten-3β-ol-7-one and phloretin, due to their decreasing effect on the dipole potential, the measured rates for the $Q_A^- \rightarrow Q_B$ ET process are nearly unchanged as compared to the PLPC samples. The absence of biphasicity (or absence of the slow phase) may reflect an equilibrium of the two phases, strongly displaced towards the ET phase.

It is important to note that neither the inversion of the two phases nor the significant slowing down of the first ET process have been reported in the work of Taly *et al.*[24] when investigated below the phase transition temperature of DMPC. However, in that case electron microscopy clearly indicated that protein-protein interactions were dominant.

The effects that we observe here are, therefore, intimately associated to the presence of the cholesterol derivatives.

It is quite difficult to give a definitive interpretation, but our data strongly suggest that the amplitude of the dipole potential does influence proton-coupled ET processes by modulating the free energy barrier for proton transfer. Further experiments, in particular analyzing mutants modified in their proton transfer capabilities, and or H bond distribution would help in a more definitive conclusion of the strong effects of cholesterol and 6-ketocholestanol on the Q_A^- to Q_B electron transfer process.

Effects of the cholesterol derivatives on the P^+AQ^- decay kinetics

In contrast to the observed slowing down of the $Q_A^- \rightarrow Q_B$ first electron transfer decay kinetics when the 6-ketocholestanol and cholesterol are present, the $P^+AQ^- \rightarrow PAQ$ charge recombination decays are accelerated in the presence of the same derivatives. In the presence of 5-cholesten-3β-ol-7-one and phloretin, the $P^+AQ^- \rightarrow PAQ$ decays are only slightly accelerated as compared to PLPC samples. So when comparing the first electron transfer process to the $P^+AQ^- \rightarrow PAQ$ charge recombination process, the effects of the cholesterol analogues can be analyzed in terms of three categories:

First electron transfer rate constants:

PLPC > 5-cholesten-3β-ol-7-one and phloretin > 6-ketocholestanol and cholesterol

$P^+AQ^- \rightarrow$ PAQ charge recombination rate constants:

PLPC < 5-cholesten-3β-ol-7-one and phloretin < 6-ketocholestanol and cholesterol

It is proposed above that the increase of the dipole potential due to the presence of the cholesterol derivatives slows down the entry of protons into the RCs perpendicular to the membrane due to an increase of the free energy barrier for this process. Since the electron staying on AQ goes back to H_A and then to P^+ to achieve the $P^+AQ^- \rightarrow PAQ$ process, and since this process also takes place perpendicular to the membrane, it would be consistent for the same changes of the dipole potential to have an opposite effect on the the $Q_A^- \rightarrow Q_B$

electron transfer and on the electron transfer back to P^+ from AQ^- (or similarly the energy level of P^+AQ^- would be increased by the dipole potential).

Both effects observed on the $Q_A^- \rightarrow Q_B$ first proton-coupled electron transfer reaction and on the $P^+AQ^- \rightarrow PAQ$ recombination process would expected to be therefore be modulated oppositely by the dipole potential. This would be consistent with the dipole potential influencing charge transfer reactions across the entire membrane.

Effect of the cholesterol derivatives on the equilibrium between two populations of RCs

The existence of two RC conformations evidenced by the presence of biphasic decay kinetics of the $P^+Q_A^- \rightarrow PQ_A$ charge recombinations in the WT RC from *Rps. viridis*[112] or of the $P^+Q_A^- \rightarrow PQ_A$ when Q_A is a low potential quinone such as anthraquinone in WT RC from *R. sphaeroides* have been previously suggested[100, 117]. The exact nature of the phase and of the associated equilibrium is still unknown. It had tentatively been proposed that two conformational states of the RC which would equilibrate rapidly (as compared to $P^+Q_A^-$ charge recombination in the WT) pre-existed in the dark. Under "fast" recombination conditions as for $P^+Q_A^- \rightarrow PQ_A$ in *Rps. viridis* RC (1-2 ms) or in *R. sphaeroides* RC when the native Q_A is replaced by a low potential quinone (few ms), this equilibrium can no longer establish itself, revealing a biphasic decay reflecting the presence of both states.

It has been demonstrated that pH, salt, the stiffness of the membrane, temperature and protein mutations modulate this equilibrium[25, 111, 118]. However, the presence of the two phases have never been reported, neither for the $P^+Q_B^- \rightarrow PQ_B$, nor for the $P^+Q_A^- \rightarrow PQ_A$ charge recombination at room temperature in WT *R. sphaeroides* RC with the native quinone (UQ_{10}) acting as Q_A. Here for the first time it is reported that it is possible to modulate the equilibrium time between both phases by changing the dipole potential. Indeed, in PLPC containing *R. sphaeroides* RCs, both the $P^+Q_A^- \rightarrow PQ_A$ and the $P^+Q_B^- \rightarrow PQ_B$ display

exponential decays as in RCs isolated in detergent. However, biphasicity of the two types of decays are observed in the presence of cholesterol derivatives (except for the $P^+Q_B^- \rightarrow PQ_B$ decay in the presence of 5-cholesten-3β-ol-7-one).

One also has to note here that in the work of Taly et al.[24], in DMPC liposomes below the phase transition, the $P^+Q_A^-$ and $P^+Q_B^-$ charge recombination processes were occurring *via* exponential decays. Again, this suggests that effects observed here in the presence of the cholesterol derivatives on the biphasicity of the charge recombination are specifically induced by these molecules and not by indirect protein-protein interactions.

The finding here that two RC states associated with two respective phases of the $P^+Q_A^-$ and $P^+Q_B^-$ charge recombinations[118] are revealed in WT proteins by the presence of cholesterol derivatives might be consistent with the above hypothesis of the dipole potential affecting the way that protons penetrate within the protein. A slowing down and/or an increased barrier for protons to reach their sites may affect the equilibrium between two conformational states of the RCs, which were proposed to be associated with different proton conformations. It is difficult at this stage to proceed further this hypothesis. More experiments, using the same cholesterol samples, and varying the pH, salt, lipid stiffness would help to further characterize these effects and states.

Chapter 4

Thermodynamics of ATP binding to the Na^+, K^+-ATPase

4.1 Introduction

The Na^+,K^+-ATPase is one of the most crucial enzymes of animal physiology. Throughout the animal kingdom it is responsible for pumping Na^+ and K^+ ions across the plasma membrane and thus maintaining electrochemical potential gradients for both ions across the membrane. A major function of the Na^+ electrochemical potential gradient is to act as a driving force for the uptake of essential metabolites such as glucose and amino acids. In the plant kingdom the corresponding role is played by the plasma membrane H^+-ATPase, a related enzyme to the Na^+,K^+-ATPase, which pumps H^+ ions across the plasma membrane and builds up the H^+ electrochemical gradient which plants utilize to drive metabolite absorption[119].

One of the puzzling observations in the Na^+,K^+-ATPase field is that the affinity of the E1 conformation appears to differ depending on whether it is measured by an equilibrium method or a pre-steady-state kinetic method. From ATP binding studies a single ATP binding equilibrium with a K_d in the range 0.12-0.63 μM has been detected[120-124]. In contrast, from pre-steady-state kinetic studies based on enzyme phosphorylation much higher dissociation constants have been found (K_d in the range 3.5-14 μM)[125-130]. Apparent K_d values can also be determined from steady-state kinetic measurements, but these depend on all of the rate constants and equilibrium constants of the enzymatic cycle and, therefore, cannot be compared with the results of equilibrium binding measurements. The question is whether the two different ranges of the K_d value can be explained by the classical monomeric Albers-Post

mechanism of Na^+,K^+-ATPase function. One simple explanation for the difference in behaviour could be that it is due to Mg^{2+} ions. In equilibrium ATP binding studies Mg^{2+} must be omitted to avoid phosphorylation, whereas in pre-steady-state kinetic studies it must be included to allow phosphorylation. In principle Mg^{2+} ions could complex ATP in aqueous solution and compete with the enzyme for ATP. A major aim of this chapter is, therefore, to obtain data which would allow an analysis of whether or not this is a feasible explanation.

To do this requires careful measurements of the equilibrium binding of ATP by both the enzyme and by Mg^{2+} under the same ionic strength and pH conditions. For this the technique of isothermal titration calorimetry (ITC) has been used here.

ITC has so far only been applied twice previously to the Na^+,K^+-ATPase; once to measure ouabain interaction with the enzyme[125, 127-132] and once to detect nucleotide binding[120]. Using this technique the heat released to or absorbed from the surroundings on ATP binding can be directly measured. In their studies Grell *et al.*[120] incorporated glycerol in the buffer medium. However, glycerol has not been used in any of the pre-steady-state kinetic studies and it could possibly influence the thermodynamics of ATP binding. Therefore, to allow the analysis described in the previous paragraph in this thesis the first ITC measurements of ATP binding to the Na^+,K^+-ATPase in the complete absence of glycerol have been carried out.

4.2 Results

4.2.1 Binding of Mg^{2+} to ATP

If one wishes to compare the ATP binding affinities of the enzyme obtained from equilibrium binding experiments and from kinetic studies, it is first necessary to establish the dissociation constant for the interaction of ATP with Mg^{2+} ions. The reason for this is that in equilibrium studies Mg^{2+} ions are omitted but in kinetic studies they are included. Interaction

between Mg^{2+} and ATP in the bulk solution could very well influence the enzyme's apparent affinity for ATP and this needs to be taken into account. The results of a titration of Na_2ATP with $MgCl_2$ are shown in **Fig. 4.1**.

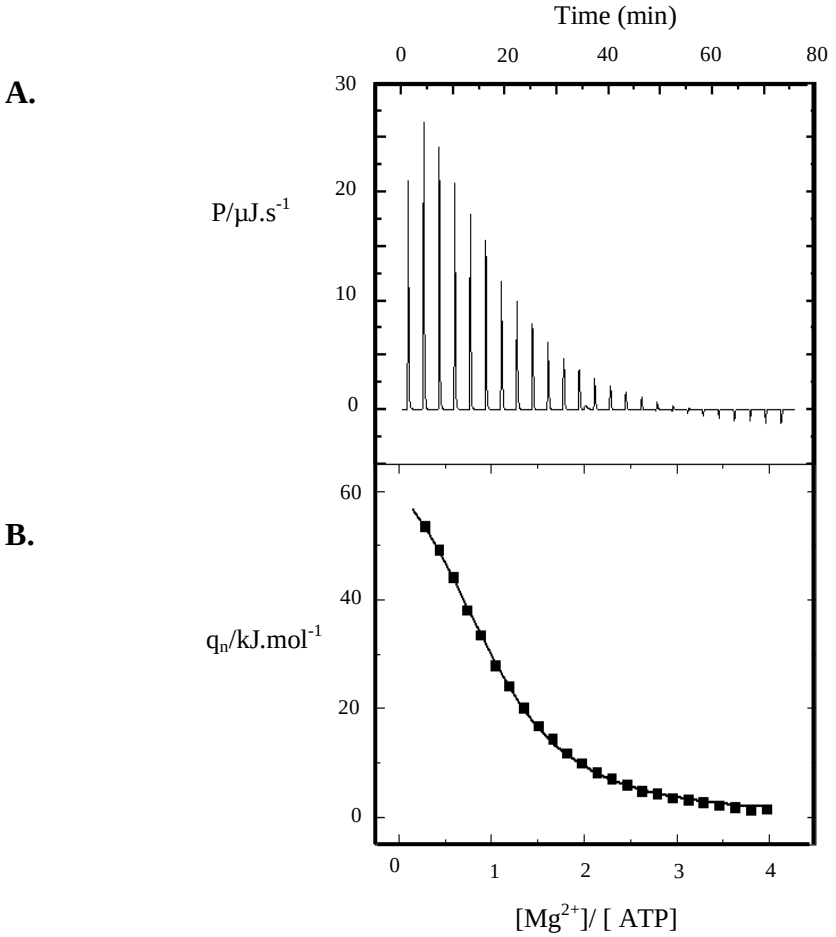

Figure 4.1: Titration of Na_2ATP with $MgCl_2$. The initial concentration of ATP in the ITC cell was 0.25 mM. The buffer of both the ATP and the $MgCl_2$ solutions contained 130 mM NaCl and 30 mM imidazole, pH 7.4. The experiment was conducted at 24°C. (A) shows the power, P, in μJ s^{-1} that needs to be applied to the sample cell to maintain isothermal conditions with respect to the reference cell. (B) shows the heat evolved from each $MgCl_2$ injection per mole of Mg^{2+} (obtained from integrating the individual heat pulses of the upper panel) versus the molar ratio of Mg^{2+} to ATP, i.e. $[Mg^{2+}]/[ATP]$. The solid line in the lower panel represents a fit of a 1:1 binding model to the data. The fit yields a Mg^{2+}-ATP binding constant, K_M, of 1.41 (± 0.06) x 10^4 M^{-1}. The other thermodynamic parameters derived from the fit are ΔH = 75 (± 2) kJ mol^{-1}, ΔG = -23.6 (± 0.1) kJ mol^{-1} and ΔS = 331 (± 5) J K^{-1} mol^{-1}.

The data can be explained by a simple 1: 1 binding equilibrium:

$$Mg^{2+} + ATP^{4-} \leftrightarrow MgATP^{2-}$$

Fitting of the data to this binding model yielded the following values: K_M = 1.41 (± 0.06) x 10^4 M^{-1} and ΔH = 75 (± 2) kJ mol^{-1}. From these fit parameters one can also calculate that ΔG = -23.6 (± 0.1) kJ mol^{-1} and ΔS = 331 (± 5) J K^{-1} mol^{-1}. Binding of Mg^{2+} by ATP is thus an endothermic reaction under these conditions.

Because ATP can undergo protonation, e.g. formation of the $HATP^{3-}$ species, and because it can also complex Na^+ ions in competition with Mg^{2+}, the value of K_M is very dependent on the pH and the NaCl concentration. Taking both of these effects into account as described by O'Sullivan and Smithers[133] yields a theoretical apparent value of K_M of 2.1 x 10^4 M^{-1} at pH 7.4 and 130 mM NaCl. This value agrees quite well with the experimental value determined here.

4.2.2 Heat signals due to ATP binding to the Na^+,K^+-ATPase

The determination of the dissociation constant for ATP to the Na^+,K^+-ATPase relies on the measurement of the heat of binding of ATP to the enzyme. Any subsequent reactions which might also produce or consume heat and which could, furthermore, perturb the ATP binding equilibrium must be excluded. It is therefore important that enzyme phosphorylation and ATP hydrolysis be prevented. In principle this can be done by removing all traces of Mg^{2+} and Ca^{2+} from the buffer solution, because both ions are capable of acting as ATP cofactors enabling phosphoryl transfer from ATP to the enzyme. In the first instance, therefore, an ATP titration was carried out using a buffer containing 5 mM of the divalent metal ion chelator EDTA. However, the heat signals associated with ATP injection showed a slow return to baseline following the initial exothermic heat pulse in **Fig. 4.2 (A)**. This slow return to baseline is not typical of a simple binding reaction. ATP binding alone would be expected to be very rapid, with equilibration occurring on a subsecond timescale[131, 134, 135].

Therefore, it appears that some other reaction is occurring. The slow return to baseline also causes technical difficulties. If one is to calculate a dissociation constant, the area under each heat pulse must be integrated to obtain the total heat evolved following each injection.

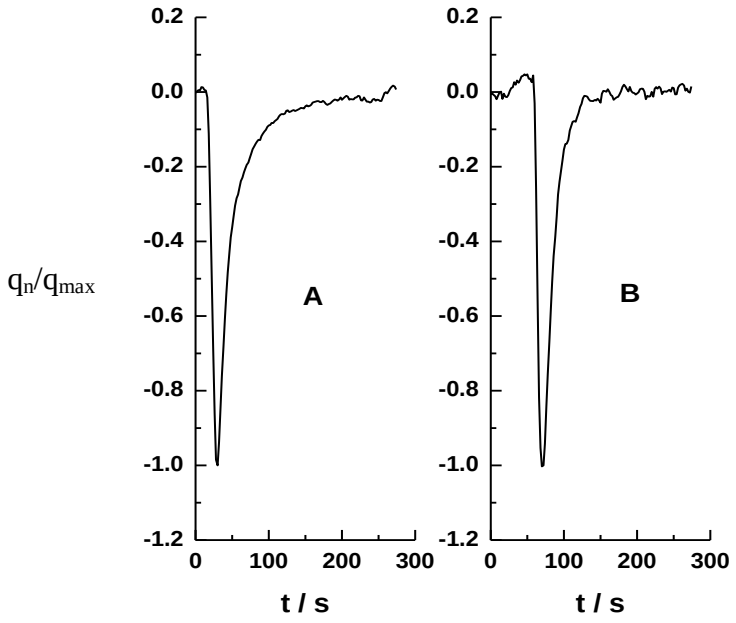

Figure 4.2: Heat signals associated with the injection of ATP into a suspension of shark Na^+,K^+-ATPase in a 30 mM imidazole buffer (pH 7.4) containing 5 mM EDTA (A) or 5 mM EDTA and 1 mM ouabain (B). The signals have been normalized for comparison. The buffer also contained 130 mM NaCl in each case. Both measurements were recorded at 24°C.

The slow return to baseline makes the actual locating of the baseline very difficult. In order to do this it was found that one had to wait for long periods of time, i.e. up to an hour, between each injection. Under these circumstances the danger exists that the protein might undergo denaturation over the course of a titration, which could last up to 24 hours. Therefore, it was crucial to locate the origin of the slow return to baseline and prevent it.

In a second ATP titration 1 mM of the specific Na^+,K^+-ATPase inhibitor ouabain was included in addition to 5 mM EDTA in the buffer solution **(Fig. 4.3)**. Ouabain is known to

inhibit the Na^+,K^+-ATPase by binding to a phosphorylated intermediate of the enzyme (E_2P) and blocking the enzyme cycle by preventing dephosphorylation[70, 131, 136]. It does not prevent ATP binding or enzyme phosphorylation (Clarke, unpublished stopped-flow data), but it does prevent enzyme cycling by competing with K^+ ions and blocking the enzyme in the E_2P state.

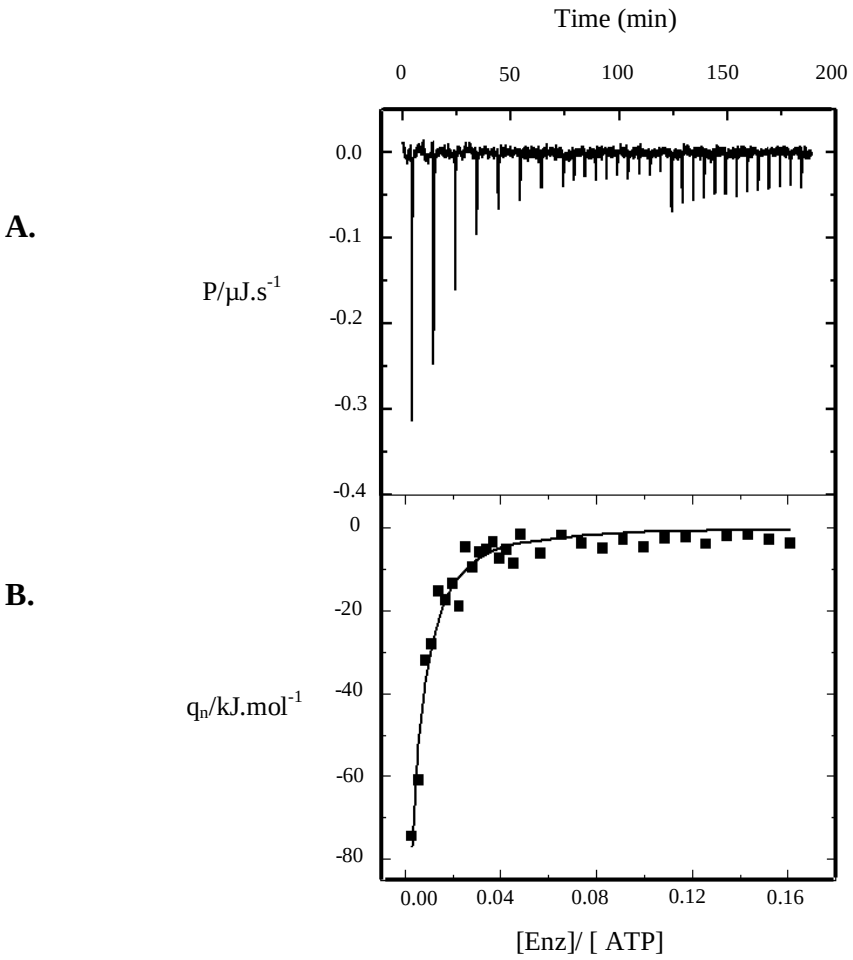

Figure 4.3: Titration of shark Na^+,K^+-ATPase-containing membrane fragments from shark rectal gland with ATP. The initial concentration of Na^+,K^+-ATPase in the ITC cell was 13.7 µM. The buffer of both the Na^+,K^+-ATPase suspension and the ATP solution contained 130 mM NaCl, 5 mM EDTA, 1 mM ouabain and 30 mM imidazole, pH 7.4. The experiment was conducted at 24°C. The upper and lower panels have the same meaning as for Fig. 4.2 except that q_n is here the heat evolved per mole of ATP injected. The negative value of P indicates heat evolution, i.e. an exothermic reaction. The increase in the power of the heat pulses at 125 min is due an increase in the injection volume at this point in order to saturate the available ATP sites. The solid line in the lower panel represents a fit of a binding model with one class of sites to the data. This model is similar to the monomer model described in the appendix, except that the possibility of a variable number of ATP binding sites per enzyme molecule was included to take into account the possibility of inaccessible sites. The fit yields an ATP dissociation constant, K_d, of 0.27 (± 0.09) µM.

Under these conditions it was found that the slow return to baseline was completely eliminated as shown in **Fig. 4.2 (B)**. Much sharper heat pulses were observed. This indicates that the slow return to baseline observed in the previous titration must have been due to Na^+,K^+-ATPase activity, and, more precisely, continuing ATP hydrolysis due to enzyme cycling. Furthermore, if it is true that enzyme phosphorylation can only occur in the presence of Mg^{2+} or Ca^{2+} ions, the results of these two titrations indicate that in the first titration 5 mM EDTA must not have been sufficient to completely remove all divalent metal ions from the buffer solution. Some trace amounts must still have been present to allow some enzyme cycling to continue, although at a low rate.

To improve the situation further it was considered replacing EDTA with CDTA. CDTA is also a divalent metal ion chelator, but it has a higher intrinsic binding constant for Mg^{2+} and Ca^{2+} than EDTA[137]. To test whether this is also the case for the apparent binding constant for Mg^{2+} under our buffer conditions of 130 mM NaCl and pH 7.4, ITC titrations of both EDTA and CDTA with $MgCl_2$ were carried out **(see Figs. 4.4 and 4.5)**. In fact it was found that EDTA appears to bind Mg^{2+} more strongly than CDTA under our experimental conditions. For EDTA a $[Mg^{2+}]$/[EDTA] ratio of approximately 3 is sufficient to completely saturate all of the EDTA with Mg^{2+} ions. In the case of CDTA one must continue the titration to a $[Mg^{2+}]$/[CDTA] ratio of greater than 8 to achieve the same level of saturation.

A further experimental finding from the titration of enzyme with ATP in the presence of EDTA (but in the absence of ouabain) was that the slow return to baseline became more pronounced as the titration proceeded and the ATP concentration increased. This can easily be explained by competition between EDTA and ATP for the trace amounts of Mg^{2+} available. By including 1 mM ouabain in the buffer medium, however, any small amount of

phosphorylated enzyme that is produced is blocked in the phosphorylated state and doesn't continue cycling.

A.

B.

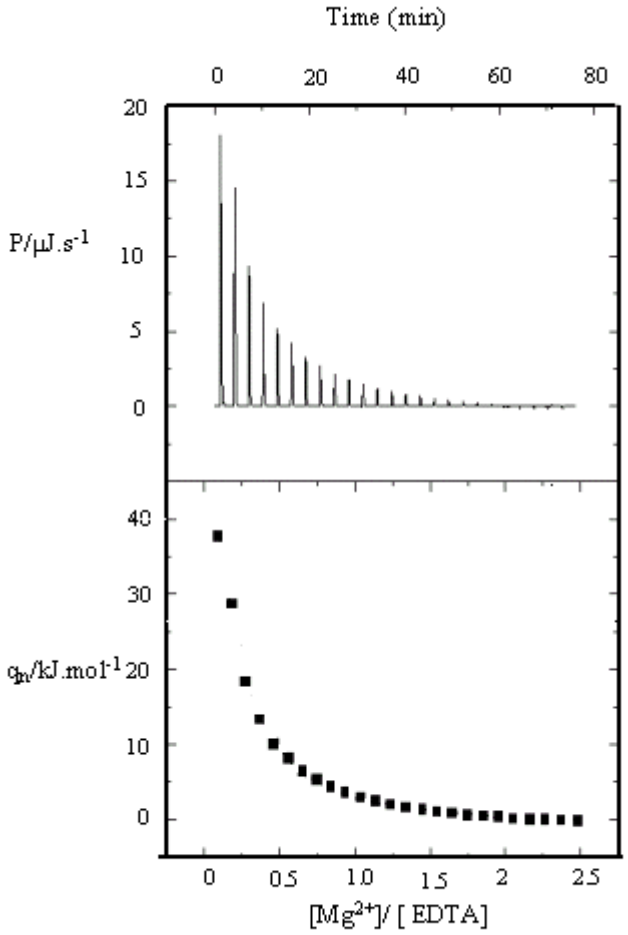

Figure 4.4: Titration of EDTA with $MgCl_2$. The initial concentration of EDTA in the ITC cell was 0.25 mM. The buffer of both the EDTA and the $MgCl_2$ solutions contained 130 mM NaCl and 30 mM imidazole, pH 7.4. The experiment was conducted at 24°C. (A) shows the power, P, in μJ s^{-1} that needs to be applied to the sample cell to maintain isothermal conditions with respect to the reference cell. (B) shows the heat evolved from each $MgCl_2$ injection per mole of Mg^{2+} (obtained from integrating the individual heat pulses of the upper panel) versus the molar ratio of Mg^{2+} to EDTA, i.e. $[Mg^{2+}]$/[EDTA].

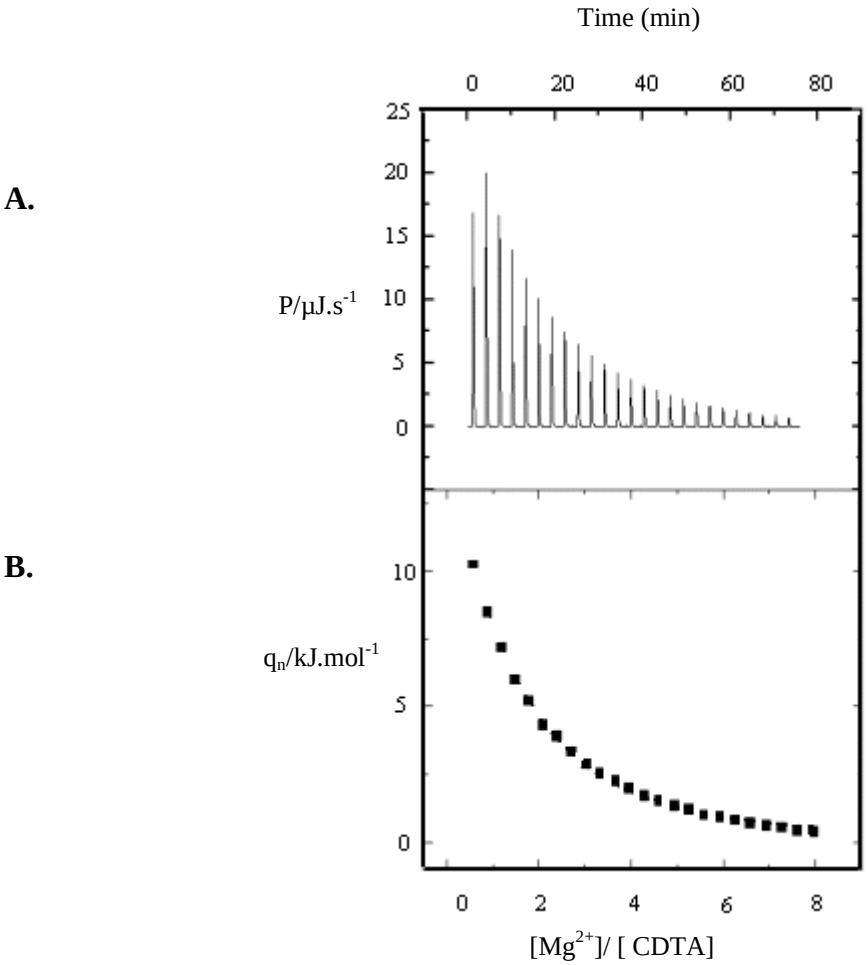

Figure 4.5: Titration of CDTA with $MgCl_2$. The initial concentration of CDTA in the ITC cell was 0.25 mM. The buffer of both the CDTA and the $MgCl_2$ solutions contained 130 mM NaCl and 30 mM imidazole, pH 7.4. The experiment was conducted at 24°C. (A) shows the power, P, in µJ s^{-1} that needs to be applied to the sample cell to maintain isothermal conditions with respect to the reference cell. (B) shows the heat evolved from each $MgCl_2$ injection per mole of Mg^{2+} (obtained from integrating the individual heat pulses of the upper panel) versus the molar ratio of Mg^{2+} to CDTA, i.e. $[Mg^{2+}]/[CDTA]$.

4.2.3 Binding of ATP to the Na^+,K^+-ATPase

The results of a titration of shark Na^+,K^+-ATPase with ATP in a pH 7.4 30 mM imidazole buffer containing 5 mM EDTA and 1 mM ouabain are shown in **Fig. 4.3**. A simple binding model with one class of sites was fitted to the data, leading to an apparent ATP dissociation constant of 0.27 (± 0.09) μM. This value agrees well with previously reported values using other techniques[122-124]. Unfortunately a reliable value of the enthalpy of binding could not be determined, because of insufficient data points at low ATP: enzyme molar ratios. However, from the initial data point of the titration one would expect ΔH to be of the order of – 75 kJ mol^{-1}.

4.3 Discussion and conclusion

The isothermal titration calorimetric data presented here indicate that ATP can bind exothermically to the E1 conformation of the Na^+,K^+-ATPase with a dissociation constant of 0.27 (± 0.09) μM. This value is consistent with previous studies using other methods[121-124]. Under the same pH and ionic strength conditions Mg^{2+} was found to bind to ATP in free solution with a dissociation constant of 71 (± 3) μM. Together the data obtained allows an analysis of the question of the effect that Mg^{2+} would be expected to have on ATP binding in pre-steady-state kinetic measurements if the enzyme existed prior to mixing with ATP in a monomeric form, i.e. αβ protomer. This analysis is presented in the following chapter..

Chapter 5

Model Simulations of ATP Binding Assays

5.1 Introduction

In this chapter theoretical simulations of the degree of saturation of the ATP binding sites are presented based on the experimental data obtained in the previous chapter for the dissociation constants of ATP with the enzyme and Mg^{2+} with ATP. The aim of the simulations is to find a mechanistic model of ATP binding which is consistent with both equilibrium and pre-steady-state kinetic measurements.

5.2 Results

5.2.1 Model Simulations of the degree of saturation of the ATP sites

To test whether competition between free Mg^{2+} and enzyme for ATP could account for the different K_d values reported in the literature from equilibrium and pre-steady-state measurements, we have carried out simulations of the expected variation of the total saturation of the ATP sites, *S*, for a monomeric model in the presence and absence of Mg^{2+} ions. The results of the simulations are shown in **Fig. 5.1**. The equations used for the simulations are described in the Appendix.

The results of these simulations **(see Fig. 5.1)** show that a monomeric model in the absence of Mg^{2+} ions predicts a hyperbolic saturation curve of the ATP sites, with half-saturation occurring in the submicromolar range, in agreement with experimental observations[121-124]. One needs to be aware here that the actual half-saturating concentration depends on how the theoretical or experimental data are plotted. Strictly speaking one should

plot the percentage saturation of the ATP sites versus the free ATP concentration. If this is done, the half-saturating free ATP concentration exactly equals the K_d for ATP binding (in the case of the simulations 0.25 μM was the value used). More commonly, however, the percentage saturation is plotted against the total concentration of ATP because this is a more directly accessible quantity. Therefore, this is the way the simulations in **Fig. 5.1** have been plotted. The half-saturating total ATP concentration, however, doesn't equal K_d. In the monomer simulation the half-saturating total ATP concentration occurs at 0.59 μM, more than twice the actual K_d. Therefore, one needs to be wary of this fact when reporting K_d values or interpreting literature data.

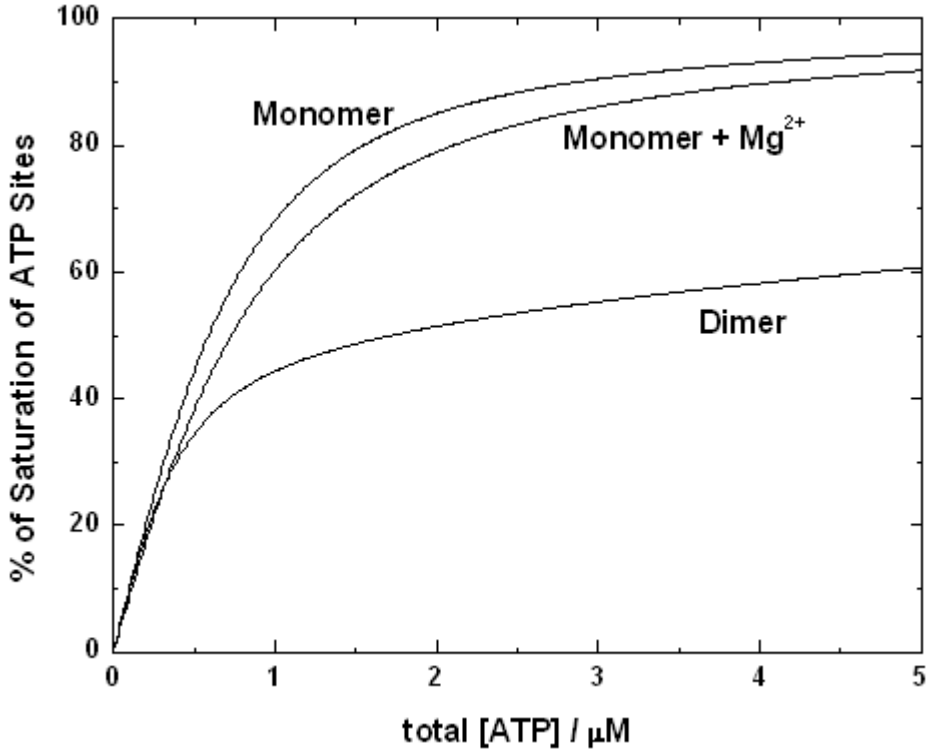

Figure 5.1: Simulated dependence of the percentages of saturation of the ATP sites of the Na^+,K^+-ATPase for a monomer model with and without the presence of Mg^{2+} ions and a cooperative dimer model. The percentage saturations are given by *S* (see the Appendix) multiplied by 100. The values of all the parameters used were: $K_1 = 4 \times 10^6\ M^{-1}$, $K_2 = 1.43 \times 10^5\ M^{-1}$, $K_M = 1.41 \times 10^4\ M^{-1}$ and $K_{MA} = 2.56 \times 10^6\ M^{-1}$. K_1 and K_2 represent the binding constants of the first and second ATP binding steps. The total protein concentration (i.e. the concentration of αβ protomers) used was 0.68 μM, which was chosen to agree with the conditions of the equilibrium titrations published[134]. For the monomer simulation with Mg^{2+} ions a Mg^{2+} concentration of 5 mM was used.

A significant difference between the conditions of equilibrium binding studies and pre-steady-state kinetic studies is that Mg^{2+} ions are excluded in equilibrium studies but included in pre-steady-state kinetic studies. Therefore, the possibility must be considered that the presence of Mg^{2+} ions could be modifying the enzyme's apparent ATP binding affinity and that this could account for the higher value of K_d generally observed in pre-steady-state kinetic studies. Certainly Mg^{2+} ions in the bathing solution could bind ATP and compete with the enzyme. This would be expected to increase the enzyme's apparent K_d for ATP. However, one must also consider that the enzyme could bind the $MgATP^{2-}$ complex. Simulations taking into account both of these effects have also been carried out and the results are shown in **Fig. 5.1**. The equations used are described in the Appendix.

There is some disagreement in the literature concerning the relative dissociation constants of free nucleotide and Mg-nucleotide complex for the enzyme. Campos and Beaugé[138] report K_d values of 1.52 μM and 0.36 μM for free ATP and $MgATP^{2-}$, respectively, i.e. they consider that the complex binds to the enzyme approximately a factor of 4 more strongly than free ATP. According to the data of Fedosova *et al.*[134], however, the Mg^{2+} complex of ADP should bind to the enzyme a factor of 1.6 more weakly than free ADP. Grell *et al.*[120] found that the affinity of ADP for the enzyme is reduced by a factor of 4 in the presence of 3 mM $MgCl_2$. Since there is no possible way that a Mg^{2+}-induced increase in ATP affinity could explain the lower affinity observed for ATP in pre-steady-state kinetic studies where Mg^{2+} is present, for the purposes of the simulations only the case that the $MgATP^{2-}$ complex binds to the enzyme more weakly than free ATP has been considered. The value of K_1 of 4×10^6 M^{-1} has been chosen based on previous measurements[82, 122, 134, 135] for the binding of free ATP. For the binding of the $MgATP^{2-}$ complex a value of K_{MA} of 2.56×10^6 M^{-1} has been used. This value is based on the 1.56 fold lower K_d found by Fedosova *et al.*[134] for the $MgADP^{2-}$ complex relative to free ADP.

The results of these calculations indicate that the presence of 5 mM Mg^{2+} would indeed be expected to increase the enzyme's apparent K_d for ATP. Based on the simulations shown in **Fig. 5.1** one would expect a half-saturating total ATP concentration of 0.73 μM, in comparison to 0.59 mM in the absence of Mg^{2+}. For these simulations the enzyme concentration used was 0.68 μM. This value was chosen to reproduce the conditions of the radioactivity-based equilibrium binding assay of Fedosova *et al.*[134]. If the enzyme concentration is reduced by a factor of 10 to reproduce the conditions of the fluorescence-based stopped-flow kinetic measurements of Kane *et al.*[130], corresponding simulations show that for monomeric enzyme in the presence of 5 mM $MgCl_2$ the expected half-saturating total ATP concentration would be 0.42 μM. This value is still more than an order of magnitude lower than the average value of K_d determined from pre-steady-state kinetic studies, i.e. approximately 8 μM. Therefore, a direct competition between Mg^{2+} and enzyme for ATP cannot explain the different ATP binding affinities observed in pre-steady-state kinetic and equilibrium studies.

5.2.2 ATP-induced conformational change

A possible mechanism which could in principle explain a lower K_d from equilibrium versus pre-steady state kinetic measurements is shown below:

$$E1 + ATP \leftrightarrow E1 \cdot ATP \leftrightarrow E1' \cdot ATP \rightarrow E2P$$

A mechanism such as this has been proposed by Jencks and co-workers[139, 140] based on quenched-flow measurements on sheep kidney Na^+,K^+-ATPase. The most important difference between this mechanism and the classical Albers-Post mechanism is that it includes a rate-limiting conformational change of the enzyme-ATP complex, $E1 \cdot ATP \leftrightarrow$

E'·ATP, prior to a rapid phosphoryl transfer reaction to produce the phosphoenzyme. Because the reaction E1·ATP ↔ E1'·ATP is assumed to be the rate-determining step, the maximum observed rate constant of phosphorylation when starting in the E1 state must be given by the rate constant of this reaction. Furthermore, the concentration of ATP required to achieve the half-saturating observed rate constant (i.e. K_d) must be given by the ATP concentration required to achieve half-saturation of the species immediately before the rate-determining step, i.e. E1·ATP. In contrast, in equilibrium ATP titrations one would measure the total degree of saturation of the enzyme with ATP, i.e. the sum of the degrees of saturation of E1·ATP and E1'·ATP. As long as the equilibrium constant of the reaction E1·ATP ↔ E1'·ATP is greater than 1, the apparent K_d determined by equilibrium titrations would be lower than that determined by pre-steady-state kinetic measurements, i.e. in agreement with experimental observations.

However, there are at least two pieces of evidence which contradict the attribution of the different K_d values from equilibrium and pre-steady-state kinetic measurements to such a mechanism. Firstly, if this mechanism were correct, then the maximum observed rate constant achievable for phosphorylation of the enzyme should depend on whether or not the enzyme is pre-incubated with ATP. If the E1·ATP ↔ E1'·ATP reaction is rate-determining when starting in the E1 state, then pre-equilibration with ATP such that the enzyme starts in E1'·ATP should lead to a significantly higher observed rate constant of phosphorylation. However, stopped-flow kinetic investigations of the formation of E2P using enzyme from both pig and rabbit kidney have shown that the maximum observed rate constant is always in the range 180-200 s^{-1}, whether the enzyme is pre-incubated with Na^+, ATP or Na^+ and ATP together[81]. A further argument against such a mechanism is that it predicts only a single ATP binding step. However, the careful analysis of the observed rate constants and the amplitudes of pre-steady-state kinetic data by a number of researchers have shown in fact that evidence

for two ATP binding steps can be detected[82, 141, 142]. For these reasons, a rate-determining conformational change of an enzyme-ATP complex must be rejected as an explanation of the difference in ATP binding behaviour observed in equilibrium and pre-steady-state kinetic measurements.

5.2.3 Model Simulations of the dependence of the percentage of enzyme in the E1ATP:E1ATP state for a cooperative dimer model.

If Mg^{2+} competition for ATP and a rate-determining conformational change of an enzyme-ATP complex are both rejected as possible explanations of the different K_d values observed for ATP from equilibrium and pre-steady-state kinetic measurements, the only reasonable remaining explanation is that there are in fact two ATP binding steps. Recently published crystal structures of P-type ATPases[61 143]show that there is only a single ATP binding site per α-subunit of the enzyme. Therefore, the only possibility for two ATP binding equilibria which is consistent with the crystal structures is anticooperative binding of two ATP molecules to an $(\alpha\beta)_2$ enzyme diprotomer. A mechanism describing this explanation is shown schematically below **(see Fig. 5.2)**.

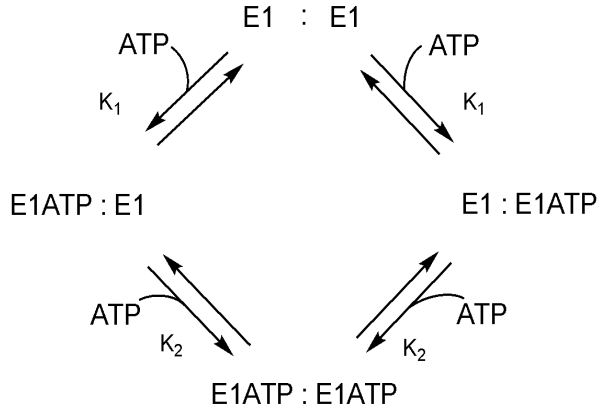

Figure 5.2: Cooperative dimer model of ATP binding. K_1 and K_2 represent the binding constants of the first and second ATP binding steps. The species E1ATP:E1 and E1:E1ATP are chemically equivalent, but they are included for statistical reasons (i.e. because E1:E1 has two available ATP binding sites). For anticooperative ATP binding $K_1 > K_2$.

In **Fig. 5.3** the result of a simulation of the degree of saturation of an enzyme dimer, S_{dim}, (i.e. the fraction of enzyme in the E1ATP:E1ATP state) as a function of the total ATP concentration based on this mechanism is shown.

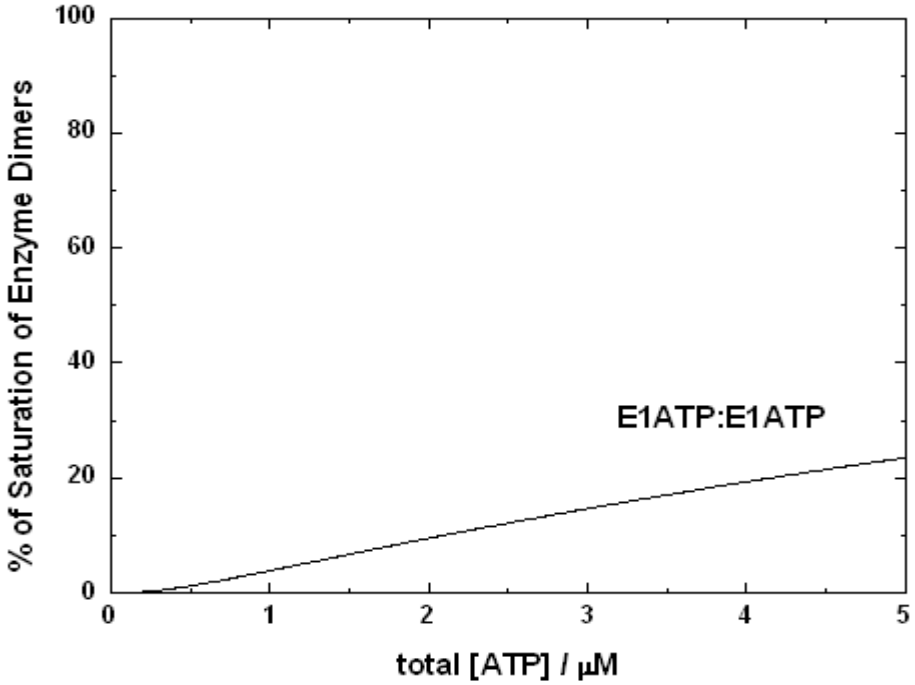

Figure 5.3: Simulated dependence of the percentage of enzyme in the E1ATP:E1ATP state for a cooperative dimer model. The percentage saturations are given by S_{dim} (see Appendix) multiplied by 100. The values of all the parameters used were: K_1 = 4 x 10^6 M^{-1} and K_2 = 1.43 x 10^5 M^{-1}. The total protein concentration (i.e. the concentration of αβ protomers) used was 0.68 μM, which was chosen to agree with the conditions of the equilibrium titrations published[134].

The equations used for the simulation are described in the Appendix. The graph shows that S_{dim} rises much more slowly with increasing ATP concentration than the total saturation of the ATP sites, *S*, for the same dimer model (cf. the Dimer curve in **Fig. 5.1**). This is, thus, consistent with the slower rise in the observed rate constant experimentally observed in pre-steady-state kinetic measurements relative to the rise in bound ATP observed in equilibrium titration experiments.

5.3 Discussion and conclusion

Simulations of the degree of saturation of the ATP sites for a monomeric enzyme model **(see Fig. 5.1)** showed that direct competition between Mg^{2+} and the enzyme cannot explain the differences observed between equilibrium and pre-steady-state kinetic results.

The simulations in **Figs. 5.1 and 5.3** are shown over the same ATP concentration range for ease of comparison. However, if one extends the simulations over a larger concentration range it is found that 50% of the enzyme is present as E1ATP:E1ATP at a total ATP concentration of 15 μM, whereas 50% of the ATP sites are occupied already at 1.7 μM. These numbers are based on a protein concentration of 0.68 μM, as used by Fedosova *et al.*[134]. If the enzyme concentration is reduced by a factor of 10 to reproduce the conditions of the pre-steady-state kinetic experiments of Kane *et al.*[130], the corresponding half-saturating total ATP concentrations are 14 μM for E1ATP:E1ATP and 1.4 μM for the ATP sites. The difference in the concentration range over which dimers are saturated by ATP as opposed to the concentration over which the ATP sites within a dimer are saturated can easily be explained if one considers the hypothetical case where half of all of the sites are occupied. Because in the dimer model the first ATP that binds to a dimer is assumed to bind with high affinity and the second with low affinity, dimers with only one ATP binding site occupied would form preferentially to dimers with both sites occupied. If one imagines a situation where every dimer has one ATP molecule bound, the total saturation of the sites would be 50%, but the percentage of completely saturated dimer would still be 0%. Thus, S_{dim} must rise more slowly than S for the dimer model.

The observed rate constant (or reciprocal relaxation time) found in pre-steady state kinetic studies of enzyme phosphorylation[125, 126, 128-130] shows an ATP concentration dependence which agrees very well with the ATP concentration dependence of S_{dim} shown here **(see Fig. 5.3)**. These studies have yielded a higher ATP dissociation constant than equilibrium binding

studies, i.e. 3.5-14 μM from pre-steady-state kinetic studies in comparison to 0.12-0.63 μM from binding studies. The higher ATP concentration required for saturation in pre-steady-state kinetic studies suggests, therefore, that the formation of a fully saturated enzyme dimer, E1ATP:E1ATP, is required for the maximum rate of phosphorylation, as previously suggested[82].

Based on the analysis presented here it seems most likely that the different ATP concentrations required for half-saturation in equilibrium and pre-steady-state kinetic studies is due to a different concentration dependence of the experimental observable, i.e. concentration of bound ATP or observed rate constant, respectively. In binding studies one is measuring the degree of total occupation of the enzyme's ATP binding sites, whereas in pre-steady-state kinetic studies the observed rate constant depends on the degree of occupation of an enzyme dimer. Both of these have different ATP concentration dependences **(cf. Figs. 5.1 and 5.3)**.

Recent crystal structure data[61] has shown that the structure of the Na^+,K^+-ATPase is very similar to that of its related enzyme, the Ca^{2+}-ATPase of sarcoplasmic reticulum. This provides strong support for the validity of comparisons between the two enzymes. Therefore, it is important at this stage to mention the work of Møller *et al.*[144] on the sarcoplasmic reticulum Ca^{2+}-ATPase. This enzyme occurs in the sarcoplasmic reticulum membrane with a high density and forms an aggregated state, similar to the Na^+,K^+-ATPase in the plasma membrane. Møller *et al.*[144] investigated the effect of protein-protein interactions on the enzyme's kinetics by comparing the kinetic behaviour of aggregated vesicular Ca^{2+}-ATPase and monomeric enzyme solubilised using the detergent $C_{12}E_8$. What they found was that detergent solubilisation decreased the enzyme's ATP affinity. For aggregated enzyme they measured an ATP K_d of 2 μM, whereas for monomeric enzyme they determined a K_d of 7 μM. This result suggests that, for the Ca^{2+}-ATPase, protein-protein interactions in the native membrane enhance the enzyme's affinity for ATP. The same could be true of the Na^+,K^+-

ATPase. This would imply that the low K_d of around 0.2 μM obtained from equilibrium titrations in the absence of Mg^{2+} actually corresponds to ATP binding to an $(\alpha\beta)_2$ protein dimer, whereas the high K_d of around 10 μM obtained from pre-steady-state kinetic studies is due to ATP binding to disaggregated protein monomers, i.e. individual αβ protomers. The conformational change of the enzyme which brings about the change in the enzyme's ATP affinity could then be attributed to protein disaggregation within the membrane.

There are both kinetic and structural data which would support such a conclusion. First of all, in the two gear pumping model which it was recently demonstrated[82] could explain stopped-flow kinetic data over an ATP concentration range of approximately 5 orders of magnitude, the higher gear of pumping following binding of ATP to both αβ protomers of the $(\alpha\beta)_2$ diprotomer involved a synchronous pumping by each αβ protomer. The simplest way that each αβ protomer could pump with the same rate constant would be if they were completely independent of one another, i.e. disaggregated with no interactions between them **(Fig. 5.4)**. Protein disaggregation following ATP binding is also supported by x-ray crystal structural data obtained on the Ca^{2+}-ATPase. Olesen *et al.*[143] have shown that an important role of ATP in the function of P-type ATPases, apart from phosphorylating the enzyme, is to maintain the cytoplasmic domains in a compact closed conformation.

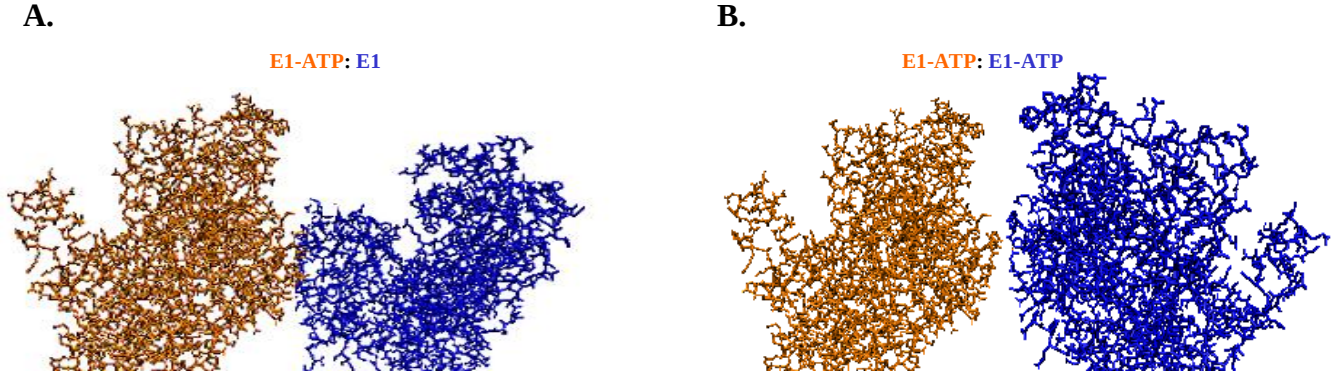

Figure 5.4: Conformational hypothesis of α-subunits of the dimer of Na^+, K^+-ATPase in the presence of one or two ATP molecules to explain the two different rates of pumping for the Na^+, K^+-ATPase when bound to one or two ATP molecules. **A:** one of the monomer's site is occupied by 1 ATP and the other is empty. **B:** both sites of the monomers are occupied. In state A the cytoplasmic domains of the two Na^+,K^+-ATPase molecules interfere with one another. In state B there is no interaction between the cytoplasmic domains.

In the absence of ATP the cytoplasmic domains of the E1 conformation are much more widely spread and, because of the high density of these enzymes in specialized membranes such as in the kidney and the shark rectal gland used here, this could easily lead to protein-protein interactions within the membrane and consequent changes in nucleotide binding affinity.

Chapter 6

Role of Mg^{2+} in the Na^+,K^+-ATPase Mechanism

6.1 Introduction

In animals, an important role of Mg^{2+} is as a cofactor of ATP and other nucleotides when they bind to proteins. In the case of ATP, the Mg^{2+} ion is complexed by the negatively charged oxygens of its phosphate groups. The Mg^{2+} is, thus, thought to help shield the negative charges of the phosphates, allowing reaction with the electron pairs of attacking groups and facilitating phosphoryl transfer[145]. One of the most important enzymes where this is the case is the Na^+,K^+-ATPase.

Although there have been a number of research groups who have investigated the role of Mg^{2+} in the function of the Na^+,K^+-ATPase[138, 145-151], much more work has focussed on the transported ions, Na^+ and K^+. The aim of the present chapter is to provide reliable data on the strength of binding of Mg^{2+} ions to the Na^+,K^+-ATPase and its role in the enzyme's mechanism. A difficulty in studying Mg^{2+} interaction with the Na^+,K^+-ATPase under physiological conditions, i.e. in the presence of ATP and Na^+ ions, is that it immediately induces phosphorylation, so that Mg^{2+} binding cannot be separated from the subsequent phosphorylation reaction. This precludes equilibrium binding studies. Therefore, one must use a kinetic approach. From steady-state kinetic studies one could obtain a K_m value for Mg^{2+} ions. However, under steady-state conditions the K_m value would be influenced by the rate constants and equilibrium constants of the entire reaction cycle of the enzyme, and it would not give an accurate reflection of the strength of binding of Mg^{2+}. Therefore, here a pre-steady-state kinetic technique (stopped-flow spectrofluorimetry) has been applied. In order to follow the kinetics of the enzyme the voltage-sensitive fluorescent probe RH421 was

utilised. This technique has previously been employed by Pratap and Robinson[151] to study the Mg^{2+} concentration dependence of the kinetics of enzyme phosphorylation and conformational changes. However, Kane *et al.*[130] later showed that the concentration of RH421 Pratap and Robinson[151] used for their studies was at an enzyme inhibitory level. Furthermore, with improved sensitivity of detection Kane *et al.*[130] found that it was possible to detect two kinetic processes in such experiments[131]. Therefore, in this chapter the effect of Mg^{2+} ions on the kinetics of enzyme phosphorylation and subsequent conformational changes has been re-investigated by the stopped-flow technique. Furthermore, together with data obtained under the same experimental conditions for Mg^{2+} binding to ATP (see Chapter 4), this allows one to analyse the question of the relative contributions of the enzyme and ATP in binding Mg^{2+} in the enzyme-ATP-Mg^{2+} complex. In the case of the E1 conformation of the enzyme, it will be shown here that, although the enzyme environment is definitely important for the catalysis of phosphoryl transfer from ATP, it is ATP itself which is totally responsible for Mg^{2+} binding.

6.2 Results

6.2.1 Rates of ATP-induced stopped-flow fluorescence traces

On mixing shark rectal gland Na^+,K^+-ATPase-containing membrane fragments labeled with RH421 with Na_2ATP (as described under Materials and Methods), an increase in fluorescence occurred **(see Fig. 6.1)**. Two exponential time functions were required to fit the data. The faster phase constituted on average 80 % of the overall amplitude and the slower phase 20 %.

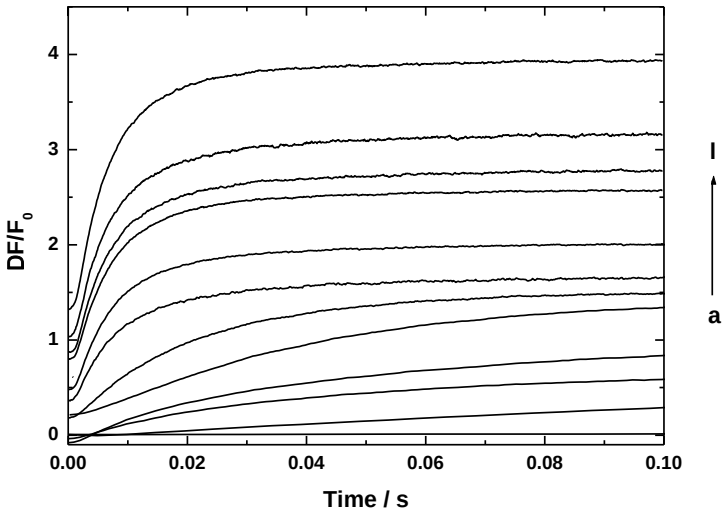

Figure 6.1: Stopped-flow fluorescence transients of Na^+,K^+-ATPase from shark rectal gland noncovalently labelled with RH421 (100 nM, after mixing). Na^+,K^+-ATPase (40 µg/ml or 270 nM, after mixing) was rapidly mixed with an equal volume of a solution containing Na_2ATP (1 mM, after mixing). Both the enzyme suspension and the Na2ATP solutions were prepared in a buffer containing 130 mM NaCl, 30 mM imidazole and either 5 mM EDTA or varying concentrations of $MgCl_2$ (pH 7.4, 24 °C). The traces have been labelled in order of increasing fluorescence intensity change. Curve a corresponds to a control experiment in the presence of 5 mM EDTA and no added $MgCl_2$. Curves b-l correspond to the following $MgCl_2$ concentrations: b) 0.0025 mM, c) 0.01 mM, d) 0.15 mM, e) 0.2 mM, f) 0.4 mM, g) 1.0 mM, h) 2.0 mM, i) 2.5 mM, j) 3.5 mM, k) 4.5 mM and l) 5.0 mM, respectively. The fluorescence of membrane-bound RH421 was measured at an excitation wavelength of 577 nm at emission wavelengths of ≥ 665 nm (RG665 glass cutoff filter).

As the $MgCl_2$ concentration of the enzyme suspension and the ATP solution was increased, the overall kinetics of the fluorescence change became faster until a saturating limit was reached, which was characterized by a reciprocal relaxation time of ~190-200 s^{-1} for the faster phase **(see Fig. 6.2)** and ~45-50 s^{-1} for the slower phase **(see Fig. 6.3)**. The fact that the kinetics of both phases saturate at constant values implies that the overall rate-determining step for each process is a first-order reaction (i.e. phosphorylation or an enzyme conformational change).

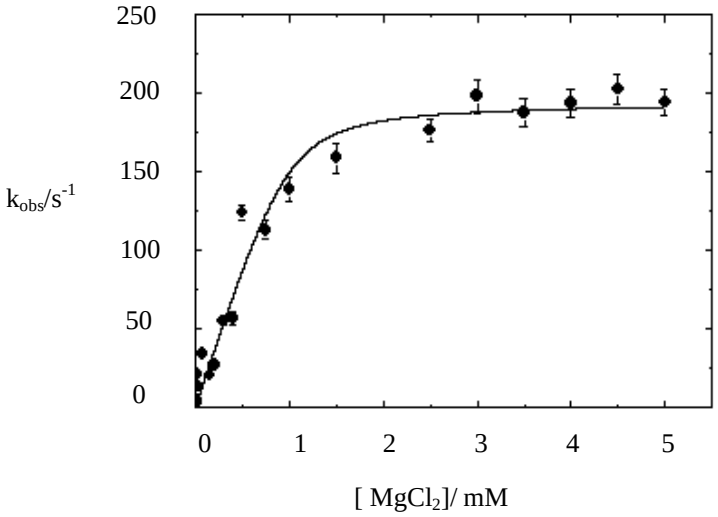

Figure 6.2: Dependence of the observed rate constant, k_{fast}^{obs}, of the fast phase of the RH421 fluorescence change on the concentration of $MgCl_2$ (after mixing) for stopped-flow experiments in which Na^+,K^+-ATPase was rapidly mixed with Na_2ATP. All of the experimental parameters were as described in the caption to Fig. 6.1. The solid line represents a nonlinear least-squares fit of the data to Eq. 5 and Eqs. 16 – 19. The calculated fit parameters were: k_1 = 195 (± 6) s^{-1} and K_E = 1.45 (± 0.22) x 10^4 M^{-1}. K_E corresponds to a dissociation constant, K_d, of 0.069 (± 0.010) mM.

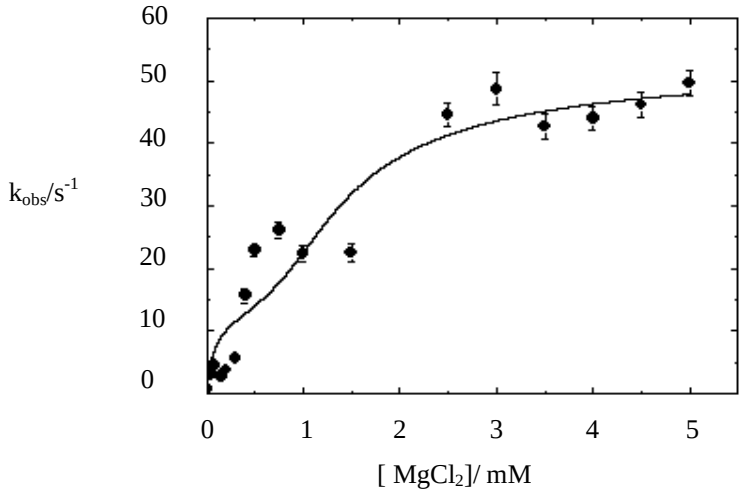

Figure 6.3: Dependence of the observed rate constant, k_{slow}^{obs}, of the slow phase of the RH421 fluorescence change on the concentration of $MgCl_2$ (after mixing) for stopped-flow experiments in which Na^+,K^+-ATPase was rapidly mixed with Na_2ATP. All of the experimental parameters were as described in the caption to Fig. 6.1. The solid line represents a nonlinear least-squares fit of the data to Eq. 10 and Eqs. 16 – 21. The calculated fit parameters were: k_4^{min} = 13 (± 4) s^{-1}, k_4^{max} = 74 (± 10) s^{-1}, K_F = 1.26 (± 0.8) x 10^3 M^{-1}. K_F corresponds to a dissociation constant, K_d, of 0.8 (± 0.5) mM.

The slower kinetics observed under nonsaturating Mg^{2+} concentrations implies that both first-order reactions are preceded by Mg^{2+} binding, i.e., the first-order reactions are preceded by Mg^{2+} binding. Therefore, any reaction scheme in which Mg^{2+} binding occurs subsequent to a slow conformational change can be excluded as a possible mechanism.

A control experiment in which 5 mM EDTA and no $MgCl_2$ were included in the buffer resulted in almost the complete disappearance of the fluorescence change **(see Fig. 6.1)**. In previous studies[130] it was shown that if 30 mM sodium orthovanadate was added to the drive syringe containing the Na^+,K^+-ATPase membrane fragments, the fluorescence change also completely disappeared. These control experiments indicate that the observed fluorescence changes are in fact due to the hydrolytic action of the Na^+,K^+-ATPase.

Based on previous studies[142, 151, 152], it is known that RH421 responds to the formation of the E2P state with an increase in fluorescence. The fast phase of the fluorescence transients observed can, therefore, confidently be attributed to the reaction $E1MgATP(Na^+)_3 \rightarrow E2MgP + 3Na^+ + ADP$. The maximum observed relaxation time for the fast phase (195 (± 6) s^{-1}) agrees well with rate constants determined[130, 149, 153] for enzyme phosphorylation using the quenched-flow technique and radioactively labelled ATP, which yield values of the order of 200 s^{-1}. Phosphorylation can thus be considered as the rate-determining step for the reaction sequence responsible for the fast fluorescence phase.

The origin of the slow phase has been previously considered in detail[126]. Based on additional stopped-flow measurements and theoretical simulations it was attributed to a relaxation of the dephosphorylation/rephosphorylation equilibrium. The meaning of this requires some explanation. In the absence of K^+ ions, as in the experiments performed here, dephosphorylation of the E2MgP species is slow, but it still occurs. Measured rate constants[131, 138, 153, 154] are in the range 2-7 s^{-1}. Following dephosphorylation, because excess ATP is present, the enzyme can undergo a conformational transition back to the E1 state and

be rephosphorylated by ATP, i.e. E2 → E1(Na^+)$_3$ + ATP → E2P + 3Na^+ + ADP (Mg^{2+} ions would also be bound to the protein, but they have been omitted here for simplicity). The rate-determining step in this rephosphorylation pathway is the conformational transition, E2 → E1(Na^+)$_3$, which based on previous measurements[81, 82] using enzyme from rabbit or pig kidney would be expected to have a rate constant in the range 65-90 s^{-1} at saturating Na^+, Mg^{2+} and ATP concentrations. Based on the Van Slyke approximation[155], the reciprocal of the overall expected rate constant for the entire pathway from E2 to E2P via ATP rephosphorylation is given by the sum of the reciprocal of the rate constants of the separate reaction steps, E2 → E1(Na^+)$_3$ and E1(Na^+)$_3$ + ATP → E2P + 3Na^+ + ADP. Taking values of 65-90 s^{-1} for the first reaction and the value of 195 s^{-1} measured here for the fast phase for the second, yields an overall expected rate constant in the range 49-62 s^{-1}.

Enzyme dephosphorylation and rephosphorylation via ATP, therefore, represent a coupled equilibrium which must relax subsequent to the initial phosphorylation of the enzyme by ATP. According to kinetic theory the reciprocal relaxation time for the relaxation of any first order or pseudo-first order process is simply given by the sum of the forward and backward rate constants. Therefore, adding the rate constants given above for dephosphorylation and rephosphorylation yields an expected reciprocal relaxation time of 51-69 s^{-1}. The observed rate constant measured here of 45-50 s^{-1} for the slow phase at a saturating $MgCl_2$ concentration is slightly below this range, but this small difference could be explained by the different source of the enzyme, i.e. shark rectal gland in comparison to pig or rabbit kidney for the previous studies on which this calculation was based.

Further evidence[131] supporting the assignment of the slow phase to the relaxation of the dephosphorylation/rephosphorylation equilibrium comes from measurements in which 7 mM KCl was included in the buffer prior to mixing with ATP. Under these conditions an increase in fluorescence was still observed, but the fluorescent transient was then

monoexponential. This can be explained by an acceleration of the dephosphorylation reaction by K^+ ions. The rate constant for K^+-stimulated dephosphorylation has been estimated based on stopped-flow measurements[82, 156] to have a value of around 312 s^{-1}. Adding this value to the rate constant for rephosphorylation given above (49-62 s^{-1}), then yields an expected observed rate constant for relaxation of the dephosphorylation/rephosphorylation equilibrium of 361-374 s^{-1}. This is far greater than the maximum reciprocal relaxation time found here for the fast phase due to initial ATP phosphorylation of 195 (±6) $^{-1}$. Therefore, under K^+-saturating conditions the dephosphorylation/rephosphorylation equilibrium would be expected to relax instantaneously on the time-scale of the initial phosphorylation, which is consistent with the experimental observation of only a single phase under these conditions.

6.2.2 Amplitudes of ATP-induced stopped-flow fluorescence traces

The total amplitudes of the fluorescence change, $\Delta F/F_0$, are shown in **Fig. 6.4**. $\Delta F/F_0$ was found to increase approximately linearly with increasing Mg^{2+} concentration.

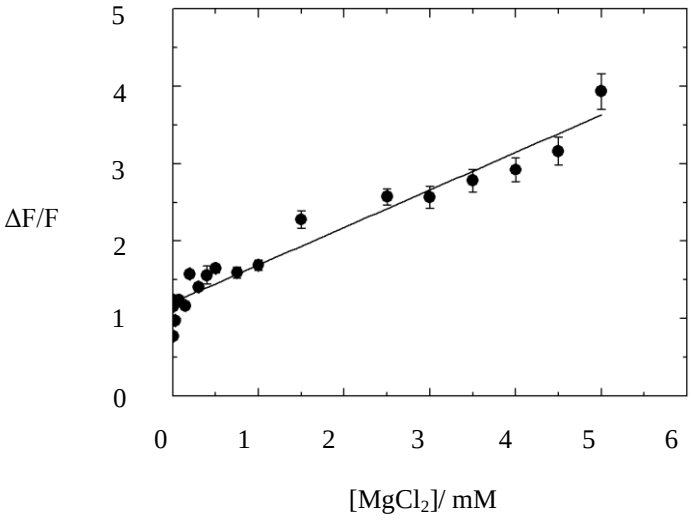

Figure 6.4: Dependence of the total amplitude, $\Delta F/F_0$, (i.e. the fast phase plus the slow phase) of the RH421 fluorescence change on the concentration of $MgCl_2$ (after mixing) for stopped-flow experiments in which Na^+,K^+-ATPase was rapidly mixed with Na_2ATP. All of the experimental parameters were as described in the caption to Fig. 6.1. The solid line represents a least-squares fit of the data to a straight line. The calculated fit parameters were: y-intercept = 1.21 (± 0.06) and slope = 0.48 (± 0.03) mM^{-1} (r^2 = 0.95). Within experimental error the fitted curve passed through the origin.

At very low Mg^{2+} concentrations it appears that there is a more rapid increase (perhaps hyperbolic) in $\Delta F/F_0$ with increasing Mg^{2+} concentration which is overlayed by the linear increase. A rapid increase in $\Delta F/F_0$ at low Mg^{2+} concentrations makes sense, because in the absence of Mg^{2+} ions no phosphorylation by ATP can occur at all.

Because RH421 responds to the formation of the E2P state with an increase in fluorescence[142, 151, 152] the increase in fluorescence amplitude observed here with increasing Mg^{2+} concentration could be due to an increase in the rate of E2P formation relative to the rate of E2P breakdown with increasing Mg^{2+} concentration.

Another explanation could be that Mg^{2+} increases the accessibility of the enzyme towards phosphorylation by ATP.

A third explanation could be that increasing Mg^{2+} concentrations increases the sensitivity of RH421 towards E2P formation. The kinetic results shown in **Fig. 6.2** clearly demonstrate that the rate of formation of E2P is accelerated by Mg^{2+} ions. However, the other two explanations of ATP accessibility and RH421 sensitivity may also be contributing to the fluorescence amplitude increase.

6.2.3 Mg^{2+}-dependence of the degree of phosphorylation

To resolve the question of the origin of the Mg^{2+}-induced linear increase in $\Delta F/F_0$ observed in the stopped-flow experiments **(see Fig. 6.4)**, direct measurements of the degree of phosphorylation of the Na^+,K^+-ATPase by radioactively labelled ATP at varying Mg^{2+} concentrations were carried out by Prof. Flemming Cornelius (University of Aarhus, Denmark). The results obtained (data not shown) show that the degree of phosphorylation does indeed increase with the concentration of Mg^{2+}, i.e. consistent with the results of **Fig. 6.2** showing an increase in the rate of formation of E2P. However, the degree of phosphorylation reaches a saturating level at a $MgCl_2$ concentration of around 0.5 mM,

whereas $\Delta F/F_0$ continues to rise linearly up to at least 5 mM **(see Fig. 6.4)**. Therefore, the dependence of $\Delta F/F_0$ on Mg^{2+} can't be explained by an increased phosphorylation level. The only reasonable explanation would appear to be that the sensitivity of RH421 towards E2P formation increases with the Mg^{2+} concentration. This could possibly be caused by Mg^{2+} binding to the lipid phase of the membrane, to which the dye is also sensitive[157].

It is worth noting that half-saturation of the level of phosphoenzyme occurs at a Mg^{2+} concentration of the order of 10 μM. This is much lower than the half-saturating concentration observed for the observed rate constant for the fast phase **(see Fig. 6.2)**, which occurs at approximately 1 mM. One reason for this is that a lower ATP concentration of 25 μM was used for the radioactivity measurements in comparison to 1 mM for stopped-flow. This would decrease competition for the available Mg^{2+} from unbound ATP in solution (discussed in more detail later). However, a more fundamental reason for the difference is that the half-saturating Mg^{2+} concentration observed in the measurements of the phosphoenzyme level depends not only on the strength of binding of Mg^{2+} to the enzyme but also on the relative rates of enzyme phosphorylation and dephosphorylation under the experimental conditions used. Because phosphorylation is known to be much faster than dephosphorylation under these conditions[131, 158], the phosphoenzyme level saturates at a concentration far below that which would be expected based alone on the dissociation constant of Mg^{2+} for the enzyme.

6.2.4 Model simulations of the stopped-flow fluorescence transients

In order to gain a deeper understanding of the $MgCl_2$ concentration dependence of the observed kinetic behaviour computer simulations of the fluorescence transients were carried

out. These were based on the assignment of the fast and slow kinetic phases described above. Accordingly, the sequence of reaction steps used was:

$$E1MgATP(Na^+)_3 \xrightarrow{k_1} E1MgP(Na^+)_3 \qquad (1)$$

$$E2MgP(Na^+)_3 \underset{k_{-2}}{\overset{k_2}{\rightleftharpoons}} E2MgP + 3Na^+ + ADP \qquad (2)$$

$$E2MgP \underset{k_{-3}}{\overset{k_3}{\rightleftharpoons}} E2Mg \qquad (3)$$

Remember that k_{-3} represents the rate constant for rephosphorylation of the enzyme by continuing around the enzymatic cycle via E1 and undergoing phosphorylation by ATP; it is not the rate constant for "back-door" phosphorylation by inorganic phosphate. Reaction (3) thus actually represents the entire Albers-Post-cycle as a single equilibrium. Reaction (2) describes the Na^+ binding equilibrium to the E2P state. Reaction (1) is required for the initial turnover of the enzyme after mixing with ATP. For subsequent turnovers this reaction is incorporated in the reverse direction of reaction (3).

Simulations based on this model show that a biphasic fluorescence increase is expected as long as the fluorescence of dye associated with enzyme in the E2Mg state is greater than that of dye associated with the initial $E1MgATP(Na^+)_3$ state. This agrees with the results of previous stopped-flow experiments showing that the fluorescence of RH421 decreases when the enzyme undergoes the transition from the E2 state to the $E1(Na^+)_3$ state[131, 159, 160]. In fact, as shown previously[126], a biphasic fluorescence increase would also be expected for a mechanism involving only reactions (1) and (3), i.e. ignoring Na^+ dissociation from the $E2MgP(Na^+)_3$ state. This would require the fluorescence level of the E2 state to be greater than that of the E2MgP state. However, since evidence exists[152, 154, 161] that fluorescence changes of RH421 associated with the Na^+,K^+-ATPase arise predominantly

from steps involving ion binding to or release from the enzyme, the complete reaction scheme (1)-(3) has been used here.

Based on the simulations the observed two phase-fluorescence increase can be understood as follows. Initially the enzyme is in the low fluorescent state E1MgATP$(Na^+)_3$. The fast phase of the fluorescence increase on mixing with ATP can be explained by phosphorylation of the enzyme and its conversion into the higher fluorescent state E2MgP. The slow phase of the fluorescence increase is attributed to the conversion of some of the enzyme into the other high fluorescent state E2Mg.

6.2.5 Fitting of the fast phase of the stopped-flow kinetic data

Because ATP phosphorylation of the enzyme by ATP also requires a Mg^{2+} ion to bind as a cofactor, under conditions of excess Na^+, ATP and Mg^{2+} over enzyme the initial formation of the E2MgP state can be considered as a pseudo first-order reaction, which requires complete saturation of the Mg^{2+} binding sites to relax with its maximum rate constant. Under these conditions it can be shown[130] that, if one neglects competition between enzyme and unbound ATP for Mg^{2+}, the expected dependence of the observed rate constant for the fast phase, k_{fast}^{obs}, on the Mg^{2+} concentration is given by:

$$k_{fast}^{obs} = k_1 \cdot \frac{\left[Mg^{2+} \right]}{K_d + \left[Mg^{2+} \right]} \qquad (4)$$

where k_1 is the overall rate constant for phosphorylation of the enzyme and its conversion into the E2P state and K_d is the apparent dissociation constant of Mg^{2+} and enzyme in the E1ATP state. The term $[Mg^{2+}]/(K_d + [Mg^{2+}])$ represents the fraction of Mg^{2+} sites of E1ATP occupied by Mg^{2+} or, in other words, the degree of saturation of the Mg^{2+} sites. Equation (4)

predicts a hyperbolic dependence of k_{fast}^{obs} on the Mg^{2+} concentration. However, in fact the situation is more complicated, because, if the dissociation constants of ATP and enzyme for Mg^{2+} are of a similar order of magnitude, excess unbound ATP would compete effectively with the enzyme for the available Mg^{2+}. This effect, therefore, needs to be taken into account if one wishes to derive accurate values of k_1 and K_d.

Equation (4) can be written in a more model-independent form as:

$$k_{fast}^{obs} = k_1 S_{E1} \qquad (5)$$

where S_{E1} represents the degree of saturation of the Mg^{2+} sites on the E1ATP$(Na^+)_3$ species. Competition between enzyme and free ATP for Mg^{2+} can be taken into account as described in the Appendix. Equations (A6)-(A9) (see Appendix) allow one to calculate a value of S_{E1} for any given values of the binding constants of enzyme and ATP for Mg^{2+} and then, in combination with eq. (5), to fit this model to the experimental k_{fast}^{obs} data. Following this procedure leads to values of k_1 and K_d of 195 (± 6) s^{-1} and 0.069 (± 0.010) mM, respectively. The value of k_1 agrees quite well with measurements on enzyme from other sources, which have also yielded values of k_1 close to 200 s^{-1} under comparable experimental conditions[81, 82, 130, 131]. The value of K_d is indistinguishable from the dissociation constant of ATP alone for Mg^{2+} of 0.071 (± 0.003) mM under the same buffer conditions (see Chapter 4).

The salt concentrations are important here, because it appears that Mg^{2+} can also interact with the Na^+ transport sites[162, 163] and ATP can also be complexed by Na^+ ions, both of which could make the apparent K_d measured very dependent on the NaCl concentration. In the absence of any other added ions Grisham and Mildvan[148] reported that Mg^{2+} binding to the enzyme in the absence of ATP and the absence of added salt occurred with an apparent K_d of 0.15 mM, whereas in a buffer containing 100 mM NaCl and 10 mM KCl, i.e. comparable

to the conditions here of 130 mM NaCl., the apparent K_d was 1.0 mM. This value can't be directly compared to the K_d determined here, though, because Grisham and Mildvan[148] were measuring direct binding of Mg^{2+} to the enzyme, whereas here the binding of Mg^{2+} to an enzyme-ATP complex has been measured. From steady-state activity measurements Garrahan et al.[164] determined a K_m value for Mg^{2+} of 12-13 μM. However, this value also can't be directly compared to the K_d value determined here, because in steady-state measurements subsequent enzyme reactions would perturb the initial Mg^{2+} binding equilibrium.

6.2.6 Fitting of the slow phase of the stopped-flow kinetic data

In the case of the slow phase, which was attributed to the relaxation of reaction (3) above, under saturating conditions the observed rate constant should be given by the sum of the forward and backward rate constants:

$$k_{slow}^{obs} = k_3^{obs} + k_{-3}^{obs} \qquad (6)$$

The *obs* superscripts are used to indicate that under non-saturating conditions these rate constants of reaction (3) could also depend on the Mg^{2+} concentration due to coupling to other reactions. In fact the backward reaction of reaction (3) involves at least two steps:

$$E2Mg \xrightarrow{k_4^{obs}} E1Mg(Na^+)_3 + ATP \xrightarrow{k_1^{obs}} E2P + 3Na^+ + ADP \qquad (7)$$

ATP and Na^+ binding reactions have not been explicitly included here, because it is assumed that these reactions are fast equilibria and that both ATP and Na^+ are present at saturating concentrations. Furthermore, the reverse reaction of the conformational change of unphosphorylated enzyme ($E1Mg(Na^+)_3 \rightarrow E2Mg$) has been neglected, because in the

absence of K^+ and the presence of high concentrations of both Na^+ and ATP the E1/E2 equilibrium would be expected to lie far on the side of E1. According to the Van Slyke approximation[155] for sequential irreversible reactions the overall observed rate constant for this reaction sequence can be approximated by:

$$\frac{1}{k_{-3}^{obs}} = \frac{1}{k_4^{obs}} + \frac{1}{k_1^{obs}} \qquad (8)$$

k_1^{obs} is the same as the experimentally determined k_{fast}^{obs}. Therefore, substituting from eq. (5), rearranging and substituting the resulting expression for k_{-3}^{obs} into eq. (6) gives:

$$k_{slow}^{obs} = k_3^{obs} + \frac{k_4^{obs} k_1 S}{k_1 S + k_4^{obs}} \qquad (9)$$

This equation does in fact predict an approximately hyperbolic increase in k_{slow}^{obs} with increasing Mg^{2+} concentration as experimentally observed **(see Fig. 6.3)** with a saturating value given by $k_4^{obs}k_1/(k_1 + k_4^{obs})$. The Mg^{2+} concentration dependence of k_{slow}^{obs} could, thus, be explained by Mg^{2+}-stimulation of the phosphorylation reaction, as is the case for the fast phase. In the first instance, therefore, eqs. (9) and (A6)-(A9) (from Appendix) were fitted to the experimental observed rate constant data with the assumption that k_3^{obs} and k_4^{obs} are both independent of the Mg^{2+} concentration. An adequate fit to the data could, however, only be achieved if K_E, the binding constant of Mg^{2+} to E1ATP$(Na^+)_3$, was also allowed to vary. The best-fit value of K_E was a factor of 10 lower than that already determined from the analysis of the fast phase (i.e. K_d was a factor of 10 higher). Because this situation would be inconsistent, the possibility that k_4^{obs} is also Mg^{2+}-dependent needs to be considered.

A Mg^{2+}-dependence of k_4^{obs} could come about if Mg^{2+} binding to E2 stimulates the E2 → E1 transition via an allosteric effect. This is already well known to be the case for ATP[159]. To consider such an effect eq. (9) must be modified to:

$$k_{slow}^{obs} = k_3^{obs} + \frac{\left[k_4^{min} + \left(k_4^{max} - k_4^{min}\right) S_{E2}\right] k_1 S_{E1}}{k_1 S_{E1} + \left[k_4^{min} + \left(k_4^{max} - k_4^{min}\right) S_{E2}\right]} \quad (10)$$

where k_4^{min} and k_4^{max} represent the minimum and maximum values of k_4 when the E2 state of the enzyme has no bound Mg^{2+} ions and when it is saturated by Mg^{2+}, respectively. S_{E1} and S_{E2} represent the degrees of saturation of the E1 and E2 states by Mg^{2+}. S_{E1} can be calculated, taking into account competition from the excess unbound ATP, according to eqs. (A6)-(A9) (see Appendix). Analogous equations can be written for the E2 state to allow the calculation of S_{E2}.

A fit of eq. (10) to the experimental data is shown in **Fig. 6.3**. The fit was carried out using a fixed value of K_{ATP}, taken from calorimetric measurements (see Chapter 4), and fixed values of k_1 and K_E, based on the values determined from the analysis of the fast phase (see the previous section). The only parameters allowed to vary were k_3^{obs}, k_4^{min}, k_4^{max} and K_F (the binding constant of Mg^{2+} to the E2ATP conformation of the protein). It was found that the value of k_3^{obs}, the rate constant for dephosphorylation, was indistinguishable from zero and could in fact be removed from eq. (10) with no change to the fit. This is interesting, because previous direct measurements of the rate constant for dephosphorylation in the absence of K^+ but in the presence of Mg^{2+} have yielded values[131, 138, 154, 158] in the range 2-7 s^{-1}. Therefore, this result suggests that Mg^{2+} may also have an allosteric effect in accelerating the rate of dephosphorylation. However, this possibility should be investigated by more direct measurements than those reported here. An allosteric effect of Mg^{2+} on k_3 hasn't been included eq. (10). This could be done, but with the number of fit parameters already included in the equation a significantly better fit to the experimental data would not be obtained. The values of the other parameters obtained from the fit were: k_4^{min} = 13 (± 4) s^{-1}, k_4^{max} = 74 (± 10) s^{-1} and K_F = 1.3 (± 0.8) x 10^3 M^{-1}. The value of K_F corresponds to a dissociation constant

of Mg^{2+} with the E2ATP conformation of the protein of 0.8 (± 0.5) mM. In comparison with the E1ATP$(Na^+)_3$ conformation this represents an order of magnitude weaker binding of Mg^{2+}. It is interesting that this parallels a much weaker binding of ATP itself to the E2 conformation relative to the E1 conformation[159]. In contrast to the E1 conformation, therefore, it seems that the enzyme environment of the E2 conformation does weaken Mg^{2+} binding to ATP.

The value of k_4^{max} derived from the fitting of 74 s^{-1} is consistent with the values in the range 65-90 s^{-1} previously found[81, 82] for the E2 → E1$(Na^+)_3$ transition in the presence of saturating concentrations of Mg^{2+} and ATP for Na^+,K^+-ATPase from pig and rabbit kidney. The lower value of k_4^{min}, the rate constant for the same transition but in the absence of Mg^{2+}, of 13 s^{-1} is in accordance with the idea that Mg^{2+} has an allosteric effect similar to ATP in accelerating this reaction. One needs to be in mind, however, that although the fit shown in **Fig. 6.3** is completely consistent with the data obtained for the fast phase, there are a much larger number of rate constants and equilibrium constants affecting the relaxation of the slow phase. This makes it difficult to give precise estimates of the parameters in the fitting model. For this reason, as in the case of dephosphorylation reaction, the effect of Mg^{2+} on the E2 → E1$(Na^+)_3$ transition should be investigated by more direct means.

6.3 Discussion and conclusion

The kinetics of Na^+- and Mg^{2+}-dependent partial reactions of the Na^+,K^+-ATPase from shark rectal gland have been investigated via the stopped-flow technique by mixing enzyme-containing membrane fragments fluorescently labeled with the probe RH421 with ATP at varying Mg^{2+} concentrations. As in the case of previous stopped-flow studies using the same technique[81, 82, 130, 131], two kinetic phases were observed, both associated with a

fluorescence increase. The faster phase is attributed to the phosphorylation of the enzyme and its conversion to the E2MgP state. The slower phase is attributed to a subsequent relaxation of the dephosphorylation/rephosphorylation (via ATP) equilibrium and build up of some enzyme in the E2Mg state. Because of the high quality of the data obtained, here for the first time the Mg^{2+} concentration dependence of the reciprocal relaxation times associated with both phases could be analysed.

It was found that both phases showed similar roughly hyperbolic increases in their observed rate constants to saturating values, but the observed rate constant of the fast phase saturated at a lower Mg^{2+} concentration than the slow phase. The Mg^{2+} concentration dependences of the fast phase can be explained by Mg^{2+}-stimulation of the enzyme's phosphorylation by acting as a cofactor of ATP. This phase involves the direct phosphorylation of enzyme in the $E1Mg(Na^+)_3$ state by ATP. The slow phase also involves phosphorylation by ATP, but after the enzyme has proceeded once around its enzymatic cycle, i.e. after dephosphorylation and a conformational change back to the initial $E1Mg(Na^+)_3$ state. Since the slow phase also involves enzyme phosphorylation, the Mg^{2+} concentration dependence of its observed rate constant can also partly be explained by Mg^{2+}-stimulation of ATP phosphorylation. However, the fact that the slow phase saturates at a higher Mg^{2+} concentration than the fast phase implies that this is not the only effect. The concentration dependence of the slow phase could be explained by an additional stimulation by Mg^{2+} of the $E2ATP \rightarrow E1ATP(Na^+)_3$ reaction.

The fact that within experimental uncertainty the reciprocal relaxation time of the slow phase at an infinitely low Mg^{2+} concentration is indistinguishable from zero, implies that the dephosphorylation rate constant of the enzyme in the absence of both K^+ and Mg^{2+} is also indistinguishable from zero. This result would suggest that Mg^{2+} plays an allosteric role in accelerating the dephosphorylation reaction to some extent. A similar allosteric role has

recently been proposed for ATP[82], with which Mg^{2+} complexes. However, further more direct measurements of the dephosphorylation reaction and the effects of varying Mg^{2+} concentrations on it would be desirable.

From crystal structures[143] of the related P-type ATPase, the Ca^{2+}-ATPase, it is known that Mg^{2+} binds to the enzyme in a complex with a nucleotide, (i.e., ATP under physiological conditions but its inert analogue AMPPCP in the crystals). It is, therefore, interesting to compare the Mg^{2+} dissociation constant determined here with the dissociation constant of Mg^{2+} with ATP in free solution. This has been determined using isothermal titration calorimetry (see Chapter 4) under the same buffer conditions as used here for the stopped-flow measurements to be 0.071 (± 0.003) mM. This is indistinguishable from the value of K_d determined in this chapter in the presence of the enzyme, i.e. 0.069 (± 0.010) mM. This implies that the enzyme environment of the E1 state has no effect on the strength of complexation of Mg^{2+} by ATP. Therefore, although the enzyme specifically binds ATP, the Mg^{2+} ion necessary for phosphorylation is only bound indirectly to the E1 conformation of the enzyme via ATP.

Chapter 7

Effect of cholesterol, its oxidised derivatives and perchlorate on the activity of the Na^+, K^+-ATPase

7.1 Introduction

In previous chapters it was shown that cholesterol and its derivatives have an effect on the kinetics of photosynthetic reaction centres from purple bacteria. It is likely that ion pumps would also be influenced by the electrical properties of the membrane as well as steric factors such as the membrane thickness and the order of the surrounding lipid. Other studies showed that the electrical dipole potential of cell membranes was directly correlated to the quantity of cholesterol present in the membrane[13]. Thus, one of the topics investigated in this chapter is the effect of cholesterol and different cholesterol derivatives on the Na^+, K^+-ATPase activity.

Cornelius[165] described the effect of cholesterol on the Na^+, K^+-ATPase activity. His results suggested that cholesterol interacts directly with the Na^+, K^+-ATPase as an essential effector perhaps by influencing its conformational mobility or protein-protein interactions. In a study from Castuma *et al.*[166] cholesterol within the lipid bilayer was found to decrease the mobility of the phospholipids and increase the order of the bilayer.

In this chapter fluorescence experiments are described to better understand how the dipole potential and membrane orientational polarisability might affect Na^+, K^+-ATPase activity. The pumping of ions across a membrane against an electrochemical potential gradient leads to the formation of unstable enzyme intermediates, which can relax to a lower energy state only if they release ions to the other side of the membrane with the higher electrochemical potential for that ion. Surrounding lipid could in principle stabilise those enzyme intermediates via dipole reorientation and so could partially dissipate the free energy

of ATP hydrolysis and inhibit ion pumping. Here we investigated the degree of energy stabilisation by cholesterol and its derivatives via measurements of the Stokes shift of a probe molecule, di-8-ANEPPS. To fully elucidate the effect of lipid-protein interactions on ATP hydrolysis and ion transport by the Na^+,K^+-ATPase, it is necessary to reconstitute it in liposomes of defined synthetic phospholipids.

In 1955 it was already found [167] that bromide, nitrate and iodide could cause a change in the tension in the muscle. It was proposed that the effect is a result of ions adsorbing to the surface of muscle membrane with an order of effectiveness given by the so-called Hofmeister series first described by Hofmeister[168, 169]. The Hofmeister series was originally based on the ability of the studied ions to precipitate a given protein. It has been suggested[170] that the effect of salts on the molecular organization of water is an important factor but it is still unclear how such a modification in the water molecule organization can have an effect on protein function. Lyotropic anions, such as perchlorate, are known to alter the kinetics of individual partial reactions of the ion pump Na^+, K^+-ATPase[171]. However, its effect on the enzyme's overall steady-state activity has not yet been studied. This has also been investigated in this chapter.

7.2 Results

7.2.1 Enzyme activity in the presence of cholesterol and chemical analogues

Liposomes have been synthezised with phosphatidylcholine in the presence of different cholesterol derivatives and then mixed with membrane fragment containing Na^+, K^+-ATPase. The activity of the enzyme has been investigated by the decrease in UV absorption of NADH over the course of time due to its oxidation in the presence of pyruvate

kinase-lactate dehydrogenase and phosphoenolpyruvate. The activity of the enzyme was measured for each type of liposome and has been compared to the activity of enzyme in membrane fragments. The determination of the specific activity of the Na^+, K^+-ATPase was calculated from the rate of change of the absorbance of NADH. The relative errors in the enzyme activity values are all within the range 2-3%. The results are shown **Table 7.1**.

24ºC, pH 7.4 (50 mol% of cholesterol and its derivatives)	Enzyme activity (µmol Pi/mg/h)
PLPC	609 ± 12
PLPC+ 4-cholesten-3-one	850 ± 17
PLPC+ 5-cholesten-3-*β*-ol-7-one	911 ± 18
PLPC+ coprostanol	566 ± 11
PLPC+ cholesterol	708 ± 28
PLPC+ 6-ketocholestanol	280 ± 5

Table 7.1: Effect of cholesterol and derivatives on enzyme specific activity contained in synthetic liposomes. Enzyme was included in PLPC with cholesterol derivatives. Buffer conditions: 5 mM $MgCl_2$, 25 mM Tris-HCl, pH 7.4, 10 mM KCl and 130 mM NaCl.

As shown in **Table 7.1**, the activity of the Na^+, K^+-ATPase when inserted into vesicle membranes dropped significantly from 1850 µmol Pi/mg/h in membrane fragments to 609 µmolPi/mg/h when reconstituted in PLPC vesicles. When cholesterol is added to the vesicles the enzyme's activity increased to 708 µmol Pi/mg/h. This is also observed for 4-cholesten-3-one (850 µmol Pi/mg/h) and 5-cholesten-3-*β*-ol-7-one (911 µmol Pi/mg/h). Interestingly, the results are very different for the cholesterol derivatives 6-ketocholestanol and coprostanol. The enzyme activity decreases from 609 µmol Pi/mg/h for PLPC to 566 µmol Pi/mg/h for coprostanol and 280µmol Pi/mg/h for 6-ketocholestanol. It is important to note that 5-cholesten-3-*β*-ol-7-one is the derivative that has the greatest effect on the enzyme's activity and is also the only derivative studied that decreases the dipole potential[13].

7.2.2 Orientational polarizability measurements on phosphatidylcholine vesicles

Di-8-ANEPPS is a well-established probe for quantifying the dipole potential and the orientational polarizability of lipid membranes[13, 21, 23, 172]. Fluorescence excitation spectra have been recorded for di-8-ANEPPS bound to phosphatidylcholine vesicles containing the enzyme in the presence of cholesterol and its chemical analogues and the orientational polarizability has been calculated using the method described in Materials and Methods. The results are shown in **Fig. 7.2**.

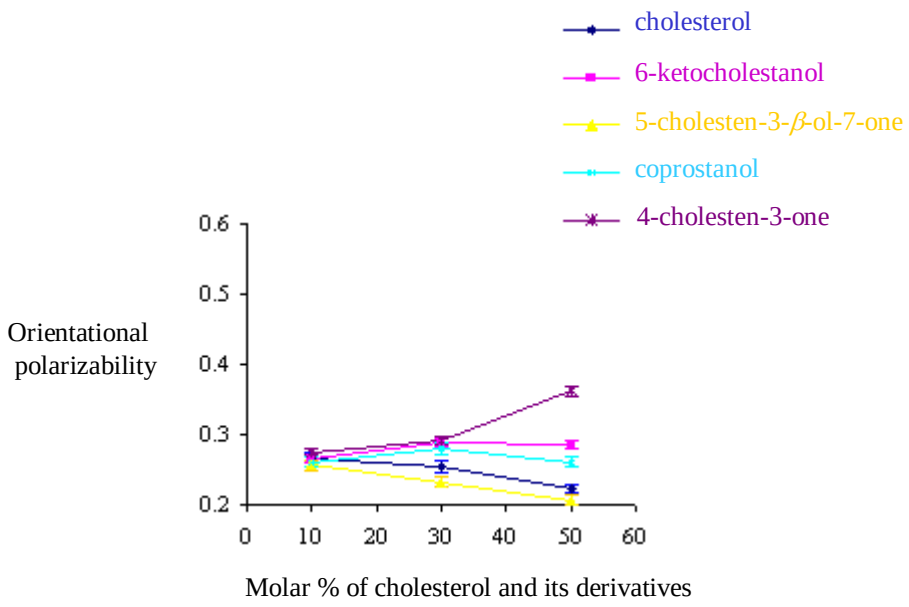

Figure 7.2: Graph representing the orientational polarizability versus the molar percent of cholesterol and its derivatives present in vesicles. Effect of cholesterol derivatives concentration on the orientational polarizability, Δf, of the dye [di-8-ANEPPS]= 7μM, [PC]= 2mM and 10, 30 or 50 mol% of cholesterol, 6-ketocholestanol, 5-cholesten-3-*β*-ol-7-one, coprostanol and 4-cholesten-3-one have been added to the vesicles containing Na^+,K^+-ATPases. Buffer conditions: 5 mM $MgCl_2$, 25 mM Tris-HCl, pH 7.4, 10 mM KCl and 130 mM NaCl. Orientational polarizability values were deducted from Stokes shifs magnitudes.

The relative errors in the orientational polarizability values are all within the range 5-10% based on the errors in the paramaters in the equation to calculate the orientational polarizability (see Materials and Methods).

It was found that with vesicles composed only of phosphatidylcholine and containing enzyme the orientational polarizability was 0.23. When 10 mol% of cholesterol and its derivatives were added to the vesicles the orientational polarizability value for each type of molecule was comparable to the value of phosphatidylcholine in the absence of sodium perchlorate, i.e. no significant change is observed. No significant change is observed at 30 mol% for coprostanol, 6-ketocholestanol and 4-cholesten-3-one compared to the same derivatives at 10 mol% **(Fig. 7.2)**. However, for 5-cholesten-3-β-ol-7-one the orientational polarizability is slightly decreased at 30 mol% compared to its value at 10mol% **(Fig. 7.2)**. If the vesicles containing the enzyme were mixed with 50 mol% it appears that there is an increase in the orientational polarizability for 4-cholesten-3-one from 0.27 at 10 mol% to 0.36 at 50 mol% **(Fig. 7.2)**. A significant decrease in orientational polarizability is also observed for cholesterol and 5-cholesten-3-β-ol-7-one that shifts from 0.26 at 10 mol% to 0.22 at 50 mol% and from 0.25 at 10 mol% to 0.20, at 50 mol% respectively **(Fig. 7.2)**.

On the other hand, no significant changes were observed for 6-ketocholestanol and coprostanol. In general one can observe that the difference between cholesterol and its derivatives on the orientational polarizability is greatest when their percentage in the vesicle is $\geq$50 mol%.

5-cholesten-3-β-ol-7-one and cholesterol show the greatest difference at 50 mol%. Interestingly 5-cholesten-3-β-ol-7-one and cholesterol have opposite effects on the dipole potential as cholesterol increases the dipole potential and 5-cholesten-3-β-ol-7-one decreases it. This is because their dipole moments are in opposite directions when within the bilayer.

The same experiment has been repeated in the presence of 50 mM of sodium perchlorate, which is known to decrease the dipole potential value[157] and the results are displayed in **Fig. 7.3**. When sodium perchlorate is added to the preparation with vesicles composed only of phosphatidylcholine and containing enzyme the orientational polarizability

was shifted from 0.23 to 0.18 **(Fig. 7.3)**. Unlike the values of the orientational polarizability without sodium perchlorate significant effects are already observed at 30 mol% of cholesterol derivatives **(Fig. 7.3)**.

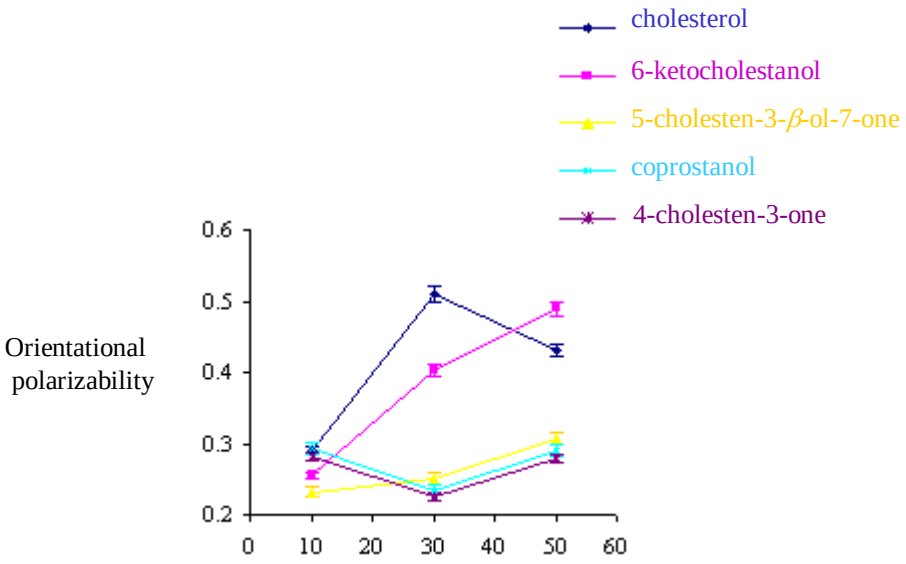

Table 7.3: Graph representing the orientational polarizability versus the molar percent of cholesterol and its derivatives present in vesicles. Effect of cholesterol derivatives concentration in presence of 50mM of sodium perchlorate on the orientational polarizability, Δf, of the dye [di-8-ANEPPS]= 7µM, [PC]= 2mM and 10, 30 or 50 mol% of cholesterol, 6-ketocholestanol, 5-cholesten-3-*β*-ol-7-one, coprostanol and 4-cholesten-3-one have been added to the vesicles containing Na^+,K^+-ATPases. Buffer conditions: 5 mM $MgCl_2$, 25 mM Tris-HCl, pH 7.4, 10 mM KCl and 130 mM NaCl and 50mM of sodium perchlorate. Orientational polarizability values were deducted from Stokes shifs magnitudes.

.

At 30 mol%, 6-ketocholestanol and cholesterol increase the orientational polarizability from 0.25 at 10 mol% to 0.40 at 30 mol% for cholesterol and 0.29 at 10mol% to 0.50 at 30 mol% for 6-ketocholestanol **(Fig. 7.3)**. The situation is quite different with coprostanol and 4-cholesten-3-one which decrease the orientational polarizability from 0.28 at 10 mol% to 0.22 at 50 mol% for 4-cholesten-3-one and 0.29 at 10 mol% to 0.23 at 50 mol% for 6-ketocholestanol. Surprisingly 5-cholesten-3-*β*-ol-7-one doesn't show any difference between 10 mol% and 30 mol% in the presence of sodium perchlorate **(Fig. 7.3)**.

In **Fig. 7.3**, 50 mol% cholesterol decreases the orientational polarizability from 0.50 at 30 mol% to 0.43 at 50 mol%. On the other hand 6-ketocholestanol, 4-cholesten-3-one, coprostanol and 5-cholesten-3-β-ol-7-one increase the orientational polarizability when the percentage goes up to 50 mol%.

It is important, here, to note that the major effect on the orientational polarizability occurs for cholesterol and 6-ketocholestanol, which were the derivatives that induced the greatest effect on the 1 ET of RC (see Chapter 3).

7.2.3 Effect of sodium perchlorate on the enzyme activity

The results of the investigation of the effect of sodium perchlorate on the Na^+, K^+-ATPase's steady-state activity are presented in **Fig. 7.4**. The highest concentration of sodium perchlorate used was 100mM.

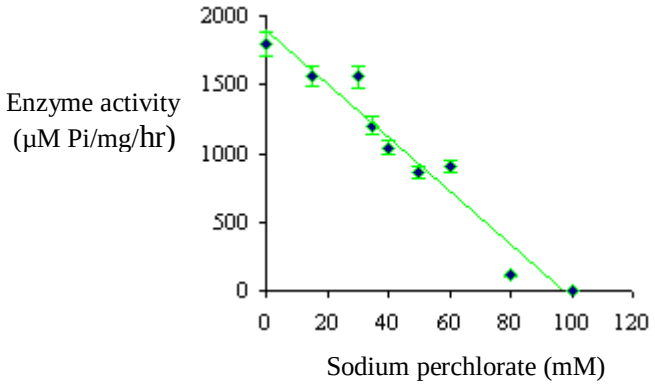

Figure 7.4: Effect of sodium perchlorate on Na^+, K^+-ATPase's activity. The experiment has been carried out on fragments membrane bound-enzyme (0.5 µM). Buffer conditions: 5 mM $MgCl_2$, 25 mM Tris-HCl, pH 7.4, 10 mM KCl and 0-10 0mM perchlorate. A control experiment has been carried out without perchlorate, 130 mM NaCl and 10 mM of KCl.; enzyme specific activity in these conditions is 1850 µmol Pi/mg/hr.

The relative errors in the enzyme's activity values presented in **Fig. 7.4** are all around 10% based on the values obtained from repeated experiments. In **Fig. 7.4**, one can notice that the enzyme's specific activity decreases steadily when sodium perchlorate is added until 0 µmol Pi/mg/hr at a concentration of sodium perchlorate of 100 mM. It is interesting to note

that the enzyme has an activity of 1850 µmol Pi/mg/h in the presence of 130 mM of NaCl but close to zero in presence of 100 mM sodium perchlorate.

7.2.4 Effect of sodium perchlorate on the fluidity of membrane fragments containing Na^+, K^+-ATPase

The results of the effect of sodium perchlorate on the fluorescence anisotropy of di-8-ANEPPS in membrane fragments containing enzyme are reported in **Fig. 7.5**. The fluorescence anisotropy of dyes such as di-8-ANEPPS that have their absorption and fluorescence transition moments oriented along the long axis of the molecule reflect the rotational mobility of the dye inside the membrane and hence the membrane fluidity at different concentrations of sodium perchlorate.

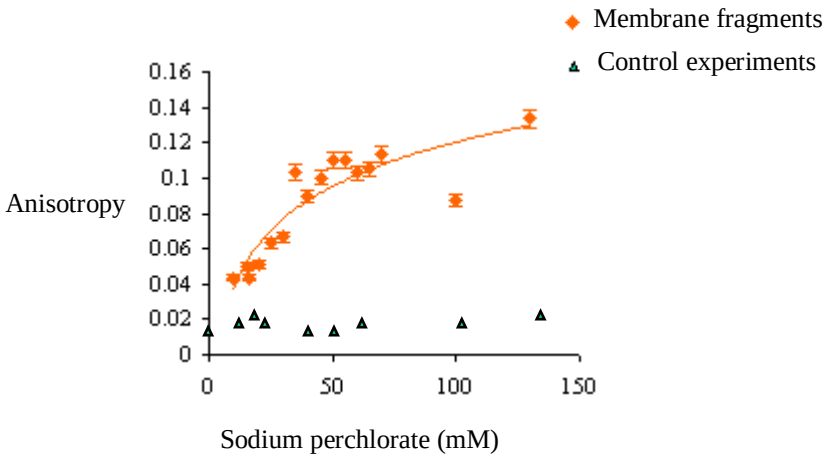

Figure 7.5: Effect of sodium perchlorate concentration on the fluorescence anisotropy of di-8-ANEPPS. The experiment has been carried out on Na^+, K^+-ATPase membrane fragments (orange) and without membrane fragments (green) as a control experiment. Buffer conditions: 5 mM $MgCl_2$, 25 mM Tris-HCl, pH 7.4, 10 mM KCl and 0-10 0mM perchlorate.

A control experiment has been carried out without membrane fragments and an increasing concentration of sodium perchlorate revealing no change in the fluorescence anisotropy. The relative errors in the fluorescence anisotropy values are all around 10% based on the average values obtained from repeated experiments. Interestingly, in the presence of

10-140 mM of sodium perchlorate the fluorescence anisotropy of the probe in the membranes increases from ~0.04 to ~0.14, indicating a perchlorate-induced increase in rigidity or decrease in fluidity of the membrane.

7.3 Discussion and conclusion

The aim of this chapter was to explain the mode of action of different cholesterol derivatives and perchlorate on the enzyme's activity. Measurements of Na^+, K^+-ATPase activity reconstituted in different kinds of vesicles demonstrate that the enzyme has a greater activity when reconstituted in vesicles containing 5-cholesten-3-β-ol-7-one and 4-cholesten-3-one. As it is known that 5-cholesten-3-β-ol-7-one causes a decrease in the dipole potential and 4-cholesten-3-one causes a large increase in dipole potential. Based on the results of the enzyme's activity for each cholesterol derivative it is not possible to conclude a direct correlation between their effect on the dipole potential and on the enzyme's activity.

The results obtained from the study of the membrane orientational polarizability for each of the cholesterol derivatives in **Fig. 7.3** show that the effect on the orientational polarizability varied significantly between the different cholesterol analogues. This suggests that the cholesterol derivatives can either increase or decrease the membrane fluidity.

The measurements of fluorescence anisotropy with membrane fragments containing Na^+, K^+-ATPase allowed a comparison of the effect of sodium perchlorate on the phospholipid mobility with its effect on the enzyme's activity. An increase in the fluorescence anisotropy is observed as the concentration of sodium perchlorate is increased. This indicates a decrease in membrane fluidity. This could directly influence ion pump activity via a steric effect, or it could influence the enzyme's activity indirectly via electrostatic effects due to a decrease in the charge mobility of the surrounding lipids. This

could suggest that the difference in the local electric field created by cholesterol derivatives might have the same mode of action as sodium perchlorate in terms of the orientation of charge and rigidity of the phospholipids. However, as the cholesterol derivatives' effects on the dipole potential or orientational polarizability don't show a correlation with their effect on the enzyme activity one may suggest that the dominant effect of perchlorate on the enzyme's activity is due to a restriction in its degree of movement.

References

1. Chiriac, R.; Luchian, T., pH modulation of transport properties of alamethicin oligomers inserted in zwitterionic-based artificial lipid membranes. *Biophys Chem* **2007,** 130, 139-47.
2. McLaughlin, S., The electrostatic properties of membranes. *Annu Rev Biophys Biophys Chem* **1989,** 18, 113-36.
3. Dani, J. A., Ion-channel entrances influence permeation. Net charge, size, shape, and binding considerations. *Biophys J* **1986,** 49, 607-18.
4. Kell, M. J.; DeFelice, L. J., Surface charge near the cardiac inward-rectifier channel measured from single-channel conductance. *J Membr Biol* **1986,** 102, 1-10.
5. Mathai, J. C.; Tristram-Nagle, S.; Nagle, J. F.; Zeidel, M. L., Structural determinants of water permeability through the lipid membrane. *J Gen Physiol* **2008,** 131, 69-76.
6. Clarke, R. J.; Lüpfert, C., Influence of anions and cations on the dipole potential of phosphatidylcholine vesicles: a basis for the Hofmeister effect. *Biophys J* **1999,** 76, 2614-24.
7. Ganea, C.; Babes, A.; Lüpfert, C.; Grell, E.; Fendler, K.; Clarke, R. J., Hofmeister effects of anions on the kinetics of partial rections of the Na^+,K^+-ATPase. *Biophys J* **1999,** 77, 267-281.
8. Cordomi, A.; Edholm, O.; Perez, J. J., Effect of ions on a dipalmitoyl phosphatidylcholine bilayer. A molecular dynamics simulation study. *J Phys Chem B* **2008,** 112, 1397-408.
9. Böckmann, R. A.; Hac, A.; Heimburg, T.; Grubmüller, H., Effect of sodium chloride on a lipid bilayer. *Biophys J* **2003,** 85, 1647-55.
10. Clarke, R. J., The dipole potential of phospholipid membranes and methods for its detection. *Adv Colloid Interface Sci* **2001,** 89-90, 263-81.
11. Gawrisch, K.; Ruston, D.; Zimmerberg, J.; Parsegian, V. A.; Rand, R. P.; Fuller, N., Membrane dipole potentials, hydration forces, and the ordering of water at membrane surfaces. *Biophys J* **1992,** 61, 1213-23.
12. Le Goff, G.; Vitha, M. F.; Clarke, R. J., Orientational polarisability of lipid membrane surfaces. *Biochem Biophys Acta* **2006,** 1768, 562-570.
13. Starke-Peterkovic, T.; Turner, N.; Vitha, M. F.; Waller, M. P.; Hibbs, D. E.; Clarke, R. J., Cholesterol effect on the dipole potential of lipid membranes. *Biophys J* **2006,** 90, 4060-70.
14. Peterson, U.; Mannock, D. A.; Lewis, R. N. A. H.; Pohl, P.; McElhaney, R. N.; Pohl, E. E., Origin of membrane dipole potential: Contribution of the phospholipid fatty acid chains. *Chem Phys Lipids* **2002,** 117, 19-27.
15. Buzón, V.; Cladera, J., Effect of cholesterol on the interaction of the HIV GP41 fusion peptide with model membranes. Importance of the membrane dipole potential. *Biochem* **2006,** 45, 15768-75.
16. Cladera, J. M.; Ruysschaert, I.; O'Shea, P., Characterization of the sequence of interactions of the fusion domain of the simian immunodeficiency virus with membranes. Role of the membrane dipole potential. *Biol Chem* **1999,** 274, 29951-29959.
17. Becucci, L.; Moncelli, M. R.; Guidelli, R., Thallous ion movements through gramicidin channels incorporated in lipid monolayers supported by mercury. *Biophys J* **2002,** 82, 852-64.

18. Edmonds, D. T., A two-channel electrostatic model of an ionic counterport. *Proc R Soc Lond B Biol Sci* **1986,** 228, 71-84.
19. Rokitskaya, T. I.; Antonenko, Y. N.; Kotova, E. A., Effect of the dipole potential of a bilayer lipid membrane on gramicidin channel dissociation kinetics. *Biophys J* **1997,** 73, 850-4.
20. Maggio, B., Modulation of phospholipase A2 by electrostatic fields and dipole potential of glycosphingolipids in monolayers. *J Lipid Res* **1999,** 40, 930-9.
21. Starke-Peterkovic, T.; Turner, N.; Else, P. L.; Clarke, R. J., Electric field strength of membrane lipids from vertebrate species: membrane lipid composition and Na+-K+-ATPase molecular activity. *Am J Physiol Regul Integr Comp Physiol* **2005,** 288, R663-70.
22. Malkov, D. Y.; Pavlov, K. V.; Sokolov, V. S., Dipole potential drop due to RH-dye adsorption on the lipid bilayer and its influence on Na+/K+-ATPase activity. *Ann N Y Acad Sci* **1997,** 834, 357-60.
23. Clarke, R. J., Effect of lipid structure on the dipole potential of phosphatidylcholine bilayers. *Biochim Biophys Acta* **1997,** 1327, 269-78.
24. Taly, A.; Baciou, L.; Sebban, P., The DMPC lipid phase transition influences differently the first and the second electron transfer reactions in bacterial reaction centers. *FEBS Lett* **2002,** 532, 91-6.
25. Baciou, L.; Gulik-Krzywicki, T.; Sebban, P., Involvement of the protein-protein interactions in the thermodynamics of the electron-transfer process in the reaction centers from Rhodopseudomonas viridis. *Biochem* **1991,** 30, 1298-302.
26. Agostiano, A.; Milano, N.; Trotta, T., Trapping of a long-living charge separated state of photosynthetic reaction centers in proteoliposomes of negatively charged phospholipids. *Photosynth Res* **2005,** 83, 53-61.
27. Palmer, C. P.; Mahen, R.; Schnell, E.; Mustafa, B. A.; Djamgoz, D.; Aydar, E., Sigma-1 Receptors Bind Cholesterol and Remodel Lipid Rafts in Breast Cancer Cell Lines. *Cancer Res J* **2007,** 67, 11166-11175.
28. Brown, D., GPI-anchored proteins and detergent-resistant membrane domains. *Braz J Med Biol Res.* **1994,** 27, 309-15.
29. Maisse, C.; Rossin, A.; Cahuzac, N.; Paradisi, A.; Klein, C.; Haillot, M. L.; Hérincs, Z.; Mehlen, P.; Hueber, A. O., Lipid raft localization and palmitoylation: Identification of two requirements for cell death induction by the tumor suppressors UNC5H. *Exp Cell Res* **2008,** 314, 2544-52.
30. Welker, P.; Boehlick, A.; Mutig, K.; Salanova, M.; Kahl, T.; Schlueter, H.; Blottner, D.; Ponce-Coria, J.; Gamba, G.; Bachmann, S., Renal Na-K-Cl Cotransposrter Activity And Vasopressin-Induced Trafficking Are Lipid Raft-Dependent. *Am J Physiol Renal Physiol (in press)* **2008**.
31. Fedida-Metula, S.; Elhyany, S.; Tsory, S.; Segal, S.; Hershfinkel, M.; Sekler, I.; Fishman, D., Targeting lipid rafts inhibits Protein Kinase B by disrupting calcium homeostasis and attenuates malignant properties of melanoma cells. *Carcinogenesis (in press)* **2008**.
32. Cardaba, C. M.; Kerr, J. S.; Mueller, A., CCR5 internalisation and signalling have different dependence on membrane lipid raft integrity. *Cell Signal* **2008,** 20, 1687-94.
33. Halling, K. K.; Ramstedt, B.; Slotte, J. P., Glycosylation induces shifts in the lateral distribution of cholesterol from ordered towards less ordered domains. *Biochim Biophys Acta* **2008,** 1778, 1100-11.
34. Lu, J. X.; Caporini, M. A.; Lorigan, G. A., The effects of cholesterol on magnetically aligned phospholipid bilayers: a solid-state NMR and EPR spectroscopy study. *J Magn Reson* **2004,** 168, 18-30.

35. Holt, A.; Almeida, R. F.; Nyholm, T. K.; Loura, L. M.; Daily, A. E.; Staffhorst, R. W.; Rijkers, D. T.; Li, R. E.; Prieto, M.; Killian, J. A., Is there a preferential interaction between cholesterol and tryptophan residues in membrane proteins? *Biochem* **2008,** 47, 2638-2649.
36. Ramsammy, L. S.; Volwerk, H.; Lipton, L. C.; Brockerhoff, H., Association of cholesterol with lysophosphatidylcholine. *Chem Phys Lipids* **1983,** 32, 83-9.
37. Giordani, C.; Wakai, C.; Yoshida, K.; Okamura, E.; Matubayasi, N.; Nakahara, M., Cholesterol location and orientation in aqueous suspension of large unilamellar vesicles of phospholipid revealed by intermolecular nuclear overhauser effect. *J Phys Chem B* **2008,** 112, 2622-8.
38. Róg, T.; Stimson, L. M.; Pasenkiewicz-Gierula, M.; Vattulainen, I.; Karttunen, M., Replacing the Cholesterol Hydroxyl Group with the Ketone Group Facilitates Sterol Flip-Flop and Promotes Membrane Fluidity. *J Phys Chem B* **2008,** 112, 1946-1952.
39. Auner, B. G.; Valenta, C.; Hadgraft, J., Influence of phloretin and 6-ketocholestanol on the skin permeation of sodium-fluorescein. *J Control Release* **2003,** 89, 321-8.
40. Auner, B. G.; O'Neill, M. A.; Valenta, C.; Hadgraft, J., Interaction of phloretin and 6-ketocholestanol with DPPC-liposomes as phospholipid model membranes. *Int J Pharm* **2005,** 294, 149-55.
41. Valenta, C.; Steininger, A.; Auner, B. G., Phloretin and 6-ketocholestanol: membrane interactions studied by a phospholipid/polydiacetylene colorimetric assay and differential scanning calorimetry. *Eur J Pharm Biopharm* **2004,** 57, 329-36.
42. Antonenko, Y. N.; Bulychev, A. A., Effect of phloretin on the carrier-mediated electrically silent ion fluxes through the bilayer lipid membrane: measurements of pH shifts near the membrane by pH microelectrode. *Biochim Biophys Acta* **1991,** 1070, 474-80.
43. Sandeep, B.; Kombrabail, M. H.; S., P. B., Effect of phloretin on ionophore mediated electroneutral transmembrane translocations of H^+, K^+ and Na^+ in phospholipid vesicles *Biochim Biophys Acta* **2000,** 1510, 258-269.
44. Staley, J. T.; Irgens, R. L.; Herwig, R. P., Gas Vacuolate Bacteria from the Sea Ice of Antarctica. *Appl Environ Microbiol* **1989,** 55, 1033-36.
45. Bryant, M. P.; Pfennig, N.; Holt, J. G., Bergey's manual of systematic bacteriology. *Springer eds* **1989,** 3, 1895-1904.
46. Woese, C. R., Bacterial evolution. *Microbiol Rev* **1987,** 51, 221-71.
47. Stowell, M. H.; McPhillips, T. M.; Rees, D. C.; Soltis, S. M.; Abresch, E.; Feher, G., Light-induced structural changes in photosynthetic reaction center: implications for mechanism of electron-proton transfer. *Science* **1997,** 276, 812-6.
48. Koepke, J.; Krammer, E. M.; Klingen, A. R.; Sebban, P.; Ullmann, G. M.; Fritzsch, G., pH modulates the quinone position in the photosynthetic reaction center from Rhodobacter sphaeroides in the neutral and charge separated states. *J Mol Biol* **2007,** 371, 396-409.
49. Koepke, J.; Krammer, E. M.; Klingen, A. R.; Sebban, P.; Ullmann, G. M.; Fritzsch, G., pH modulates the quinone position in the photosynthetic reaction center from Rhodobacter sphaeroides in the neutral and charge separated states. *J Mol Biol* **2007,** 371, 396-409.
50. Debus, R. J.; Feher, G.; Okamura, M. Y., Iron-depleted reaction centers from Rhodopseudomonas sphaeroides R-26.1: characterization and reconstitution with Fe2+, Mn2+, Co2+, Ni2+, Cu2+, and Zn2+. *Biochem* **1986,** 25, 2276-87.
51. Hermes, S.; Bremm, O.; Garczarek, F.; Derrien, V.; Liebisch, P.; Loja, P.; Sebban, P.; Gerwert, K.; Haumann, M., A time-resolved iron-specific X-ray absorption

experiment yields no evidence for an Fe2+ --> Fe3+ transition during QA- --> QB electron transfer in the photosynthetic reaction center. *Biochem* **2006,** 45, 353-9.

52. Dutton, P. L.; Mosser, C. C., Quantum biomechanics of long-range electron transfer in protein: Hydrogen bonds and reorganization energies. *Proc Natl Acad Sci USA* **1994,** 91, 10247-10250.
53. Marcus, R. A., On the theory of oxidation-reduction reactions involving electron transfer. VI. Unified treatment for homogenous and electrode reactions. *J Chem Phys* **1965,** 43, 679-701.
54. Marcus, R. A.; Sutin, N., Electron transfers in chemistry and biology. *Biochim Biophys Acta* **1985,** 811, 265-322.
55. Gray, H. B.; Winkler, J. R., Electron transfer in proteins. *Annu Rev Biochem* **1996,** 65, 537-561.
56. Moser, C. C.; Keske, J. M.; Warncke, K.; Farid, R. S.; Dutton, L. P., Nature of biological electron transfer. *Nature* **1992,** 355, 796-802.
57. Gunner, M. R.; Robbertson, D. E.; Dutton, P. L., Kinetic studies on the reaction center protein from Rb. sphaeroides: The temperature and free energy dependence of electron transfer between various quinones in the QA site and the oxidized bacteriochlorophyll dimer. *J Phys Chem* **1986,** 90, 3783-3795.
58. Gunner, M. R.; Dutton, P. L., Temperature and -DG° dependence of the electron transfer from Bph- to QA in reaction center from Rhodobacter sphaeroides with different quinones as QA. *J Am Chem Soc* **1989,** 111, 3400-3412.
59. Kleinfeld, D.; Okamura, M. Y.; Feher, G., Electron transfer in reaction centers of Rhodopseudomonas sphaeroides. Determination of the charge recombination pathway of D+QAQB- and free energy and kinetic relation between QA- QB and QAQB-. *Biochim Biophys Acta* **1984,** 766, 126-140.
60. Babes, A.; Fendler, K., Na(+) transport, and the E(1)P-E(2)P conformational transition of the Na(+)/K(+)-ATPase. *Biophys J.* **2000,** 79, 2557-71.
61. Morth, J. P.; Pedersen, B. P.; Toustrup-Jensen, M. S.; Sørensen, T. L.; Petersen, J.; Andersen, J. P.; Vilsen, B.; Nissen, P., Crystal structure of the sodium-potassium pump. *Nature* **2007,** 450, 1043-9.
62. Cornelius, F.; Skou, J. C., The sided action of Na+ on reconstituted shark Na+/K+-ATPase engaged in Na+-Na+ exchange accompanied by ATP hydrolysis. II. Transmembrane allosteric effects on Na+ affinity. *Biochim Biophys Acta* **1988,** 944, 223-32.
63. Zatyka, M.; Ricketts, C.; X., d. S. G.; Minton, J.; Fenton, S.; Hofmann-Thiel, S.; Rutter, G. A.; Barrett, T. G., Sodium-potassium ATPase β1 subunit is a molecular partner of Wolframin, an endoplasmic reticulum protein involved in ER stress. *Hum Mol Genet* **2008,** 17, 190-200.
64. Gorokhova, S.; Bibert, S.; Geering, K.; Heintz, N., A novel family of transmembrane proteins interacting with ß subunits of the Na,K-ATPase. *Hum Mol Genet* **2007,** 20, 3394-3410.
65. Segall, L.; Scanzano, R.; Kaunisto, M. A.; Wessman, M.; Palotie, A.; Gargus, J. J.; Blostein, R., Kinetic alterations due to a missense mutation in the Na,K-ATPase alpha2 subunit cause familial hemiplegic migraine type 2. *J Biol Chem* **2004,** 279, 43692-6.
66. Austgen, L., The Na,K-ATPase. *Hypertext for biomedical science* **2006**.
67. Skou, J., The influence of some cations on an adenosine triphosphatase from peripheral nerves. *Biochim Biophys Acta* **1989,** 1000, 439-46.
68. Hassett, A.; Blattler, W.; Knowles, J. R., Pyruvate kinase: is the mechanism of phospho transfer associative or dissociative? *Biochemistry* **1982,** 21, 6335-6340.

69. Williams, N. H., Magnesium Ion Catalyzed ATP Hydrolysis. *Am Chem Soc* **2000,** 122, 12023 -12024.
70. Kaplan, J. H., Biochemistry of Na,K-ATPase. *Annu Rev Biochem* **2002,** 71, 511-35.
71. Argüello, J. M.; Whitis, J.; Cheung, M. C.; Lingrel, J. C., Functional role of oxygen-containing residues in the fifth transmembrane segment of the Na,K-ATPase alpha subunit. *Arch Biochem Biophys* **1999,** 364, 254-63.
72. Vilsen, B.; Andersen, J. P.; Petersen, J.; Jørgensen, P. L., Occlusion of 22Na+ and 86Rb+ in membrane-bound and soluble protomeric alpha beta-units of Na,K-ATPase. *J Biol Chem* **1987,** 262, 10511-7.
73. Kubala, M.; Hofbauerová, K.; Ettrich, R.; Kopecký, V.; Krumscheid, R.; Plásek, J.; Teisinger, J.; Schoner, W.; Amler, E., Phe(475) and Glu(446) but not Ser(445) participate in ATP-binding to the alpha-subunit of Na(+)/K(+)-ATPase. *Biochem Biophys Res Commun* **2002,** 297, 154-9.
74. Ayuyan, A. G.; Sokolov, V. C.; Lenz, A. A.; Apell, H. J., Effect of chaotropic anions on the sodium transport by the Na,K-ATPase. *Eur Biophys J* **2006,** 35, 247-54.
75. Koenderin, J. B.; Hermsen-Harm, P. H.; P, H. G.; Swarts, P. W.; De Pont, J. J., High affinity ouabain binding by a chimeric gastric H, K-ATPase containing transmembrane hairpins. *J Biol Chem* **2000,** 278, 47240-47244.
76. Lopez, L. B.; Quintas, L. E.; Noël, F., Influence of development on Na(+)/K(+)-ATPase expression: isoform- and tissue-dependency. *Comp Biochem Physiol A Mol Integr Physiol* **2002,** 131, 323-33.
77. Qiu, L. Y.; Krieger, E.; Schaftenaar, G.; Swarts, H. G.; Willems, P. H.; De Pont, J. J.; Koenderink, J. B., Reconstruction of the complete ouabain-binding pocket of Na,K-ATPase in gastric H,K-ATPase by substitution of only seven amino acids. *J Biol Chem* **2005,** 280, 32349-55.
78. Glynn, I. M., The Na, K-Transporting Adenosine Triphosphatase. *Plenum Press, New York* **1985,** 3, 34-114.
79. Fahn, S.; Koval, G. J.; Albers, R. W., Sodium-potassium-activated adenosine triphosphatase of Electrophorus electric organ. I. An associated sodium-activated transphosphorylation. *J Biol Chem* **1966,** 241, 1882-9.
80. Albers, R. W.; Koval, G. J., Sodium-potassium-activated adenosine triphosphatase of Electrophorus electric organ. 3. An associated potassium-activated neutral phosphatase. *J Biol Chem* **1966,** 241, 1896-8.
81. Lüpfert, C.; Grell, E.; Pintschovius, V.; Apell, H. J.; Cornelius, F.; Clarke, R. J., Rate limitation of the Na(+),K(+)-ATPase pump cycle. *Biophys J* **2001,** 81, 2069-81.
82. Clarke, R. J.; Kane, D. J., Two gears of pumping by the sodium pump. *Biophys J* **2007,** 93, 4187-96.
83. Okamura, M. Y.; Isaacson, R. A.; Feher, G., Primary acceptor in bacterial photosynthesis: obligatory role of ubiquinone in photoactive reaction centers of Rhodopseudomonas spheroides. *Proc Natl Acad Sci USA* **1975,** 72, 3491-5.
84. Sebban, P., pH effect on the biphasicity of the P+QA- charge recombination kinetics in the reaction centers from Rhodobacter sphaeroides, reconstituted with anthraquinone. *Biochim Biophys Acta* **1988,** 936, 124-132.
85. Straley, S. C.; Parson, W. W.; Mauzerall, D. C.; Clayton, R. K., Pigment content and molar extinction coefficients of photochemical reaction centers from Rhodopseudomonas spheroides. *Biochim Biophys Acta* **1973,** 305, 597-609.
86. Miksovska, J.; Kálmán, L.; Schiffer, M.; Maróti, P.; Sebban, P.; Hanson, D. K., In bacterial reaction centers rapid delivery of the second proton to QB can be achieved in the absence of L212Glu. *Biochem* **1997,** 36, 12216-26.

87. Mancino, L. J.; Dean, D. P.; Blankenship, R. E., Kinetics and thermodynamics of the P870+QA-®P870QB- reaction in isolated reaction centers from the photosynthetic bacterium Rhodopseudomonas sphaeroides. *Biochim Biophys Acta* **1984,** 764, 46-54.
88. Kleinfeld, D.; Okamura, M. Y.; Feher, G., Electron transfer in reaction centers of Rhodopseudomonas sphaeroides. I. Determination of the charge recombination pathway of D+QAQ(-)B and free energy and kinetic relations between Q(-)AQB and QAQ(-)B. *Biochim Biophys Acta* **1984,** 766, 126-40.
89. Marcus, R. A.; Sutin, N., Electron transfer in chemistry amd biology. *Biochem Biophys Acta* **1985,** 934, 314-328.
90. Schwartz, A., *Methods in pharmacology*. New York, 1971; Vol. 1, p 1-200.
91. Cornelius, F.; Skou, J. C., Reconstitution of (Na+ + K+)-ATPase into phospholipid vesicles with full recovery of its specific activity. *Biochim Biophys Acta* **1984,** 772, 357-73.
92. Loew, L. M.; Bonneville, G. W.; Surow, J., Charge shift optical probes of membrane potential. Theory. *Biochem* **1978,** 17, 4065-71.
93. Clarke, R. J.; Zouni, A.; Holzwarth, J. F., Voltage sensitivity of the fluorescent probe RH421 in a model membrane system. *Biophys J* **1995,** 68, 1406-15.
94. Shuvalov, V. A.; Yakovlev, A. G., Energy level of P+B- with respect to P* found from recombination fluorescence measurements in pheophytin-modified reaction centres. *Membr Cell Biol* **1998,** 12, 563-9.
95. Cheap, H.; Tandori, J.; Derrien, V.; Benoit, M.; de Oliveira, P.; Koepke, J.; Lavergne, J.; Maroti, P.; Sebban, P., Evidence for delocalized anticooperative flash induced proton binding as revealed by mutants at the M266His iron ligand in bacterial reaction centers. *Biochem* **2007,** 46, 4510-21.
96. Tandori, J.; Baciou, L.; Alexov, E.; Maroti, P.; Schiffer, M.; Hanson, D. K.; Sebban, P., Revealing the involvement of extended hydrogen bond networks in the cooperative function between distant sites in bacterial reaction centers. *J Biol Chem* **2001,** 276, 45513-5.
97. Graige, M. S.; Feher, G.; Okamura, M. Y., Conformational gating of the electron transfer reaction QA-.QB --> QAQB-. in bacterial reaction centers of Rhodobacter sphaeroides determined by a driving force assay. *Proc Natl Acad Sci USA* **1998,** 95, 11679-84.
98. Tiede, D. M.; Vázquez, J.; Córdova, J.; Marone, P. A., Time-resolved electrochromism associated with the formation of quinone anions in the Rhodobacter sphaeroides R26 reaction center. *Biochem* **1996,** 35, 10763-75.
99. Li, J.; Gilroy, D.; Tiede, D. M.; Gunner, M. R., Kinetic phases in the electron transfer from P+QA-QB to P+QAQB- and the associated processes in Rhodobacter sphaeroides R-26 Reaction centres *Biochem* **1998,** 37, 2818-2829.
100. Sebban, P.; Wraight, C. A., Heterogeneity of the P+QA- recombination kinetics in reaction centers from Rhodopseudomonas viridis: the effect of pH and temperature. *Biochim Biophys Acta* **1989,** 974, 54-65.
101. Rostovtseva, T. K.; Petrache, H. I.; Kazemi, N.; Hassanzadeh, E.; Bezrukov, S., Interfacial polar interactions affect gramicidin channel kinetics. *Biophys J* **2008,** 94, L23-5.
102. Cladera, J.; O'Shea, P., Intramembrane molecular dipoles affect the membrane insertion and folding of a model amphiphilic peptide. *Biophys J.* **1998,** 74, 2434-42.
103. Milhiet, P. E.; Giocondi, M. C.; Baghdadi, O.; Ronzon, F.; Roux, B.; Le Grimellec, C., Spontaneous insertion and partitioning of alkaline phosphatase into model lipid rafts. *EMBO Rep* **2002,** 3, 485-90.

104. Watanabe, J.; Morita, T.; Kimura, S., Effects of dipole moment, linkers, and chromophores at side chains on long-range electron transfer through helical peptides. *J Phys Chem B* **2005,** 109, 14416-25.
105. Cladera, J.; O'Shea, P.; Hadgraft, J.; Valenta, C., Influence of molecular dipoles on human skin permeability: Use of 6-ketocholestanol to enhance the transdermal delivery of bacitracin. *J Pharm Sci* **2003,** 92, 1018-27.
106. Szabo, G., Dual mechanism for the action of cholesterol on membrane permeability. *Nature* **1974,** 252, 47-9.
107. McIntosh, T. J.; Magid, A. D.; Simon, S. A., Cholesterol modifies the short-range repulsive interactions between phosphatidylcholine membranes. *Biochem* **1989,** 28, 17-25.
108. McIntosh, T. J.; Magid, A. D.; Simon, S. A., Cholesterol modifies the short-range repulsive interactions between phosphatidylcholine membranes. *Biochem* **1988,** 26, 7325-32.
109. Vitha, M. F.; Clarke, R. J., Comparison of excitation and emission ratiometric fluorescence methods for quantifying the membrane dipole potential. *Biochim Biophys Acta* **2007,** 1768, 107-14.
110. Shopes, R. J.; Wraight, C. A., Charge recombination from the P+QA- state in reaction centers from Rhodopseudomonas viridis. *Biochim Biophys Acta* **1987,** 893, 409-25.
111. Parot, P.; Thiery, J.; Verméglio, A., Charge recombination at low temperature in photosynthetic bacteria reaction centers: Evidence for two conformation states. *Biochim Biophys Acta* **1987,** 893, 534-543.
112. Shopes, R. J.; Wraight, C. A., Charge recombination from the P+QA- state in reaction centers from Rhodopseudomonas viridis. *Biochim Biophys Acta* **1987,** 893, 409-25.
113. Woodbury, N. W.; Parson, W. W., Nanosecond fluorescence from isolated photosynthetic reaction centers of Rhodopseudomonas sphaeroides. *Biochim Biophys Acta* **1984,** 767, 345-61.
114. Sebban, P.; Barbet, J. C., Intermediate states between P* and Pf in bacterial reaction centers, as detected by the fluorescence kinetics. *Biochim Biophys Acta* **1984,** 165, 107-110.
115. Rivasa, E.; Costa, B.; Gulik-Krzywickic, T.; Reiss-Husson, F., Phospholipid and pigment alterations after fusion between Rhodobacter sphaeroides chromatophores and acidic liposomes *Biochim Biophys Acta* **1987,** 904, 290-300.
116. Fritzsch, G.; Koepke, J.; Diem, R.; Kuglstatter, A.; Baciou, L., Charge separation induces conformational changes in the photosynthetic reaction centre of purple bacteria. *Acta Crystallogr D Biol Crystallogr* **2002,** 58, 1660-3.
117. Baciou, L.; Rivas, E.; Sebban, P., P+QA- and P+QB- charge recombinations in Rhodopseudomonas viridis chromatophores and in reaction centers reconstituted in phosphatidylcholine liposomes. Existence of two conformational states of the reaction centers and effects of pH and o-phenanthroline. *Biochem* **1990,** 29, 2966-76.
118. Baciou, L.; Sebban, P., Influences of the lipidic environment on the reaction centre's function. *Photochem photobiol* **1995,** 94, 4020-30.
119. Pedersen, B. P.; Buch-Pedersen, M. J.; Morth, J. P.; Palmgren, M. G.; Nissen, P., Crystal structure of the plasma membrane proton pump. *Nature* **2007,** 450, 1111-4.
120. Grell, E.; Lewitzki, E.; Schacht, A.; Stoltz, M., Nucleotide/Protein interaction: Energetic and structural features of Na, K-ATPase. *J Therm Anal Calorim* **2004,** 77, 471-481.
121. Esmann, M.; Fedosova, N. U.; Marsh, D., Osmotic stress and viscous retardation of the Na,K-ATPase ion pump. *Biophys J* **2008,** 94, 2767-76.

122. Fedosova, N. U.; Champeil, P.; Esmann, M., Rapid filtration analysis of nucleotide binding to Na,K-ATPase. *Biochem* **2003,** 42, 3536-43.
123. Hegyvary, C.; Post, R. L., Binding of adenosine triphosphate to sodium and potassium ion-stimulated adenosine triphosphatase. *J Biol Chem* **1971,** 246, 5234-40.
124. Norby, J. G.; Jensen, J., Binding of ATP to brain microsomal ATPase. Determination of the ATP-binding capacity and the dissociation constant of the enzyme-ATP complex as a function of K+ concentration. *Biochim Biophys Acta* **1971,** 233, 104-16.
125. Borlinghaus, R.; Apell, H. J., Current transients generated by the Na+/K+-ATPase after an ATP concentration jump: dependence on sodium and ATP concentration. *Biochim Biophys Acta* **1988,** 939, 197-206.
126. Clarke, R. J.; Kane, D. J.; Apell, H. J.; Roudna, M.; Bamberg, E., Kinetics of Na^+ -dependent conformational changes of rabbit kidney Na^+,K^+ -ATPase. *Biophys J* **1998,** 75, 1340-1353.
127. Fendler, K.; Jaruschewski, S.; Hobbs, A. S.; Albers, W.; Froehlich, J. P., Pre-steady-state charge translocation in NaK-ATPase from eel electric organ. *J Gen Physiol* **1993,** 102, 631-66.
128. Friedrich, T.; Bamberg, E.; Nagel, G., Na+,K(+)-ATPase pump currents in giant excised patches activated by an ATP concentration jump. *Biophys J* **1996,** 71, 2486-500.
129. Froehlich, J. P.; Hobbs, A. S.; Albers, R. W., Evidence for parallel pathways of phosphoenzyme formation in the mechanism of ATP hydrolysis by the electrophorus Na, K-TPase. *Curr Top Membr Transport* **1983,** 19, 513-535.
130. Kane, D. J.; Fendler, K.; Grell, E.; Bamberg, E.; Taniguchi, K.; Froehlich, J. P.; Clarke, R. J., Stopped-flow kinetic investigations of conformational changes of pig kidney Na+,K+-ATPase. *Biochem* **1997,** 36, 13406-20.
131. Kane, D. J.; Grell, E.; Bamberg, E.; Clarke, R. J., Dephosphorylation kinetics of pig kidney Na+,K+-ATPase. *Biochem* **1998,** 37, 4581-91.
132. Grell, E.; Schick, E.; Lewitzki, E., Membrane receptor calorimetry: cardiac glycoside interaction with Na, K-ATPase *Thermochim Acta* **2001,** 380, 245-254.
133. O'Sullivan, W. J.; Smithers, G. W., Stability constants for biologically important metal-ligand complexes. *Methods Enzymol* **1979,** 63, 294-336.
134. Fedosova, N. U.; Champeil, P.; Esmann, M., Nucleotide Binding to Na,K-ATPase: The Role of Electrostatic Interactions. *Biochem* **2002,** 41, 1267-73.
135. Montes, M. R.; González-Lebrero, R. M.; Garrahan, P. J.; Rossi, R. C., Quantitative analysis of the interaction between the fluorescent probe eosin and the Na+/K+-ATPase studied through Rb+ occlusion. *Biochem* **2004,** 43, 2062-9.
136. Stürmer, W.; Apell, H. J., Fluorescence study on cardiac glycoside binding to the Na,K-pump. Ouabain binding is associated with movement of electrical charge. *FEBS letters* **1992,** 300, 1-4.
137. Klodos, I.; Skou, J. C., The effect of chelators on Mg2+, Na+-dependent phosphorylation of (Na+ + K+)-activated ATPase. *Biochim Biophys Acta* **1977,** 481, 667-79.
138. Campos, M.; Beaugé, L., Effects of magnesium and ATP on pre-steady-state phosphorylation kinetics of the Na+,K(+)-ATPase. *Biochim Biophys Acta* **1992,** 1105, 51-60.
139. Ghosh, M. C.; Jencks, W. P., Phosphorylation of the sodium-potassium adenosinetriphosphatase with adenosine triphosphate and sodium ion that requires subconformations in addition to principal E1 and E2 conformations of the enzyme. *Biochem* **1996,** 35, 12587-90.

140. Keillor, J. W.; Jencks, W. P., Phosphorylation of the sodium--potassium adenosinetriphosphatase proceeds through a rate-limiting conformational change followed by rapid phosphoryl transfer. *Biochem* **1996,** 35, 2750-3.
141. Tsuda, T.; Kaya, S.; Yokoyama, T.; Hayashi, Y.; Taniguchi, K., ATP and acetyl phosphate induces molecular events near the ATP binding site and the membrane domain of Na+,K+-ATPase. The tetrameric nature of the enzyme. *J Biol Chem* **1998,** 273, 24339-45.
142. Cornelius, F., Rate determination in phosphorylation of shark rectal Na,K-ATPase by ATP: temperature sensitivity and effects of ADP. *Biophys J* **1999,** 77, 934-42.
143. Olesen, C.; Picard, M.; Winther, A. M.; Gyrup, C.; Morth, J. P.; Oxvig, C.; Møller, J. V.; Nissen, P., The structural basis of calcium transport by the calcium pump. *Nature* **2007,** 450, 1036-42.
144. Møller, J. V.; Lind, K. E.; Andersen, J. P., Enzyme kinetics and substrate stabilization of detergent-solubilized and membraneous (Ca2+ + Mg2+)-activated ATPase from sarcoplasmic reticulum. Effect of protein-protein interactions. *J Biol Chem* **1980,** 255, 1912-20.
145. Voet, D.; Voet, J. G., Biochemistry 2nd Edn. Wiley, *New York,USA eds* **1995,** 377.
146. Campos, M.; Beaugé, L., Binding of manganese ions to the Na+/K+-ATPase during phosphorylation by ATP. *Biochim Biophys Acta* **1988,** 944, 242-8.
147. Richards, D. E., Occlusion of cobalt ions within the phosphorylated forms of the Na+-K+ pump isolated from dog kidney. *J Physiol* **1988,** 404, 497-51.
148. Grisham, C. M.; Mildvan, A. S., Magnetic resonance and kinetic studies of the mechanism of sodium and potassium ion-activated adenosine triphosphatase. *J Biol Chem* **1974,** 249, 3187-97.
149. Märdh, S.; Post, R. L., Phosphorylation from adenosine triphosphate of sodium- and potassium-activated adenosine triphosphatase. Comparison of enzyme-ligand complexes as precursors to the phosphoenzyme. *J Biol Chem* **1977,** 252, 633-8.
150. Patchornik, G.; Munson, K.; Goldshleger, R.; Shainskaya, A.; Sachs, G.; Karlish, S. J., The ATP-Mg2+ binding site and cytoplasmic domain interactions of Na+,K+-ATPase investigated with Fe2+-catalyzed oxidative cleavage and molecular modeling. *Biochem* **2002,** 41, 11740-9.
151. Pratap, P. R.; Robinson, J. D., Rapid kinetic analyses of the Na+/K(+)-ATPase distinguish among different criteria for conformational change. *Biochim Biophys Acta* **1993,** 1151, 89-98.
152. Stürmer, W.; Bühler, R.; Apell, H. J.; Läuger, P., Charge translocation by the Na,K-pump: II. Ion binding and release at the extracellular face. *J Membr Biol* **1991,** 121, 163-76.
153. Hobbs, A. S.; Albers, R. W.; Froehlich, J. P., Complex time dependence of phosphoenzyme formation and decomposition in electroplax Na,K-ATPase. *Prog Clin Biol Res* **1988,** 268A, 307-14.
154. Apell, H. J.; Roudna, M.; Corrie, J. E.; Trentham, D. R., Kinetics of the phosphorylation of Na,K-ATPase by inorganic phosphate detected by a fluorescence method. *Biochem* **1996,** 35, 10922-30.
155. Segel, I. H., Enzyme kinetics: behaviour and analysis of rapid equilibrium and steady state enzyme systems. *Wiley, New York USA eds* **1975,** 19, 142.
156. Kong, B. Y.; Clarke, R. J., Identification of potential regulatory sites of the Na+,K+-ATPase by kinetic analysis. *Biochem* **2004,** 43, 2241-50.
157. Clarke, R. J.; Lüpfert, C., Influence of anions and cations on the dipole potential of phosphatidylcholine vesicles: Basis for the Hofmeister effect. *Biophys J* **1999,** 76, 2614-2624.

158. Hobbs, A. S.; Albers, R. W.; Froehlich, J. P., Potassium-induced changes in phosphorylation and dephosphorylation of (Na+ + K+)-ATPase observed in the transient state. *J Biol Chem* **1980,** 255, 3395-402.
159. Clarke, R. J.; Apell, H. J.; Kong, B. Y., Allosteric effect of ATP on Na(+),K(+)-ATPase conformational kinetics. *Biochem* **2007,** 46, 703-44.
160. Kane, D. J.; Fendler, K.; Grell, E.; Bamberg, E.; Taniguchi, K.; Froehlich, J. P.; Clarke, R. J., Stopped-flow kinetic investigations of conformational changes of pig kidney Na^+, K^+-ATPase. *Biochem* **1997,** 36, 13406-13420.
161. Klodos, I., Partial reactions in Na, K and H,K-ATPase studied with voltage-sensitive fluorescent dyes. In the sodium pump : Structure mechanism, hormonal control and its role in disease. *Steinkopff Verlag, Darmstadt, Germany eds* **1994**, 517-528.
162. Schneeberger, A.; Apell, H. J., Ion selectivity of the cytoplasmic binding sites of the Na,K-ATPase: II. Competition of various cations. *J Membr Biol* **2001,** 179, 263-73.
163. Schneeberger, A.; Apell, H. J., Ion selectivity of the cytoplasmic binding sites of the Na,K-ATPase: I. Sodium binding is associated with a conformational rearrangement. *J Membr Biol* **1999,** 168, 221-8.
164. Garrahan, P. J.; Rossi, R. C.; Rega, A. F., The interaction of K+, Na+, Mg2+, and ATP with the (Na,K)-ATPase. *Ann N Y Acad Sci* **1982,** 402, 239-52.
165. Cornelius, F., Cholesterol modulation of molecular activity of reconstituted shark Na^+,K^+-ATPase. *Biochem Biophys Acta* **1995,** 1235, 205-212.
166. Castuma, C.; Brenner, R. R.; De Lucce-Gattas, E. A.; Shreier, S.; Lamy-Freund, M. T., Cholesterol modulation of lipid-protein interactions in liver microsomal membrane: a spin label study *Biochem* **1991,** 30, 9492-9497.
167. Cacace, M. G.; Landau, E. M.; Ramsden, J. J., The Hofmeister series: salt and solvent effects on interfacial phenomena. *Q Rev Biophys* **1997,** 30, 241-77.
168. Hofmeister, F., Zur Lehre von der Wirkung des Salze. *Arch.exp.Pathol.Pharmacol* **1888,** 24, 247-260.
169. Hofmeister, F., Zur Lehre von der Wirkung der Saltze. *Arch.exp.Pathol.Pharmacol* **1890,** 27, 395-413.
170. Post, R. L.; Suzuki, K., A Hofmeister effect on the phosphoenzyme of Na,K-ATPase. *Soc Gen Physiol Ser* **1991,** 46, 201-9.
171. Suzuki, K.; Post, R. L., Equilibrium of phosphointermediates of sodium and potassium ion transport adenosine triphosphatase: action of sodium ion and Hofmeister effect. *J Gen Physiol* **1997,** 109, 537-54.
172. Gross, E.; Bedlack, R. S.; Loew, L. M., Dual-wavelength ratiometric fluorescence measurement of the membrane dipole potential. *Biophys J* **1994,** 67, 208-16.
173. Holmgren, M.; Wagg, J.; Bezanilla, F.; Rakowski, R. F.; De Weer, P.; Gadsby, D. C., Three distinct and sequential steps in the release of sodium ions by the Na+/K+-ATPase. *Nature* **2000,** 403, 898-901.

Appendix

Chapter 3

1. Composition of RM medium

	for 1 l
10 % $(NH4)_2SO_4$	*6.67 mg*
10 % DL- Malic acid, pH 6.8	*26.7 ml*
Super salts	*66.7 ml*
0.64 M Potassium phosphate buffer	*10 ml*
Peptone	*1 g*
Yeast extract	*1 g*
1M $MgCl_2$	*533 µl*
1M CaCl2	*333 µl*
H_2O	*888 ml*

The RM medium was autoclaved for 30 minutes and after cooling kanamycin (30 µg/ml) was added.

2. 10 % Malic acid

	for 1 l
DL-Malic acid	*100 g*
NaOH	*60 g*
H_2O	*up to 1 l, pH 6.8.*

3. Super salts

	for 1 l
Na_2EDTA	*0.4 g*
$MgSO_4.7H_2O$	*4.0 g*
$CaCl_2.2H_2O$	*1.7 g*
$FeSO_4$	*0.24 g*
Thiamine-HCl	*0.02 g*
Trace elements	*20 ml*

H_2O	*980 ml*

4. Trace elements

	for 250 ml
$MnSO_4.H_2O$	*0.397 g*
H_3BO_3	*0.7 g*
$Cu(NO_3)_2.3\ H_2O$	*0.01 g*
$ZnSO_4.7\ H_2O$	*0.06 g*
$(NH_4)_6Mo_7O_{24}.4\ H_2O$	*1.06 g*

5. RCV Agar

A.

10 % $(NH4)_2SO_4$	*10 ml*
10 % DL- Malic acid, pH 6.8	*40 ml*
Super salts	*100 ml*
0.64 M Potassium phosphate buffer	*15 ml*
H_2O	*335 ml*

B.

Agar	*20 g*
H_2O	*500 ml*

A and B components were autoclaved separately and mixed after both being cooled to 50 ℃. Kanamycin (30mg/ml) was added.

Chapter 5

Computer simulations of equilibrium titrations and the concentration dependence of pre-steady state kinetic data were performed using the commercially available program Berkeley-Madonna 8.0 (University of California, Berkeley) via a globally-convergent variation of the Newton-Raphson method to find the roots of eqs. (A2), (A3) and (A8).

Single site model without Mg^{2+}. Binding of ATP to the E1(Na^+)$_3$ conformation of the enzyme can be described by the equilibrium,

$$E1+ATP \overset{K1}{\leftrightarrow} EATP$$

,where K_1 is the apparent binding constant of ATP to the enzyme. Taking into account mass balance of the enzyme, the concentration of E1ATP is:

$$[E1ATP] = \frac{K_1[E]_{tot}[ATP]}{1+K_1[ATP]} \qquad (A1)$$

where $[E]_{tot}$ is the total concentration of enzyme. Taking into account mass balance for ATP the free ATP concentration, [ATP], is related to the total enzyme concentration and the total ATP concentration, $[ATP]_{tot}$ by:

$$[ATP] + \frac{K_1[E]_{tot}[ATP]}{1+K_1[ATP]} - [ATP]_{tot} = 0 \quad (A2)$$

Solving for the roots of eq. (A2) allows [ATP] to be calculated and then, by substitution into eq. (A1), [E1ATP] as well.

For the analysis of equilibrium titrations and pre-steady-state kinetic data, the degree of saturation, *S*, of the ATP binding sites as a function of [ATP] needs to be calculated. *S* is given by $[E1ATP]/[E]_{tot}$. [E1ATP] can be determined from eq. (A1) after solving for [ATP] from eq. (A2).

Single site model including Mg^{2+}. Equilibrium binding assays can never yield the apparent K_d of the enzyme for ATP in the presence of Mg^{2+}, because under these conditions the enzyme would immediately undergo phosphorylation and continue cycling until all the ATP was consumed. Therefore, the equilibrium condition can never be fulfilled. However, if sufficient equilibrium binding information is available for the individual equilibria involved from separate binding studies, a theoretical K_d can be calculated for comparison with that obtained in pre-steady-state kinetic studies.

Under these conditions it is necessary to consider three separate equilibria:

$$E1+ATP \overset{K1}{\leftrightarrow} EATP$$

$$Mg^{2+}+ATP \overset{KM}{\leftrightarrow} MgATP$$

$$Mg^{2+}+ATP \overset{KMA}{\leftrightarrow} MgATP$$

In theory there is a fourth equilibrium, i.e. the binding of Mg^{2+} ions to the enzyme. However, experimentally the Mg^{2+} concentration of the bulk solution is far in excess of the enzyme, so that the small amount of Mg^{2+} lost from the bulk by binding to the enzyme is negligible. It is also assumed that Mg^{2+} is far in excess of the ATP concentration, so that the free Mg^{2+} concentration can be approximated by the total concentration, $[Mg^{2+}]_{tot}$. Taking into account mass balance for ATP under these conditions [ATP] is related to $[E]_{tot}$, $[Mg^{2+}]_{tot}$ and $[ATP]_{tot}$ by:

$$[\mathrm{ATP}]+\frac{K_1[\mathrm{E}]_{\mathrm{tot}}[\mathrm{ATP}]}{1+K_1[\mathrm{ATP}]+K_{MA}K_M\left[\mathrm{Mg}^{2+}\right]_{\mathrm{tot}}[\mathrm{ATP}]}+K_M\left[\mathrm{Mg}^{2+}\right]_{\mathrm{tot}}[\mathrm{ATP}]$$
$$+\frac{K_{MA}K_M[\mathrm{E}]_{\mathrm{tot}}\left[\mathrm{Mg}^{2+}\right]_{\mathrm{tot}}[\mathrm{ATP}]}{1+K_1[\mathrm{ATP}]+K_{MA}K_M\left[\mathrm{Mg}^{2+}\right]_{\mathrm{tot}}[\mathrm{ATP}]}-[\mathrm{ATP}]_{\mathrm{tot}}=0 \qquad \text{(A3)}$$

Solving for the roots of eq. (A3) allows [ATP] to be calculated. The concentrations of E1ATP and E1MgATP can then be determined from:

$$[\mathrm{E1ATP}] = \frac{K_1[\mathrm{E}]_{\mathrm{tot}}[\mathrm{ATP}]}{1+K_1[\mathrm{ATP}]+K_{MA}K_M\left[\mathrm{Mg}^{2+}\right]_{\mathrm{tot}}[\mathrm{ATP}]} \quad \text{(A4)}$$

$$[\mathrm{E1MgATP}] = \frac{K_{MA}K_M[\mathrm{E}]_{\mathrm{tot}}\left[\mathrm{Mg}^{2+}\right][\mathrm{ATP}]}{1+K_1[\mathrm{ATP}]+K_{MA}K_M\left[\mathrm{Mg}^{2+}\right]_{\mathrm{tot}}[\mathrm{ATP}]} \quad \text{(A5)}$$

The total degree of saturation of the ATP sites under these conditions is given by S = ([E1ATP]+[E1MgATP)/$[\mathrm{E}]_{\mathrm{tot}}$.

Cooperative dimer model. From stopped-flow kinetic experiments[82] it was found that ATP binding was better described by a cooperative binding of two ATP molecules to an enzyme dimer (see Fig. 5.2). Taking into account mass balance for the enzyme, the equilibrium concentrations of enzyme dimer with one and two molecules of ATP bound are given by:

$$[\mathrm{E1ATP{:}E1}] = \frac{K_1[\mathrm{E}]_{\mathrm{tot}}[\mathrm{ATP}]}{1+2K_1[\mathrm{ATP}]+K_1K_2[\mathrm{ATP}]^2} \quad \text{(A6)}$$

$$[\mathrm{E1ATP{:}E1ATP}] = \frac{K_1K_2[\mathrm{E}]_{\mathrm{tot}}[\mathrm{ATP}]^2}{2+4K_1[\mathrm{ATP}]+2K_1K_2[\mathrm{ATP}]^2} \quad \text{(A7)}$$

In eq. (A6), [E1ATP:E1] represents the sum of the concentrations of the two species E1ATP:E1 and E1:E1ATP. These two species are chemically indistinguishable, but for statistical reasons it is important to consider both, because this takes into account the fact that there are two sites available on a protein dimer for the first ATP molecule to bind whereas there is only one site available for the second ATP molecule. Taking into account mass balance for ATP, [ATP] is related to $[\mathrm{E}]_{\mathrm{tot}}$ and $[\mathrm{ATP}]_{\mathrm{tot}}$ by:

$$[\mathrm{ATP}]+\frac{K_1[\mathrm{E}]_{\mathrm{tot}}[\mathrm{ATP}]+K_1K_2[\mathrm{E}]_{\mathrm{tot}}[\mathrm{ATP}]^2}{1+2K_1[\mathrm{ATP}]+K_1K_2[\mathrm{ATP}]^2}-[\mathrm{ATP}]_{\mathrm{tot}}=0 \qquad \text{(A8)}$$

Solving for the roots of eq. (A8) allows [ATP] to be calculated and then, by its substitution into eqs. (A6) and (A7), [E1ATP:E1] and [E1ATP:E1ATP] as well.

If one wishes to fit or simulate equilibrium titrations and pre-steady-state kinetic data, the total degree of saturation, *S*, of the ATP sites for the cooperative dimer model is given by ([E1ATP:E1]+2[E1ATP:E1ATP])/$[E]_{tot}$. Note that in this expression, as in the case of eq. (A6), [E1ATP:E1] actually represents the sum of the concentrations of the two species E1ATP:E1 and E1:E1ATP. The fraction of enzyme dimer, S_{dim}, totally saturated with ATP, i.e. in the form E1ATP:E1ATP, is given by [E1ATP:E1ATP]/($[E]_{tot}$/2).

Chapter 6

Simulations

Computer simulations of the time course of fluorescence changes experimentally observed via stopped-flow were performed using the commercially available program Berkeley Madonna 8.0 (University of California, Berkeley) via the variable step-size Rosenbrock integration method for stiff systems of differential equations. The simulations yield the time course of the concentration of each enzyme intermediate involved as well as the total fluorescence. Based on the reaction scheme 1-3, the differential rate equations describing the changes in the concentrations of all the enzyme intermediates are:

$$\frac{d\left[\mathrm{E1MgATP(Na^+)_3}\right]}{dt}=-k_1\left[\mathrm{E1MgATP(Na^+)_3}\right] \qquad \text{(A1)}$$

$$\frac{d\left[\mathrm{E2MgP(Na^+)_3}\right]}{dt}=k_1\left[\mathrm{E1MgATP(Na^+)_3}\right]-k_2\left[\mathrm{E2MgP(Na^+)_3}\right]+k_{-2}[\mathrm{E2MgP}] \qquad \text{(A2)}$$

$$\frac{d[\mathrm{E2MgP}]}{dt} = k_2\left[\mathrm{E2MgP(Na^+)_3}\right] - k_{-2}[\mathrm{E2MgP}] - k_3[\mathrm{E2MgP}] + k_{-3}[\mathrm{E2Mg}] \qquad \text{(A3)}$$

$$\frac{d[\mathrm{E2Mg}]}{dt} = k_3[\mathrm{E2MgP}] - k_{-3}[\mathrm{E2Mg}] \qquad \text{(A4)}$$

The total fluorescence, *F*, is due to contributions from fluorescence levels, *f*, of the probe associated with each of the enzyme conformational states. Because the fluorescence increases following mixing with ATP and the enzyme starts in the E1MgATP(Na^+)$_3$ state, the fluorescence level of this state has been defined to be zero. Because the major changes in fluorescence are thought to involve the binding or release of ions[152, 154, 162], the fluorescence level of the E1MgP(Na^+)$_3$ has also been taken to be zero. The total fluorescence is then given by

$$F = f_{\mathrm{E2MgP}}[\mathrm{E2MgP}] + f_{\mathrm{E2Mg}}[\mathrm{E2Mg}] \qquad \text{(A5)}$$

Numerical integration of Eqs. A1-A4 and calculation of the fluorescence using Eq. A5 yield a biexponential fluorescence transient with both phases associated with a fluorescence increase (as experimentally observed) using any values of f_{E2MgP} and f_{E2Mg} as long as they are both greater than zero. Based on the experimental results obtained, at saturating Mg^{2+} concentrations the values of k_1, k_3 and k_{-3} used were 237 s^{-1}, 5 s^{-1} and 63 s^{-1}, respectively. The values of k_2 and k_{-2} for Na^+ release and binding to the E2MgP state were both chosen to have values of 1000 s^{-1}. This is based on the electrical measurements of Holmgren et al.[173], which showed reciprocal relaxation times of $\geq$ 1000 s^{-1} for the release of Na^+ from the phosphorylated enzyme. For the purposes of the simulations normalized enzyme concentrations were used. Thus, the initial concentration of E1MgATP(Na^+)$_3$ was taken as 1.0 and the initial concentrations of all other enzyme species were taken as 0.0.

Data fitting

Nonlinear least squares fitting of equations describing the Mg^{2+} concentration dependence of the stopped-flow fluorescence amplitudes to the data was performed using Origin 6.0 (Microcal Software, Northampton, MA, USA). Nonlinear least squares fitting of equations describing the Mg^{2+} concentration dependence of the observed rate constants to the data were performed using Mathematica via a globally-convergent variation of the Newton-Raphson methods to find the roots of Eqs. A6 and A7.

Immediately after mixing with ATP but prior to any phosphorylation occurring the following equilibria would be expected to exist in solution:

$$E1ATP\ (Na^+)_3 + Mg^{2+} \leftrightarrow E1MgATP(Na^+)_3$$

$$ATP + Mg^{2+} \leftrightarrow MgATP$$

K_E and K_{ATP} represent the association constants for these two equilibria. It is assumed that because the enzyme is saturated by ATP and Na^+ there is no enzyme in the $E1(Na^+)_3$, E1ATP or E1 states and, therefore, binding of Mg^{2+} to these states has been ignored. Furthermore, it is also assumed that under conditions of excess ATP and Mg^{2+} over enzyme the concentrations of $E1MgATP(Na^+)_3$ and $E1ATP(Na^+)_3$ can be neglected when calculating the total ATP concentration and that the concentration of $E1MgATP(Na^+)_3$ can also be neglected when calculating the total Mg^{2+} concentration. Under these conditions, taking into account mass balance for ATP, the free ATP concentration is related to the total Mg^{2+} concentration, $[Mg^{2+}]_{tot}$, and the total ATP concentration, $[ATP]_{tot}$, by:

$$[ATP] + \frac{K_{ATP}[ATP]\left[Mg^{2+}\right]_{tot}}{1+K_{ATP}[ATP]} - [ATP]_{tot} = 0 \qquad (A6)$$

Solving for the roots of Eq. A6 allows [ATP] to be calculated for any values of $[Mg^{2+}]_{tot}$ and $[ATP]_{tot}$. Considering mass balance for Mg^{2+}, the free Mg^{2+} concentration is related to the $[Mg^{2+}]_{tot}$ and the total enzyme concentration, $[E]_{tot}$, by:

$$\left[Mg^{2+}\right]+K_{ATP}\left[ATP\right]\left[Mg^{2+}\right]+\frac{K_E\left[E\right]_{tot}\left[Mg^{2+}\right]}{1+K_E\left[Mg^{2+}\right]}-\left[Mg^{2+}\right]_{tot}=0 \qquad (A7)$$

Once Eq. A6 has been solved for [ATP], this can then be used to solve for the roots of Eq. A7 to find $[Mg^{2+}]$ for any values of $[Mg^{2+}]_{tot}$ and $[E]_{tot}$. Taking into account mass balance for the enzyme, from the expression for the association constant of Mg^{2+} with the enzyme, the concentration of $E1MgATP(Na^{+})_3$, the species which must be produced to allow phosphorylation to occur, is:

$$\left[E1MgATP(Na^{+})_3\right]=\frac{K_E\left[E\right]_{tot}\left[Mg^{2+}\right]}{1+K_E\left[Mg^{2+}\right]} \qquad (A8)$$

The degree of saturation, S_{E1}, of the Mg^{2+} sites on the E1 conformation of the enzyme is given by:

$$S_{E1}=\frac{\left[E1MgATP(Na^{+})_3\right]}{\left[E\right]_{tot}} \qquad (A9)$$

After the enzyme has been mixed with ATP and cycling has begun, Mg^{2+} could also bind to the E2 conformation of the enzyme according to the following equilibrium:

$$E2ATP+Mg^{2+} \leftrightarrow E2MgATP$$

K_F represents the association constant for this equilibrium. In a similar fashion to the E1 conformation one can find the free Mg^{2+} concentration when the enzyme is in the E2 conformation by solving an analogous expression to Eq. A7, i.e.

$$\left[Mg^{2+}\right]+K_{ATP}\left[ATP\right]\left[Mg^{2+}\right]+\frac{K_F\left[E\right]_{tot}\left[Mg^{2+}\right]}{1+K_F\left[Mg^{2+}\right]}-\left[Mg^{2+}\right]_{tot}=0 \qquad (A10)$$

Eq. A6 can still be used to calculate the free ATP concentration. The degree of saturation, S_{E2}, of the Mg^{2+} sites on the enzyme is given by:

$$S_{E2}=\frac{K_F\left[Mg^{2+}\right]}{1+K_F\left[Mg^{2+}\right]} \qquad (A11)$$